BRITTLE FRACTURE CHARACTERISTICS OF A THICK- WALLED CYLINDER WITH AN FGM COATING AT THE INNER SURFACE

by

Lumaya Ahmed

Submitted in partial fulfillment of the requirements for the degree of

MASTER OF SCIENCE IN MECHANICAL ENGINEERING

Department of Mechanical Engineering

BANGLADESH UNIVERSITY OF ENGINEERING AND TECHNOLOGY

Dhaka 1000, Bangladesh.

June, 2012

This thesis titled "**Brittle Fracture Characteristics of a Thick -Walled Cylinder with an FGM Coating at the Inner Surface",** submitted by **Lumaya Ahmed**, Student No. 1009102054**P** Session October 2009 has been accepted as satisfactory in partial fulfillment of the requirement for the degree of MASTER OF SCIENCE IN MECHANICAL ENGINEERING on June 25th, 2012.

BOARD OF EXAMINERS

1._____   Chairman

Dr. Md. Afsar Ali
Professor
Department of Mechanical Engineering
Bangladesh University of Engineering and Technology
Dhaka-1000, Bangladesh.

2._____   Member
                                                                (Ex-Officio)

Dr. Md. Ehsan
Professor and Head
Department of Mechanical Engineering
Bangladesh University of Engineering and Technology
Dhaka-1000, Bangladesh.

3._____   Member

Dr. Monon Mahbub
Assistant Professor
Department of Mechanical Engineering
Bangladesh University of Engineering and Technology
Dhaka-1000, Bangladesh.

4._____   Member
                                                                (External)

Dr. Md. Shamimur Rahman
Associate Professor
Department of Mechanical Engineering
Rajshahi University of Engineering and Technology
Rajshahi, Bangladesh.

CANDIDATE'S DECLARATION

It is hereby declared that this thesis or any part of it has not been submitted elsewhere for the award of any degree or diploma.

Signature of the Candidate

_____

Lumaya Ahmed

Dedicated to my parents

TABLE OF CONTENTS

LIST OF FIGURES

LIST OF TABLE

LIST OF SYMBOLS

A	Dispersed Material
B	Parent/Base material
E	Young's modulus of FGM
E_0	Young's modulus of material B
F	Geometric Factor
l	Crack length
K_I	Stress intensity factor
F_I	Normalized stress intensity factor
K_{IC}^a	Apparent fracture toughness of FGM
K_C	Intrinsic fracture toughness of FGM
K_C^B	Intrinsic fracture toughness of material B
V_A	Volume fraction of material A
V_B	Volume fraction of material B
ΔT	Difference between processing and room temperatures
γ	Bulk modulus
S_f	Strength factor
σ_u	Ultimate strength of material B
R_o	Outer radius of the cylinder
R_i	Inner radius of the cylinder
r	Any radius
p	Internal pressure
p_c	Critical pressure
μ	Shear modulus of rigidity
ν	Poisson's ratio
ε	Strain
ε^*	Incompatible thermal eigenstrain
ε_e	Equivalent eigenstrain
u	Dispalcement components
α	Coefficient of thermal expansion

σ_s^h	Stress component in uncracked homogenized cylinder
σ_s^d	Stress component of the disturbed field for crack
T_s	Traction along crack surface
$\Phi(z)$, $\Psi(z)$	Complex potential functions
K_0	Kolosov's constant
b_1, b_2	Components of Burger vector
σ_θ, σ_r	Circumferential and radial stress component respectively
ε_k	Small positive quantity
F_{obj}	Objective function
n	Number of layers in FGM coating
CT	Coating thickness

ACKNOWLEDGEMENTS

ABSTRACT

This study is concerned with the brittle fracture characteristics of a thick-walled cylinder with a functionally graded material (FGM) coating at the inner surface having two diametrically opposed edge cracks. First, the uncracked cylinder with the FGM coating is homogenized by simulating the nonhomogenous material properties with an equivalent eigenstrain. The homogenized cylinder is then considered to have two diametrically-opposed edge cracks for the analysis. Second, the cracks in the homogenized cylinder are represented by continuous distribution of edge dislocations. Representing the cracks by continuous distribution of edge dislocations, a method is then formulated to calculate the stress intensity factor (SIF), which is used to evaluate apparent fracture toughness of the cylinder. Also, the method is applied to the inverse problem of evaluating optimum material distribution intending to realize prescribed apparent fracture toughness in the cylinder with an FGM coating. For numerical results, a thick-walled cylinder with TiC/Al_2O_3 (Titanium carbide and Aluminium oxide) FGM coating at its inner surface is considered. The effects of material distribution profile, cylinder wall thickness, application temperature, coating thickness (CT) and number of cracks on both the apparent fracture toughness and stress intensity factor are investigated in details. It is found that all of these factors play an important role in the fracture characteristics of the thick walled cylinder with FGM coating. The numerical results of inverse problem reveals that the apparent fracture toughness in a thick-walled cylinder with an FGM coating depends significantly on the material distributions, and can be controlled within possible limits by choosing an optimum material distribution profile.

CHAPTER 1
INTRODUCTION

1.1 Background

Functionally graded materials (FGMs) are a new generation of engineered materials which are a nonhomogeneous mixture of two or more distinct material phases, such as different ceramics or ceramics and metals. The key distinguishing feature of these materials is that the composition, or in other words, the material distribution of each constituent material, continuously varies with space variables. This continuously varying material distribution induces chemical, material, and microstructural gradients, and makes functionally graded materials different in behavior from homogeneous materials and traditional composite materials [1, 2]. It is noted that a traditional composite is homogeneous from the view point of macroscopic study and does not have gradient in microstructure. The concept of a typical FGM body consisting of two different materials *A* and *B* is illustrated in Fig. 1.1. The left surface of the FGM plate shown in Fig. 1.1(a) has 100% material *A* while the right surface of the plate has 100% material *B*. In between these two surfaces, the material distribution (composition) denoted by the volume fractions V_A and V_B of the constituents *A* and *B*, respectively, continuously changes as shown in Fig. 1.1(b). The material distribution shown in Fig. 1.1(b) may vary linearly, exponentially, or following any power function depending on the desired properties and application of FGMs.

The functionally graded materials are tailorable in their properties via the design of the gradients in chemistry and microstructure, which again depend on the material distribution. Therefore, they allow control over their mechanical, thermal, and chemical properties to meet varying demands of applications. A specific property of FGMs can be optimized by properly selecting their material distribution profiles.

As mentioned earlier, traditional composites are homogeneous mixtures of two or more ingredients, and they, therefore, involve a compromise between the desirable properties of the component materials. On the other hand, as a significant proportion of an FGM

may contain the pure form of each component, the need for compromise is eliminated. The properties of both components can, therefore, be fully utilized. For example, the toughness of a metal can be mated with the refractoriness of a ceramic, without any compromise in the toughness of the metal side or the refractoriness of the ceramic side. From a mechanics viewpoint, the main advantages of material property grading appear to be improved bonding strength, toughness, wear and corrosion resistance, and reduced residual and thermal stresses. Usually, an FGM is made of a ceramic and a metal to resist severe environmental effects, such as wear, corrosion, and large temperature field at the ceramic side and ensure toughness and thermal conductivity on the metal side.

Initially, the purpose of these materials was to develop superheat resistant material for propulsion systems and airframes of spacecraft. Now they are also used as high temperature, wear- and corrosion-resistant materials. Apart from these, their applications have been extended from structural to five other functional areas: electronics, chemical, optical, nuclear, and biological. From a mechanics point of view the prime advantages of the composition gradation are improved bonding strength, toughness, and wear and corrosion resistance, and reduced residual and thermal stresses. Some other specific applications of FGMs are listed below.

Aeronautics: outer wall of spaceplane, parts of rocket engine, etc.
Industrial materials: forming tools, wear resistant linings for handling large heavy abrasive ore particles, heat exchanger tubes, etc.
Optoelectronics: optical fibers.
Energy materials: thermoelectric materials for optoelectric conversion and sun energy-laser conversion, etc.
Biomaterials: artificial bones, joints, and teeth.

As FGMs have wide applications in many branches of engineering, it is necessary to identify their probable failure modes and design them against those failures. It is recognized that the fracture failure is one of the most common failure modes for FGMs. Although the absence of sharp interfaces in FGMs largely reduces material property mismatch, crack may occur when they are subjected to external loadings [1, 2]. In most of the cases, the failure process starts with the formation of microcracks at locations of corrosion pits, surface flaws, or stress concentration. These microcracks are coalesced

into a local dominant crack, which would then propagate under cyclic or sustained loading. Even very small mechanical imperfection has adverse effect on the fracture strength. Therefore, fracture analysis of these materials is important in order to understand, quantify, and improve their toughness.

The study of fracture of solids is carried out from one of the three points of view, namely microscopic or atomic, microstructural, and macroscopic or continuum mechanics. From the viewpoint of engineering applications, macroscopic theories of fracture are important which classify fracture as brittle and ductile. Brittle fracture is associated with low energy, and for unstable loading conditions, it usually takes place under high fracture velocities. Ductile fracture is associated with large deformations, high energy dissipation rates, and slow fracture velocities. Again loading of cracked body is usually accompanied by inelastic deformation and other nonlinear effect in the neighborhood of the crack tip, except for the case of ideally brittle materials [3]. But in the situations where inelastic deformation and nonlinear effects are very small compared to the crack size and any other characteristic length of the body, the linear theory is adequately justified to address the problem of stress distribution in the cracked body. The microstructure is also a factor that affects the fracture characteristics of solids. However, in the idealized case of FGMs, the effect of microstructure is neglected and materials are assumed to be simple nonhomogeneous with continuous change of material properties.

Another important factor in the fracture study of FGMs is the eigenstrain, which is a generic name of such nonelastic strains as thermal expansion, phase transformation, initial strains, plastic strains and misfit strains [4]. The incompatibility of this eigenstrain produces eigenstress, which affect the fracture strength of FGMs. In FGMs, eigenstrain is induced due to nonuniform coefficient of thermal expansion (CTE) when FGMs are cooled from sintering temperature.

1.2 Manufacturing Processes of FGMs

At the beginning, the manufacturing of an FGM was challenging and costlier. Now-a-days, a good number of manufacturing techniques have been developed by various researchers, some of which are industrially used for mass production. Some common manufacturing techniques of FGMs are: electrophoretic deposition, chemical vapor

3

deposition (CVD), physical vapor deposition (PVD), plasma spraying, electrochemical gradation, centrifugal casting, powder metallurgy, etc. Among the available coating methods listed above, plasma spraying is the most potential technique for FGM coating with high-melting-point materials and accurate control of material distribution. The basic features of a plasma spray method are shown in Fig. 1.2.

The powder-form coating material to be deposited on the substrate mixes with high temperature plasma gas and melts. The mixture of molten coating material and plasma gas then strikes the substrate and deposits on it.

Now, to develop an FGM coating using this technique, two materials, instead of one, should be mixed with varying proportions with plasma gas. However, there should be a suitable mechanism to control the flow rate of two coating materials. A schematic view of FGM coating technique using plasma spray method is shown in Fig. 1.3. Here, two different materials (materials *A* and *B*) are supplied through two different ports. The volume fractions of each material can be controlled in the FGM coating being deposited on the substrate. Alternatively, two separate plasma torches can be used to deposit two materials from two torches. Controlling the volume supplied from each torch, the material distribution in the FGM coating can be controlled.

1.3 Motivation of the Present Work

It is pointed out earlier that the original purpose of FGMs was to develop a thermal barrier coating for a high temperature gradient field. However, their outstanding advantages have now stimulated the interest of researchers towards the development of new potential structural applications. Consequently, enormous studies have already been carried out to analyze various aspects of FGM beams [5, 6], plates [7-11], cylinders [12-15], and spheres [16]. For instance, Loghman *et al.* [16] investigated the magnetothermoelastic creep behavior of thick-walled spheres made of functionally graded materials (FGM) placed in uniform magnetic and distributed temperature fields and subjected to an internal pressure using method of successive elastic solution. Xiang and Yang [17] considered thermal load for the analysis of free and forced vibration of a laminated functionally graded Timoshenko beam of variable thickness. A Timoshenko beam of FGMs was also considered to investigate the post-buckling behavior in response

4

to the thermal load [18]. Nonlinear transient analysis was carried out for functionally graded ceramic-metal plates under thermal loading by Praveen and Reddy [19] using finite element method (FEM). Transient waves in FGM plates and cylinders were studied by Han *et al.* [20, 21].

FGM circular cylinders were considered by Obata and Noda [13] and Liew *et al.* [14] to analyze the thermal stresses. FGM circular cylinders were also considered by Afsar and his co-workers [22] for the analysis of brittle fracture characteristics by taking into account the effect of incompatibility of eigenstrain developed in the cylinder due to nonuniform CTE as a result of temperature change.

Over the past few years FGM cylinders have been considered to study and analyze, both theoretically and experimentally, their responses to mechanical and thermal loadings for various geometries in various fracture mechanisms. Most of these studies are concerned with the direct problems in which the fracture characteristics of FGM cylinders are analyzed only for certain assumed functional forms of material properties e.g. exponential and power functions. Also, the eigenstrain induced in the materials due to nonuniform CTE after cooling from sintering temperature was not taken into account in most of the above-mentioned analyses. In fact, the assumed functional forms of material properties are not justified for designing with FGMs to exhibit a desired characteristic suitable for a particular application, as the assumed properties may not be physically realizable to introduce the desired characteristic. Moreover all these studies were concerned with a cylinder wholly made of FGM. But in practice, it is not feasible to manufacture a thick- walled cylinder with gradation of material throughout the entire wall thickness because of manufacturing limitation as well as huge cost involvement. On the other hand, from engineering points of view, the entire cylinder wall with graded material is not important in order to meet the requirements of an application. Only a thin coating can satisfy the requirements of an application and is more feasible from technical points of view. This motivated the author to consider the problem of a thick-walled cylinder with only an FGM coating at the inner surface for the analysis of brittle fracture characteristics. The incompatible eigenstrain developed due to nonuniform co-efficient of thermal expansion, is also taken into account in this study.

1.3 Objectives

The specific objectives of the study are

a) To develop a method for the analysis of stress intensity factor (SIF) and apparent fracture toughness (AFT) for two diametrically opposed edge cracks in a thick-walled cylinder with an FGM coating at the inner surface.

b) To verify the validity of the developed method by comparing the results of stress intensity factors calculated for a homogenous cylinder with those available in the literature.

c) To investigate the effect of material distributions, cylinder wall thickness, application temperature, FGM coating thickness (CT) and number of cracks on both SIF and AFT.

d) To apply the developed method in evaluating optimum material distribution in the FGM coating corresponding to prescribed apparent fracture toughness in the cylinder by using inverse method.

The study is carried out from a macroscopic viewpoint of fracture theories for the idealized case in which the microstructure of the material is neglected and the material is assumed to be isotropic. Further, the material is assumed to be perfectly brittle or with small scale plastic deformation.

CHAPTER 2
LITERATURE REVIEW

A series of papers on the crack problems of FGMs have appeared in the literature in which the material properties have been assumed to vary following an exponential function [23-27] or power functions [28-30]. Gu and Asaro [24] considered a semi-infinite crack in a strip of an isotropic, functionally graded material under edge loading and in-plane deformation conditions. Their results showed that the fracture modes of the cracks in FGMs are inherently mixed when they are not parallel to the direction of material property variation, *i.e.* there are typically both normal and shear tractions ahead of the crack tips because of the non-symmetry in the material properties. The crack problems of FGMs with the exponential variation of material properties and involving various geometries discussed above were solved for mechanical loadings. Numerous researchers have also carried out a number of studies for cracked FGM bodies subjected to thermal loadings assuming the same exponential function for the material properties. Jin and Noda [31], Noda and Jin [32] have studied crack problems of FGMs under steady thermal loading in order to reduce the thermal stresses and the thermal stress intensity factors. All of these authors, in their research work, conclude that the appropriate selection of the mechanical and the thermal nonhomogeneous parameters of the material reduces the thermal stresses and, hence, the thermal stress intensity factors. Bao and Wang [28] studied multiple cracking in functionally graded ceramic/metal coatings and considered both mechanical and thermal loads. The gradation in the FGM coating was taken to be of a power function, both linear and nonlinear. It was found that the gradation of the coating could significantly reduce the crack driving force. It was also found that under mechanical loading the effect of different gradations on the crack driving force was relatively small. However, under thermal loading, the influence of coating gradation could be significant.

From the above reviews discussed so far, it can be summarized that the various aspects of crack problems of functionally graded materials have been studied, both analytically and experimentally, under various mechanical and thermal loading conditions, and for various geometries. However, these studies are concerned with the direct problems in which the fracture characteristics of FGM bodies can be analyzed only for certain

assumed functions of the material properties e.g. exponential and power functions.

An important aspect of FGM bodies still remaining to be dealt with is the inverse problems in which the improved characteristics of FGM bodies under mechanical and thermal loadings can be prescribed and the corresponding material composition profiles via the material properties can be obtained by inverse calculation. A general inverse design procedure for FGMs was addressed by Hirano and Wakashima [33] to determine both the basic material combination and optimum material distribution profile with respect to the objective structural shape and the thermomechanical boundary conditions. Markworth and Saunders [34] considered the inverse problem of optimizing an assumed functional form for the spatially dependent material distributions subject to certain constraints such as maximizing or minimizing the heat flux across the material. Further references of the inverse problems to design FGMs with various geometries subject to various constraints can be found in Refs. [35-40]. In all the references mentioned above, the inverse problems were considered in order to design FGMs optimally from the viewpoint of thermal characteristics. The analytical solution to the inverse problems of designing FGMs from the viewpoint of fracture characteristics turns out to be very complicated due to their nonhomogenous material properties. Obviously, the inverse problems cannot be restricted to certain assumed functions for the material property distributions as Zuiker [41] pointed out that these assumed property distributions are not physically realizable for certain material composition profiles which may be obtained by the inverse problems. Afsar and Sekine [42] dealt with the inverse problem of calculating material distribution for prescribed apparent fracture toughness in FGM coatings around a circular hole in infinite elastic media. They also considered semi-infinite FGM media with a single [43] and periodic [44] edge cracks and computed material distribution profiles for improved fracture characteristics. In another work [45], they calculated the optimum material distribution in a thick-walled FGM circular pipe with a single edge crack for desired apparent fracture toughness. However, Shannon [46] found that two diametrically-opposed radial edge cracks represent the worst geometry of multiple cracking which can occur in vessels of large diameter ratio.

It is found that all the above mentioned studies were concerned with the thick-walled FGM cylinder, i.e., the entire cylinder wall was composed of FGM, having the material gradation of throughout the entire cylinder wall which is not feasible in practice due to manufacturing limitation and huge cost involvements. From engineering perspective, the

entire cylinder wall with graded material is not essential to meet the requirements of an application. An FGM coating on the cylinder can satisfy the requirements of the application and is more feasible from technical point of view. So the present study focuses on a thin FGM coating at the inner surface of a thick-walled cylinder. The approximation method [45] developed for the FGM cylinder has been extended in the present study for the FGM coating at the inner surface of a thick-walled cylinder.

CHAPTER 3

APPROXIMATION METHOD OF STRESS INTENSITY FACTOR FOR CYLINDER WITH FGM COATING

3.1 Method of Homogenization

The presence of nonhomogeneity in FGMs complicates the analytical study of fracture characteristics of these materials due to some mathematical difficulties. Because of this complexity, it has been a trend of analyzing the fracture characteristics of these materials by assuming the material properties as certain functional forms e.g. exponential or power functions of space variables to simplify the problem. However, in designing FGMs i.e. in the inverse problems where material distributions have to be determined to achieve desired fracture characteristics, special functional forms of the properties cannot be assumed. This is due to the fact that the material distributions obtained by inverse calculation may not conform to the assumed functional forms of the material properties. Therefore, the inverse problem of determining material distributions requires an alternate method by which the problem can be treated for any arbitrary variation of material properties in FGMs. In this study, an approximation method of calculating stress intensity factor (SIF) developed by Afsar [43] is adopted for a thick-walled cylinder with FGM coating. A brief outline of the method is given in the following paragraph.

According to the approximation method, the cylinder with FGM coating is first homogenized by simulating the material nonhomogeneities by a distribution of equivalent eigenstrain. The distribution of equivalent eigenstrain is such that the elastic fields in both the cylinder with FGM coating and homogenized cylinder for the same loading condition are identical. Then a method is formulated to calculate the stress intensity factor for the cracks in the homogenized cylinder. Since the equivalent eigenstrain is determined from the condition of identical elastic fields in the uncracked cylinder with FGM coating and homogenized cylinder, the elastic field in the cracked homogenized cylinder cannot exactly represent the elastic field in the cracked cylinder with FGM coating. So, the stress intensity factors calculated for the cracks in the homogenized cylinder with the equivalent eigenstrain represent the approximate values of stress intensity factors for the same cracks in the corresponding cylinder with FGM coating and that is why it is referred to as an approximation method.

The principle of superposition is used to determine the resultant stress field in the cracked homogenized cylinder. Initially, the stress field in the uncracked homogenized cylinder is determined for external loading, and incompatible and equivalent eigenstrains. This stress field is disturbed by the presence of two diametrically opposed edge cracks. The disturbed stress field is then determined. Finally, the resultant stress field in the cracked homogenized cylinder is obtained by the principle of superposition. The disturbed stress field is such that the following boundary condition along the crack surface is satisfied,

$$\sigma_s^d + \sigma_s^h = T_s \tag{3.1}$$

where σ_s^h the stress component along the prospective crack line is in the uncracked homogenized cylinder, σ_s^d is the stress component of the disturbed field due to the presence of the cracks, and T_s is the traction applied to the crack surface. The disturbed stress field can be determined by representing the crack by a continuous distribution of edge dislocations.

3.2 Apparent Fracture Toughness of FGMs

Three independent kinematic movements of the crack surfaces with respect of each other are possible [3] as shown in Fig.3.1. According to these relative movements of the crack surfaces, crack propagation is classified as mode I (Fig.3.1 (a)), mode II (Fig.3.1 (b)), and mode III (Fig.3.1 (c)). In this study, only mode I will be considered which is most prone to occur in the cylinder under internal pressure.

The stress intensity factors for a crack in homogeneous cylinders in absence of any initial stresses or eigenstrains can be expressed, in general, for mode I as [48].

$$K_I = Fp\sqrt{\pi l} \tag{3.2}$$

where F is a geometric factor that depends on the geometry of the crack and the cracked body and the loading configuration, l is the crack length, and p is the applied internal pressure. The factor F is given by Bowie *et al.* [49] and for convenience it is reproduced here in Fig. 3.2 and Table 3.1.

The intrinsic fracture toughness of a homogeneous cylinder for a specific crack length l can be determined from the above expression when the applied pressure p approaches its

critical value p_C, since p_C alone contributes to the crack driving force.

On the other hand, in cylinder with FGM coating, the effective crack driving force is obtained due to the resultant effects of the critical pressure p_C and the induced incompatible eigenstrain resulting from nonuniform coefficient of thermal expansion when the cylinders with FGM coating are cooled from sintering temperature. However, apparently it seems that the crack extension in FGM coated cylinders occurs due to the applied critical pressure p_C alone. Therefore, the above expression gives the apparent fracture toughness in the case of cylinder coated with FGM, when p is substituted by p_C. Thus the apparent fracture toughness k_{IC}^a of the cylinder having an FGM coating can be defined by

$$K_{IC}^a = F p_c \sqrt{\pi d} \tag{3.3}$$

3.3 Intrinsic Fracture Toughness

The intrinsic fracture toughness of FGMs represents the fracture resistance that an FGM actually possesses. It is related to the effective critical stress acting at the crack tip. Therefore, in determining the intrinsic fracture toughness of FGM coated cylinders, the stress arising from the incompatible eigenstrain will also have to be considered along with the applied critical pressure.

Again, the intrinsic fracture toughness of this type of cylinders can be determined from their effective properties. If a material *A* is dispersed in a matrix material *B* and forms an *A/B* FGM coating of the cylinder, the intrinsic fracture toughness can be determined from the following equation [50].

$$K_C = \frac{E}{E_0} K_C^B \tag{3.4}$$

where K_C^B is the intrinsic fracture toughness of material *B*, E_0 is the Young's modulus of material *B*, and *E* is the effective Young's modulus of *A/B* FGM, which can be obtained by using an appropriate model of mixture rule.

3.4 Effective Properties of FGMs

To calculate the effective properties of FGMs, an appropriate and reliable model of mixture rule is required. In the case of FGMs, conventional mixture rules for composites cannot be used as the microstructure in FGMs varies with the volume fraction of the constituents. Also, a dispersive phase at one side of FGMs transforms to matrix phase on the other side. So, special attention is needed to derive a mixture rule for FGMs. Among various models of mixture rule, the model introduced by Nan *et al.* [51] is adopted in this study to calculate the effective properties of the cylinder with FGM coating, as it appears to be more accurate for the entire range of volume fractions of the constituents. For an FGM whose constituents are *A* and *B*, this mixture rule is given by

$$V_A \frac{\gamma_A - \gamma}{3\gamma_A + 4\mu} + V_B \frac{\gamma_B - \gamma}{3\gamma_B + 4\mu} = 0 \tag{3.5a}$$

$$V_A \frac{\mu_A - \mu}{\mu_A + Y} + V_B \frac{\mu_B - \mu}{\mu_B + Y} = 0 \tag{3.5b}$$

$$\alpha = V_A \alpha_A \frac{\gamma_A (3\gamma + 4\mu)}{\gamma (3\gamma_A + 4\mu)} + V_B \alpha_B \frac{\gamma_B (3\gamma + 4\mu)}{\gamma (3\gamma_B + 4\mu)} \tag{3.5c}$$

$$Y = \frac{\mu(9\gamma + 8\mu)}{(6\gamma + 12\mu)} \tag{3.5d}$$

$$E = \frac{9\gamma\mu}{(3\gamma + \mu)} \tag{3.5e}$$

where *V* is the volume fraction, γ is the bulk modulus, *E* is the Young's modulus and μ is the shear modulus of elasticity, *α* is the coefficient of thermal expansion. The subscripts *A* and *B* denote the respective properties of the constituent materials, and the non-subscripted variables are used to denote the effective properties of the FGM.

CHAPTER 4

THEORETICAL FORMULATION OF THE CRACK PROBLEM

Cylinders with an FGM coating have potential applications because of their outstanding advantages over their counterparts of homogeneous materials. They can withstand adverse condition of temperature, pressure, and environment. However, due to some inherent imperfections introduced during manufacturing, cracks can initiate and ultimately cause failure. Most common is the initiation of edge cracks that may propagate in the material gradient direction under internal pressure

4.1 Modeling of the Problem

In the present study, a model of thick-walled cylinder with an FGM coating at the inner surface is considered. The analytical model of the problem is shown in Fig. 4.1. The Cartesian coordinate system x-y and the polar coordinate system r-θ have the same origin at the center of the cylinder. R_i, R_o and CT denote the inner, outer radii and coating thickness of the cylinder, respectively. The FGM coating is assumed to be composed of two materials A and B, the volume fractions of which are denoted by V_A and V_B, respectively. The homogenous part of the cylinder consists of material B only. The material distribution varies in radial direction only. Therefore, all the material properties are the functions of r only. Due to nonuniform co-efficient of thermal expansion, an incompatible eigenstrain $\varepsilon^*(r)$ [4] is developed in the cylinder when it is cooled from sintering temperature. This incompatible eigenstrain causes an eigenstress [4] which plays an important role to the characterize the fracture behavior of the cylinder. Thus, this incompatible eigenstrain is taken into account and is given by

$$\varepsilon^* = -\alpha\Delta T$$

In the present study, two diametrically-opposed edge cracks emanating from the inner surface of the cylinder are considered. The crack surfaces and the inner surface of the cylinder are assumed to be under uniform applied pressure, p. The problem is treated under plain strain condition.

4.2 Development of the Method of Stress Intensity Factors and Apparent Fracture Toughness

As stated earlier, the nonhomogenous material properties of FGMs complicate the analytical study of fracture characteristics of these materials due to some mathematical difficulties. Therefore, an approximation method developed by Sekine and Afsar [43] is adopted to calculate stress intensity factors for cracks in the thick-walled cylinder with an FGM coating. According to the approximation method, the cylinder with FGM coating is first homogenized by simulating the material nonhomogenities by a distribution of equivalent eigenstrain. The distribution of equivalent eigenstrain is such that the elastic fields in both the uncracked FGM and homogenized cylinders are identical for same loading condition. Then a method is formulated to calculate the stress intensity factor and apparent fracture toughness for the cracks in the homogenized cylinder with the induced thermal and equivalent eigenstrains.

The present study focuses on a thin FGM coating at the inner surface of a thick -walled cylinder for the analysis of AFT and SIF against two diametrically- opposed edge cracks. Taking into account the incompatible eigenstrain and based on the approximation method [43] developed by Sekine and Afsar, an approach of evaluating AFT and SIF is introduced. The effects of material distribution, cylinder wall thickness, application temperature, FGM coating thickness and number of cracks on both AFT and SIF are investigated in details using the developed approach.

4.2.1 Equivalent eigenstrain for homogenization

The cylinder is subjected to an internal pressure p. Thus the effective crack driving force is produced due to the combined effect of internal pressure p and the eigenstress associated with the incompatible eigenstrain. By considering an additional eigenstrain, called equivalent eigenstrain [22], the cylinder with the FGM coating is replaced by a homogenous cylinder of material B only. The distribution of equivalent eigenstrain is such that the elastic fields in both the uncracked cylinder with FGM coating and homogenized cylinders are identical. For homogenization therefore, an alternate approach [43] is adopted here in order to determine the elastic field in the cylinder with FGM coating. According to this approach, the FGM region of the cylinder is radially

15

divided into n number of layers of infinitesimal thicknesses (Fig. 4.2 shows one half of the cylinder). The homogenous outer portion of the cylinder is represented as $(n+1)$th layer, consisting of material B only, in which the properties are constant. Each layer, which is the part of FGM coating, is assumed to have constant volume fractions and material properties but differs from the other FGM layers. The inner and outer radii of the ith layer are, respectively, denoted by r_{i-1} and r_i, where $r_o = R_i$ and $r_{n+1} = R_o$. The pressures at the inner and outer surfaces of the ith layer are, respectively, P_{i-1}^f and P_i^f which are the resultant of pressures due to the applied internal pressure p and the incompatible eigenstrain ε_i^* in the ith layer. Thus the resultant stress field in the ith layer can be readily derived for axisymmetric and plain strain condition given by Bieniek et $al.$ [52]

$$\sigma_{r,f}^i = \frac{c_i^2 P_{i-1}^f}{1-c_i^2}\left[1-\frac{r_i^2}{r^2}\right] - \frac{P_i^f}{1-c_i^2}\left[1-c_i^2\frac{r_i^2}{r^2}\right] \qquad ; R_i \leq r \leq R_{CT} \qquad (4.1a)$$

$$\sigma_{\theta,f}^i = \frac{c_i^2 P_{i-1}^f}{1-c_i^2}\left[1+\frac{r_i^2}{r^2}\right] - \frac{P_i^f}{1-c_i^2}\left[1+c_i^2\frac{r_i^2}{r^2}\right] \qquad ; R_i \leq r \leq R_{CT} \qquad (4.1b)$$

$$\sigma_{z,f}^i = \frac{2\nu_i}{1-c_i^2}(c_i^2 P_{i-1}^f - P_i^f) \qquad ; R_i \leq r \leq R_{CT} \qquad (4.1c)$$

where

$$c_i = \frac{r_{i-1}}{r_i} \qquad (4.2a)$$

$$\sigma_{r,f}^{n+1} = \frac{R_{CT}^2 P_n}{R_o^2 - R_{CT}^2}\left[1-\frac{R_o^2}{r^2}\right] \qquad ; R_{CT} < r \leq R_o \qquad (4.2b)$$

$$P_i^f = p_i^f + p_i^{*f} \qquad (4.2c)$$

The first term at the right hand side of Eq. (4.2c) appears due to the applied internal pressure p while the second term appears due to the incompatible eigenstrain. The strain and the displacement components in the ith layer are obtained as [45]

$$\varepsilon_{r,f}^i = \frac{(1+\nu_i)(1-2\nu_i)}{E_i(1-c_i^2)}\left[(c_i^2 P_{i-1}^f - P_i^f) - \frac{c_i^2}{1-2\nu_i}\frac{r_i^2}{r^2}(P_{i-1}^f - P_i^f)\right] + (1+\nu_i)\varepsilon_i^* \qquad (4.3a)$$

16

$$\varepsilon_{\theta,f}^i = \frac{(1+\nu_i)(1-2\nu_i)}{E_i(1-c_i^2)}\left[(c_i^2 P_{i-1}^f - P_i^f) + \frac{c_i^2}{1-2\nu_i}\frac{r_i^2}{r^2}(P_{i-1}^f - P_i^f)\right] + (1+\nu_i)\varepsilon_i^* \quad (4.3b)$$

$$u_i^f = \frac{(1+\nu_i)(1-2\nu_i)r_i}{E_i(1-c_i^2)}\left[c_i^2 P_{i-1}^f\left\{\frac{r}{r_i} + \frac{1}{1-2\nu_i}\frac{r_i}{r}\right\} - P_i^f\left\{\frac{r}{r_i} + \frac{c_i^2}{1-2\nu_i}\frac{r_i}{r}\right\}\right] + (1+\nu_i)\varepsilon_i^* r \quad (4.4)$$

The unknown pressures P_i^f and P_i^{*f} are determined by solving the following systems of simultaneous linear equations, which are obtained from the condition that $(u_i^f - u_{i+1}^f)$ vanishes at $r = r_i$,

$$\delta_{i,i-1}^f r_{i-1} p_{i-1}^f + \delta_{i,i}^f r_i p_i^f + \delta_{i,i+1}^f r_{i+1} p_{i+1}^f = 0 \; ; i = 1,2,........,n \quad (4.5a)$$

$$\delta_{i,i-1}^f r_{i-1} p_{i-1}^{*,f} + \delta_{i,i}^f r_i p_i^{*,f} + \delta_{i,i+1}^f r_{i+1} p_{i+1}^{*,f} = r_i\left[(1+\nu_{i+1})\varepsilon_{i+1}^* - (1+\nu_i)\varepsilon_i^*\right]; i = 1,2,......,n \quad (4.5b)$$

where

$$\delta_{i,i-1}^f = \frac{2c_i(1-\nu_i^2)}{E_i(1-c_i^2)} \quad (4.6a)$$

$$\delta_{i,i}^f = -\frac{1+\nu_i}{E_i(1-c_i^2)}\left[1+c_i^2-2\nu_i\right] - \frac{1+\nu_{i+1}}{E_{i+1}(1-c_{i+1}^2)}\left[1+c_{i+1}^2-2\nu_{i+1}c_{i+1}^2\right] \quad (4.6b)$$

$$\delta_{i,i+1}^f = \frac{2c_{i+1}(1-\nu_{i+1}^2)}{E_{i+1}(1-c_{i+1}^2)} \quad (4.6c)$$

and

$$p_0^f = p \quad (4.7a)$$

$$p_{n+1}^f = 0 \quad (4.7b)$$

$$p_0^{*,f} = 0 \quad (4.7c)$$

$$p_{n+1}^{*,f} = 0 \quad (4.7d)$$

Now we consider a homogeneous cylinder with the same geometry and determine the elastic field due to the same applied internal pressure p and the same incompatible eigenstrain following the same technique as the layered cylinder. Here it should be noted that the material properties for all the layers are same. The stress field in the ith layer of the layered homogeneous cylinder determined in this way is given by Bieniek et al. [52]

$$\sigma_{r,h_0}^i = \frac{c_i^2 P_{i-1}^h}{1-c_i^2}\left[1-\frac{r_i^2}{r^2}\right] - \frac{P_i^h}{1-c_i^2}\left[1-c_i^2\frac{r_i^2}{r^2}\right] \qquad ; R_i \le r \le R_{CT} \quad (4.8a)$$

$$\sigma^{i}_{\theta, h_0} = \frac{c_i^2 P^h_{i-1}}{1-c_i^2}\left[1+\frac{r_i^2}{r^2}\right] - \frac{P^h_i}{1-c_i^2}\left[1+c_i^2\frac{r_i^2}{r^2}\right] \qquad ; R_i \leq r \leq R_{CT} \qquad (4.8b)$$

$$\sigma^{i}_{z, h_0} = \frac{2v_0}{1-c_i^2}(c_i^2 p^h_{i-1} - p^h_i) \qquad ; R_i \leq r \leq R_{CT} \qquad (4.8c)$$

$$\sigma^{n+1}_{r, h_0} = \frac{R_{CT}^2 P_n}{R_o^2 - R_{CT}^2}\left[1 - \frac{R_o^2}{r^2}\right] \qquad ; R_{CT} < r \leq R_o \qquad (4.8d)$$

where

$$P^h_i = p^h_i + p^{*h}_i \qquad (4.9)$$

As before, the first term at the right hand side of Eq. (4.9) appears due to the applied internal pressure p while the second term appears due to the incompatible eigenstrain. The strain and displacement components are obtained as [45]

$$\varepsilon^{i}_{r, h_0} = \frac{(1+v_0)(1-2v_0)}{E_0(1-c_i^2)}\left[(c_i^2 P^h_{i-1} - P^h_i) - \frac{c_i^2}{1-2v_0}\frac{r_i^2}{r^2}(P^h_{i-1} - P^h_i)\right]$$
$$+ (1+v_0)\varepsilon^{*}_i \qquad (4.10a)$$

$$\varepsilon^{i}_{\theta, h_0} = \frac{(1+v_0)(1-2v_0)}{E_0(1-c_i^2)}\left[(c_i^2 P^h_{i-1} - P^h_i) + \frac{c_i^2}{1-2v_0}\frac{r_i^2}{r^2}(P^h_{i-1} - P^h_i)\right]$$
$$+ (1+v_0)\varepsilon^{*}_i \qquad (4.10b)$$

$$u^{h_0}_i = \frac{(1+v_0)(1-2v_0)r_i}{E_0(1-c_i^2)}\left[c_i^2 P^h_{i-1}\left\{\frac{r}{r_i} + \frac{1}{1-2v_0}\frac{r_i}{r}\right\} - P^h_i\left\{\frac{r}{r_i} + \frac{c_i^2}{1-2v_0}\frac{r_i}{r}\right\}\right]$$
$$+ (1+v_0)\varepsilon^{*}_i r \qquad (4.11)$$

The unknown pressures P^h_i and P^{*h}_i are determined by solving the following systems of simultaneous linear equations, which are obtained from the condition of $(u^{h_0}_i - u^{h_0}_{i+1}) = 0$ at $r = r_i$

$$\delta^{h}_{i,i-1} r_{i-1} p^h_{i-1} + \delta^{h}_{i,i} r_i p^h_i + \delta^{h}_{i,i+1} r_{i+1} p^h_{i+1} = 0 \quad ; \quad i = 1,2,.......,n \qquad (4.12a)$$

$$\delta^{h}_{i,i-1} r_{i-1} p^{*,h}_{i-1} + \delta^{h}_{i,i} r_i p^{*,h}_i + \delta^{h}_{i,i+1} r_{i+1} p^{*,h}_{i+1} = (1+v_0)(\varepsilon^{*}_{i+1} - \varepsilon^{*}_i)r_i \quad ; \quad i = 1,2,.......,n \qquad (4.12b)$$

where

$$\delta^{h}_{i,i-1} = \frac{2c_i(1-v_0^2)}{E_0(1-c_i^2)} \qquad (4.13a)$$

18

$$\delta_{i,i}^h = -\frac{1+\nu_0}{E_0}\left[\frac{1}{1-c_i^2}(1+c_i^2-2\nu_0)-\frac{1}{1-c_{i+1}^2}(1+c_{i+1}^2-2\nu_0 c_{i+1}^2)\right] \tag{4.13b}$$

$$\delta_{i,i+1}^h = \frac{2c_{i+1}(1-\nu_0^2)}{E_0(1-c_{i+1}^2)} \tag{4.13c}$$

and

$$p_0^h = p \tag{4.14a}$$

$$p_{n+1}^h = 0 \tag{4.14b}$$

$$p_0^{*,h} = 0 \tag{4.14c}$$

$$p_{n+1}^{*,h} = 0 \tag{4.14d}$$

Now we consider a distribution of equivalent eigenstrain $\varepsilon_{j,e}^i$ in the ith layer of the homogeneous cylinder, where $j = r$, θ and z. This equivalent eigenstrain induces an elastic field in the homogeneous cylinder. Superposition of this elastic field with that given by Eqs. (4.8) and (4.10) yields equivalence between the elastic fields in the FGM and the homogeneous cylinders. From the equivalence of the stress fields, we can write

$$\sigma_{r,f}^i = \sigma_{r,h_0}^i + \sigma_{r,e}^i \tag{4.15a}$$

$$\sigma_{\theta,f}^i = \sigma_{\theta,h_0}^i + \sigma_{\theta,e}^i \tag{4.15b}$$

$$\sigma_{z,f}^i = \sigma_{z,h_0}^i + \sigma_{z,e}^i \tag{4.15c}$$

where

$\sigma_{j,e}^i$ is the stress component in the ith layer of the homogeneous cylinder due to the equivalent eigenstrain $\varepsilon_{j,e}^i$

From the equivalence of the total strains, we obtain

$$\varepsilon_{r,f}^i = \varepsilon_{r,h_0}^i + e_{r,e}^i + \varepsilon_{r,e}^i \tag{4.16a}$$

$$\varepsilon_{\theta,f}^i = \varepsilon_{\theta,h_0}^i + e_{\theta,e}^i + \varepsilon_{\theta,e}^i \tag{4.16b}$$

$$\varepsilon_{z,f}^i = \varepsilon_{z,h_0}^i + e_{z,e}^i + \varepsilon_{z,e}^i \tag{4.16c}$$

where

$e_{j,e}^{i}$ is the component of the elastic strain in the ith layer of the homogeneous cylinder associated with the equivalent eigenstrain $\varepsilon_{j,e}^{i}$

The elastic strain $e_{j,e}^{i}$ is related to the stress $\sigma_{j,e}^{i}$ by Hooke's law as follows

$$e_{r,e}^{i} = \frac{1}{E_0}\left[\sigma_{r,e}^{i} - \nu_0\sigma_{\theta,e}^{i} - \nu_0\sigma_{z,e}^{i}\right] \tag{4.17a}$$

$$e_{\theta,e}^{i} = \frac{1}{E_0}\left[\sigma_{\theta,e}^{i} - \nu_0\sigma_{r,e}^{i} - \nu_0\sigma_{z,e}^{i}\right] \tag{4.17b}$$

$$e_{z,e}^{i} = \frac{1}{E_0}\left[\sigma_{z,e}^{i} - \nu_0\sigma_{r,e}^{i} - \nu_0\sigma_{\theta,e}^{i}\right] \tag{4.17c}$$

By setting the strain components $\varepsilon_{z,f}^{i}$ and ε_{z,h_0}^{i} to zero for plane strain and making use of Eqs. (4.1), (4.3), (4.8), (4.10) and (4.15)-(4.17) the expression for the equivalent eigenstrain in the ith layer of the homogeneous cylinder can be derived as [45]

$$
\begin{aligned}
\varepsilon_{r,e}^{i} = & \frac{(1+\nu_i)(1-2\nu_i)}{E_i(1-c_i^2)}\left[(c_i^2 P_{i-1}^f - P_i^f) - \frac{c_i^2}{1-2\nu_i}\frac{r_i^2}{r^2}(P_{i-1}^f - P_i^f)\right] \\
& - \frac{(1+\nu_0)(1-2\nu_0)}{E_0(1-c_i^2)}\left[(c_i^2 P_{i-1}^h - P_i^h) - \frac{c_i^2}{1-2\nu_0}\frac{r_i^2}{r^2}(P_{i-1}^h - P_i^h)\right] \\
& + \frac{1}{E_0(1-c_i^2)}\left[c_i^2\left(1-\frac{r_i^2}{r^2}\right)(P_{i-1}^h - P_{i-1}^f) - \left(1-c_i^2\frac{r_i^2}{r^2}\right)(P_i^h - P_i^f)\right] \\
& - \frac{\nu_0}{E_0(1-c_i^2)}\left[c_i^2\left(1+\frac{r_i^2}{r^2}\right)(P_{i-1}^h - P_{i-1}^f) - \left(1+c_i^2\frac{r_i^2}{r^2}\right)(P_i^h - P_i^f)\right] \\
& - \frac{2\nu_0}{E_0(1-c_i^2)}\left[\nu_0(c_i^2 P_{i-1}^h - P_i^h) - \nu_i(c_i^2 P_{i-1}^f - P_i^f)\right] + \frac{\varepsilon_i^*}{E_0}(E_0\nu_i - E_i\nu_0)
\end{aligned}
\tag{4.18a}
$$

$$\varepsilon^i_{\theta,e} = \frac{(1+\nu_i)(1-2\nu_i)}{E_i(1-c_i^2)}\left[(c_i^2 P^f_{i-1} - P^f_i) + \frac{c_i^2}{1-2\nu_i}\frac{r_i^2}{r^2}(P^f_{i-1} - P^f_i)\right]$$

$$-\frac{(1+\nu_0)(1-2\nu_0)}{E_0(1-c_i^2)}\left[(c_i^2 P^h_{i-1} - P^h_i) + \frac{c_i^2}{1-2\nu_0}\frac{r_i^2}{r^2}(P^h_{i-1} - P^h_i)\right]$$

$$+\frac{1}{E_0(1-c_i^2)}\left[c_i^2\left(1+\frac{r_i^2}{r^2}\right)(P^h_{i-1} - P^f_{i-1}) - \left(1+c_i^2\frac{r_i^2}{r^2}\right)(P^h_i - P^f_i)\right]$$

$$-\frac{\nu_0}{E_0(1-c_i^2)}\left[c_i^2\left(1-\frac{r_i^2}{r^2}\right)(P^h_{i-1} - P^f_{i-1}) - \left(1-c_i^2\frac{r_i^2}{r^2}\right)(P^h_i - P^f_i)\right]$$

$$-\frac{2\nu_0}{E_0(1-c_i^2)}\left[\nu_0(c_i^2 P^h_{i-1} - P^h_i) - \nu_i(c_i^2 P^f_{i-1} - P^f_i)\right] + \frac{\varepsilon^*_i}{E_0}(E_0\nu_i - E_i\nu_0) \qquad (4.18b)$$

$$\varepsilon^i_{z,e} = \frac{2}{E_0(1-c_i^2)}\left[\nu_0(c_i^2 P^h_{i-1} - P^h_i) - \nu_i(c_i^2 P^f_{i-1} - P^f_i)\right]$$

$$-\frac{2\nu_0}{E_0(1-c_i^2)}\left[c_i^2(P^h_{i-1} - P^f_{i-1}) - (P^h_i - P^f_i)\right] + \frac{\varepsilon^*_i}{E_0}(E_i - E_0) \qquad (4.18c)$$

For the next of the analysis, the cylinder with FGM coating can be replaced by the homogeneous cylinder (referred to as homogenized cylinder) of the same geometry if the equivalent eigenstrain of Eq. (4.18) is considered along with the other loadings. The equivalent eigenstrain derived above and the incompatible eigenstrain ε^*_i are piecewise continuous. The distributions of the equivalent and the incompatible eigenstrains continuous for the entire wall thickness of the non-layered homogenized cylinder as shown in Fig. 4.3 can be obtained by spline interpolation of the piecewise continuous eigenstrains. The resultant stress field in this non-layered homogenized cylinder is then derived as [45]

$$\sigma^h_r = \frac{R_i^2 p}{R_o^2 - R_i^2}\left[1 - \frac{R_o^2}{r^2}\right] + \frac{E_0}{1-\nu_0}\left[-\frac{1}{r^2}\int_{R_i}^{r} r\varepsilon^* dr + \left(1 - \frac{R_i^2}{r^2}\right)\frac{1}{R_o^2 - R_i^2}\int_{R_i}^{R_o} r\varepsilon^* dr\right]$$

$$+\frac{E_0}{2(1-\nu_0^2)}\left[-\frac{1}{r^2}\int_{R_i}^{r} r(\varepsilon^e_r + \varepsilon^e_\theta + 2\nu_0\varepsilon^e_z)dr + \int_{R_i}^{r}\frac{1}{r}(\varepsilon^e_r - \varepsilon^e_\theta)dr + C\left\{1 - \frac{R_i^2}{r^2}\right\}\right] \qquad (4.19a)$$

$$\sigma_\theta^h = \frac{R_i^2 p}{R_o^2 - R_i^2}\left[1 + \frac{R_o^2}{r^2}\right] + \frac{E_0}{1-\nu_0}\left[-\varepsilon^* + \frac{1}{r^2}\int_{R_i}^{r} r\varepsilon^* dr + \left(1 + \frac{R_i^2}{r^2}\right)\frac{1}{R_o^2 - R_i^2}\int_{R_i}^{R_o} r\varepsilon^* dr\right]$$

$$+ \frac{E_0}{2(1-\nu_0^2)}\left[-2(\varepsilon_\theta^e + \nu_0\varepsilon_z^e) + \frac{1}{r^2}\int_{R_i}^{r} r(\varepsilon_r^e + \varepsilon_\theta^e + 2\nu_0\varepsilon_z^e)dr + \int_{R_i}^{r}\frac{1}{r}(\varepsilon_r^e - \varepsilon_\theta^e)dr\right.$$

$$\left. + C\left\{1 + \frac{R_i^2}{r^2}\right\}\right] \tag{4.19b}$$

$$\sigma_z^h = \frac{2\nu_0 R_i^2 p}{R_o^2 - R_i^2} + \frac{E_0\nu_0}{1-\nu_0}\left\{-\varepsilon^* + \frac{2}{R_o^2 - R_i^2}\int_{R_i}^{R_o} r\varepsilon^* dr\right\}$$

$$+ \frac{\nu_0 E_0}{(1-\nu_0^2)}\left[-(\varepsilon_\theta^e + \nu_0\varepsilon_z^e) + \int_{R_i}^{r}\frac{1}{r}(\varepsilon_r^e - \varepsilon_\theta^e)dr + C\right] - E_0(\varepsilon^* + \varepsilon_z^e) \tag{4.19c}$$

where

$$C = \frac{1}{R_o^2 - R_i^2}\left\{\int_{R_i}^{R_o} r(\varepsilon_r^e + \varepsilon_\theta^e + 2\nu_0\varepsilon_z^e)dr - R_o^2\int_{R_i}^{R_o}\frac{1}{r}(\varepsilon_r^e - \varepsilon_\theta^e)dr\right\} \tag{4.20}$$

and ε^* and ε_j^e are the incompatible and equivalent eigenstrains, respectively, which are continuous throughout the wall thickness of the cylinder. When cylinder's FGM coating is air-cooled from the sintering temperature to the room temperature, the incompatible eigenstrain is given by,

$$\varepsilon^* = -\alpha\Delta T \tag{4.21}$$

The other two stress components are not shown as they are not relevant in the calculation of mode I stress intensity factor.

4.2.2 Stress intensity factor

Now, two diametrically-opposed edge cracks of equal length l each emanating from the inner surface of the homogenized cylinder with distributed incompatible and equivalent eigenstrains are considered as shown in Fig. 4.4. The crack surfaces and the inner surface of the cylinder are subjected to the internal pressure p. The boundary condition given by Eq. (3.1) reduces to

$$\sigma_\theta^d = -\sigma_\theta^h - p \,;\, R_i \leq r \leq R_i + l,\, \theta = 0^o \tag{4.22}$$

The stress component σ_θ^h in the uncracked homogenized cylinder has been determined in the previous article. The disturbed stress component σ_θ^d can be determined by

representing the cracks by a continuous distribution of edge dislocations. The potential functions for a discrete edge dislocation making an angle β with the positive x-axis and passing through a point at $z=h$ of a cylinder as shown in Fig. 4.5 are given by Muskhelishvili [53]

$$\Phi(z) = \frac{\mu_0}{\pi(\kappa_0+1)}\left[\frac{(ib_1-b_2)}{(z-h)}e^{i\beta} + a_0 + \sum_{k=1}^{\infty}(a_k z^k + a_{-k}z^{-k}) - \frac{2z}{R_o^2+R_i^2}(ib_1+b_2)e^{-i\beta}\right.$$

$$\left. -\frac{(ib_1-b_2)e^{i\beta}}{z}\right] \tag{4.23a}$$

$$\Psi(z) = \frac{\mu_0}{\pi(\kappa_0+1)}\left[-\frac{(ib_1+b_2)e^{-i\beta}}{z-h} + \frac{(ib_1-b_2)e^{i\beta}}{(z-h)^2}\bar{h} + \sum_{k=1}^{\infty}(a'_k z^k + a'_{-k}z^{-k}) + a'_0\right.$$

$$\left. +\frac{i(b_1-ib_2)e^{-i\beta}}{z} - \frac{2i(b_1+ib_2)e^{i\beta}}{z^3}\cdot\frac{R_o^2 R_i^2}{R_o^2+R_i^2}\right] \tag{4.23b}$$

where b_1 and b_2 are the components of Burgers vector, μ_o is the shear modulus of rigidity, κ_0 is the Kolosov's constant ($3-4\nu_o$ for plane strain; $(3-\nu_o)/(1+\nu_o)$ for plane stress) and $z=x+iy = re^{i\theta}$

and

$$a_0 = \frac{B_0}{2(R_o^2-R_i^2)} \tag{4.24a}$$

$$a_1 = \frac{\bar{B}_{-1}}{(R_o^4-R_i^4)} - \frac{2A'_1 R_i}{(\kappa_0+1)(R_o^2+R_i^2)} \tag{4.24b}$$

$$a_{-1} = \frac{\bar{A}'_1 R_i}{(\kappa_0+1)} \tag{4.24c}$$

$$a_k = \frac{\Delta K_1}{\Delta K}; \quad k \geq 2 \tag{4.24d}$$

$$a_{-k} = \frac{\Delta K_2}{\Delta K}; \quad k \geq 2 \tag{4.24e}$$

$$\Delta K_1 = R_0^2(1+k)(1-\xi^2)\xi^{2(k-1)}B_k + \left\{1-\xi^{2(k-1)}\right\}\frac{\bar{B}_{-k}}{R_o^{2(k-1)}} \tag{4.24f}$$

$$\Delta K_2 = R_0^2(1-k)(1-\xi^2)\xi^{2(k-1)}B_{-k} + R_i^{2(k+1)}\left\{\xi^{2(k-1)}-\xi^{-4}\right\}\bar{B}_k \tag{4.24g}$$

$$\Delta K = R_o^4\left[(1-k^2)(1-\xi^2)^2\xi^{2(k-1)} - \xi^{2(k-1)} + \xi^{2(k+1)} + \xi^{4k} + 1\right] \tag{4.24h}$$

$$\xi = R_i/R_o \tag{4.24i}$$

$$B_k = A''_k R_0^{-k+2} - A'_k R_i^{-k+2} \tag{4.24j}$$

$$\bar{B}_{-k} = \bar{A}''_{-k} R_o^{k+2} - \bar{A}'_{-k} R_i^{k+2} \qquad (4.24\text{k})$$

$$a'_{-1} = -\frac{\kappa_0 A'_1 R_i}{(\kappa_0 + 1)} \qquad (4.24\text{l})$$

$$a'_{-2} = \frac{(A''_0 - A'_0) R_o^2 R_i^2}{(R_o^2 - R_i^2)} \qquad (4.24\text{m})$$

$$a'_{-3} = \frac{R_o^2 R_i^3}{R_o^2 + R_i^2} \left[\frac{2\bar{A}'_1}{\kappa_0 + 1} + \frac{R_o(A''_{-1} R_i - A'_{-1} R_o)}{R_o^2 - R_i^2} \right] \qquad (4.24\text{n})$$

$$a'_k = -(1+k) R_o^2 a_{k+2} + \bar{a}_{-(k+2)} R_o^{-2(k+1)} - R_o^{-k} A''_{k+2} ; \quad k \geq 0 \qquad (4.24\text{o})$$

$$a'_{-k} = -(1-k) R_i^2 a_{-(k+2)} + \bar{a}_{k-2} R_i^{2(k-1)} - R_i^k A''_{-(k-2)}; \quad k \geq 4 \qquad (4.24\text{p})$$

The coefficients A'_k and A''_k are given in Table 4.1.

In the present study, there are two diametrically-opposed edge cracks, crack I and crack II, emanating from the inner surface. First, crack I is considered and the disturbed stress component for this crack is determined. For this crack, the discrete edge dislocation at $h = R_i + s$ is shown in Fig. 4.6. For this configuration of the dislocation, $\beta = -90^0$ so $e^{i\beta} = \cos 90^0 - i \sin 90^0 = -i$

Also, for the orientation shown, the crack tip experiences mode I deformation only. So, $b_2 = 0$. Thus the potential functions of Eqs. (4.23a) and (4.23b) reduce to

$$\Phi(z) = \frac{\mu_0 b_1}{\pi(\kappa_0 + 1)} \left[\frac{1}{(z-h)} + a_0 + \sum_{k=1}^{\infty} (a_k z^k + a_{-k} z^{-k}) + \frac{2z}{R_o^2 + R_i^2} - \frac{1}{z} \right] \qquad (4.25\text{a})$$

$$\Psi(z) = \frac{\mu_0 b_1}{\pi(\kappa_0 + 1)} \left[\frac{1}{z-h} + \frac{1}{(z-h)^2} \bar{h} + \sum_{k=1}^{\infty} (a'_k z^k + a'_{-k} z^{-k}) + a'_0 - \frac{1}{z} - \frac{2}{z^3} \cdot \frac{R_o^2 R_i^2}{R_o^2 + R_i^2} \right] \qquad (4.25\text{b})$$

The coefficients A'_K and A''_K are rearranged in Table 4.2.

If the crack is represented by a continuous distribution of edge dislocation, the potential functions are rewritten as [45]

$$\Phi(z) = \frac{\mu_0}{\pi(\kappa_0 + 1)} \int_0^l \left[\frac{1}{(z-h)} + a_0 + \sum_{k=1}^{\infty} (a_k z^k + a_{-k} z^{-k}) + \frac{2z}{R_o^2 + R_i^2} - \frac{1}{z} \right]_1 b_1(s)\,ds \qquad (4.26\text{a})$$

$$\Psi(z) = \frac{\mu_0}{\pi(\kappa_0 + 1)} \int_0^l \left[\frac{1}{z-h} + \frac{1}{(z-h)^2} \bar{h} + \sum_{k=1}^{\infty} (a'_k z^k + a'_{-k} z^{-k}) + a'_0 - \frac{1}{z} - \frac{2}{z^3} \cdot \frac{R_o^2 R_i^2}{R_o^2 + R_i^2} \right] b_1(s)\,ds \qquad (4.26\text{b})$$

where $b_1(s)$ is the dislocation density function.

24

The stresses can be expressed in terms of the complex potentials $\Phi(z)$ and $\Psi(z)$ and their complex conjugates as below [53]

$$\left[\sigma_\theta^d + i\sigma_{r\theta}^d\right]_{\mathrm{I}} = \Phi(z) + \overline{\Phi}(z) + [\bar{z}\Phi'(z) + \Psi(z)]e^{2i\theta} \tag{4.27}$$

where the over bar and the prime represent conjugate and differentiation with respect to z, respectively. Thus,

$$\Phi'(z) = \frac{\mu_0}{\pi(\kappa_0+1)}\int_0^l \left[-\frac{1}{(z-h)^2} + \sum_{k=1}^\infty (ka_k z^{k-1} - ka_{-k} z^{-k-1}) + \frac{2}{R_o^2+R_i^2} + \frac{1}{z^2}\right]b_1(s)\,ds$$

(4.28a)

$$\overline{\Phi(z)} = \frac{\mu_0}{\pi(\kappa_0+1)}\int_0^l \left[\frac{1}{(\bar{z}-\bar{h})} + \bar{a}_0 + \sum_{k=1}^\infty (\bar{a}_k \bar{z}^{-k} + \bar{a}_{-k}\bar{z}^{-k}) + \frac{2\bar{z}}{R_o^2+R_i^2} - \frac{1}{\bar{z}}\right]b_1(s)\,ds \tag{4.28b}$$

For the stresses along the crack line of crack I, $\theta = 0°$ and $z = \bar{z} = r$. Also, $\bar{b}_1 = b_1$ and for horizontal orientation of cracks $h = \bar{h} = R_i + s$ and $a_k = \overline{a_k}$

Combination of Eqs. (4.26) through (4.28) along with the above substitutions yields the stress field along the crack line as

$$\begin{aligned}
\left[\sigma_\theta^d + i\sigma_{r\theta}^d\right]_{\mathrm{I}} = \frac{\mu_0}{\pi(\kappa_0+1)}\int_0^l &\left[\frac{2}{r-h} + 2a_0 + \frac{6r}{R_o^2+R_i^2} - \frac{2}{r} + 3a_1 r \right.\\
&+ a'_{-2}r^{-2} + a'_{-3}r^{-3} + 2\sum_{k=2}^\infty a_k r^k + 2\sum_{k=2}^\infty a_{-k}r^{-k} + \sum_{k=2}^\infty ka_k r^k \\
&\left. - \sum_{k=2}^\infty ka_{-k}r^{-k} + \sum_{k=0}^\infty a'_k r^k + \sum_{k=4}^\infty a'_{-k}r^{-k} - \frac{2}{r^3}\cdot\frac{R_o^2 R_i^2}{R_o^2+R_i^2}\right]b_1(s)\,ds
\end{aligned} \tag{4.29}$$

Now, for brevity, one can define the following functions

$$f_1(h) = a_0 = \frac{B_0}{2(R_o^2-R_i^2)} = \frac{1}{2(R_o^2-R_i^2)}\left[A_0'' R_o^2 - A_0' R_i^2\right] = \frac{(h^2-R_i^2)}{h(R_o^2-R_i^2)} \tag{4.30a}$$

$$f_2(r,h) = a_1 r \frac{1}{R_o^4-R_i^4}\left[3h^2 - 2R_o^2 - \frac{R_i^4}{h^2}\right]r \tag{4.30b}$$

$$f_3(r,h) = a'_{-2}\frac{1}{r^2} = \frac{2R_i^2}{(R_o^2-R_i^2)}\left[\frac{h^2-R_0^2}{h}\right]\cdot\frac{1}{r^2} \tag{4.30c}$$

$$f_4(r,h) = a'_{-3} \frac{1}{r^3} = \frac{R_i^3 R_o^3}{(R_o^4 - R_i^4)} \left[\frac{R_i}{R_o^3} (3h^2 - 2R_o^2) - \frac{R_o R_i}{h^2} \right] \cdot \frac{1}{r^3} \qquad (4.30d)$$

$$f_5(r,h) = \sum_{k=2}^{\infty} a_k r^k \qquad (4.30e)$$

$$f_6(r,h) = \sum_{k=2}^{\infty} a_{-k} r^{-k} \qquad (4.30f)$$

$$f_7(r,h) = \sum_{k=2}^{\infty} k a_k r^k \qquad (4.30g)$$

$$f_8(r,h) = \sum_{k=2}^{\infty} k a_{-k} r^{-k} \qquad (4.30h)$$

$$f_9(r,h) = \sum_{k=0}^{\infty} a'_k r^k \qquad (4.30i)$$

$$f_{10}(r,h) = \sum_{k=4}^{\infty} a'_{-k} r^{-k} \qquad (4.30j)$$

Finally, for crack I, the stresses along the crack line can be given by

$$\left[\sigma_\theta^d + i\sigma_{r\theta}^d \right]_I = \frac{2\mu_0}{\pi(\kappa_0 + 1)} \int_0^l \left[\frac{1}{r-h} + \frac{3r}{R_o^2 + R_i^2} - \frac{1}{r} - \frac{1}{r^3} \cdot \frac{R_o^2 R_i^2}{R_o^2 + R_i^2} + f_1(h) \right.$$

$$+ \frac{3}{2} f_2(r,h) + \frac{1}{2} f_3(r,h) + \frac{1}{2} f_4(r,h) + f_5(r,h) + f_6(r,h)$$

$$\left. + \frac{1}{2} f_7(r,h) - \frac{1}{2} f_8(r,h) + \frac{1}{2} f_9(r,h) + \frac{1}{2} f_{10}(r,h) \right] b_1(s) ds . \qquad (4.31)$$

Now, crack II is considered and the discrete edge dislocation for this crack is shown in Fig. 4.6. For the configuration of the dislocation shown, $\beta = +90^0$

So, $e^{i\beta} = \cos 90^0 + i \sin 90^0 = +i$

This crack is also represented by a continuous distribution of edge dislocations. Following the similar procedure as crack I, the stresses along the crack line of crack I due to crack II is determined by setting $\theta = -180^0$ and considering b_1 as negative in Eq. (4.23). Finally, one obtains

$$\left[\sigma_\theta^d + i\sigma_{r\theta}^d\right]_{\mathrm{II}} = \frac{2\mu_0}{\pi(\kappa_0+1)}\int_0^l \left[-\frac{1}{r+h} - \frac{3r}{R_o^2+R_i^2} + \frac{1}{r} + \frac{1}{r^3}\cdot\frac{R_o^2 R_i^2}{R_o^2+R_i^2} + f_{1d}(h) \right.$$

$$+\frac{3}{2}f_{2d}(r,h) + \frac{1}{2}f_{3d}(r,h) + \frac{1}{2}f_{4d}(r,h) + f_{5d}(r,h) + f_{6d}(r,h)$$

$$\left. +\frac{1}{2}f_{7d}(r,h) - \frac{1}{2}f_{8d}(r,h) + \frac{1}{2}f_{9d}(r,h) + \frac{1}{2}f_{10d}(r,h) \right] b_1(s)ds \qquad (4.32)$$

where

$$f_{1d}(h) = \frac{(h^2 - R_i^2)}{h(R_o^2 - R_i^2)} \qquad (4.33\text{a})$$

$$f_{2d}(r,h) = -\frac{1}{R_o^4 - R_i^4}\left[3h^2 - 2R_o^2 - \frac{R_i^4}{h^2}\right]r \qquad (4.33\text{b})$$

$$f_{3d}(r,h) = \frac{2R_i^2}{(R_o^2 - R_i^2)}\left[\frac{h^2 - R_0^2}{h}\right]\cdot\frac{1}{r^2} \qquad (4.33\text{c})$$

$$f_{4d}(r,h) = -\frac{R_i^3 R_o^3}{(R_o^4 - R_i^4)}\left[\frac{R_i}{R_o^3}(3h^2 - 2R_o^2) - \frac{R_o R_i}{h^2}\right]\cdot\frac{1}{r^3} \qquad (4.33\text{d})$$

$$f_{5d}(r,h) = \sum_{k=2}^{\infty} a_k(-r)^k \qquad (4.33\text{e})$$

$$f_{6d}(r,h) = \sum_{k=2}^{\infty} a_{-k}(-r)^{-k} \qquad (4.33\text{f})$$

$$f_{7d}(r,h) = \sum_{k=2}^{\infty} ka_k(-r)^k \qquad (4.33\text{g})$$

$$f_{8d}(r,h) = \sum_{k=2}^{\infty} ka_{-k}(-r)^{-k} \qquad (4.33\text{h})$$

$$f_{9d}(r,h) = \sum_{k=0}^{\infty} a_k'(-r)^k \qquad (4.33\text{i})$$

$$f_{10d}(r,h) = \sum_{k=4}^{\infty} a_{-k}'(-r)^{-k} \qquad (4.33\text{j})$$

Now, superposition of Eqs. (4.31) and (4.32) gives the resultant circumferential stress component of the disturbed stress field along the crack line of crack I as:

27

$$\sigma_\theta{}^d = \frac{2\mu_0}{\pi(\kappa_0+1)} \int_0^l \left[\frac{1}{r-h} + g_1(r,h) + g_2(r,h) \right] b_1(s)ds \qquad (4.34)$$

where $g_1(r,h) = \left[f_1(h) + \frac{3}{2} f_2(r,h) + \frac{1}{2} f_3(r,h) + \frac{1}{2} f_4(r,h) + f_5(r,h) + f_6(r,h) \right.$

$$\left. + \frac{1}{2} f_7(r,h) - \frac{1}{2} f_8(r,h) + \frac{1}{2} f_9(r,h) + \frac{1}{2} f_{10}(r,h) \right] \qquad (4.35a)$$

$$g_2(r,h) = \left[-\frac{1}{r+h} + f_{1d}(h) + \frac{3}{2} f_{2d}(r,h) + \frac{1}{2} f_{3d}(r,h) + \frac{1}{2} f_{4d}(r,h) + f_{5d}(r,h) \right.$$

$$\left. + f_{6d}(r,h) + \frac{1}{2} f_{7d}(r,h) - \frac{1}{2} f_{8d}(r,h) + \frac{1}{2} f_{9d}(r,h) + \frac{1}{2} f_{10d}(r,h) \right] \qquad (4.35b)$$

The boundary condition along the crack line of crack I given by Eq. (4.22) reduce to

$$\frac{2\mu_0}{\pi(\kappa_0+1)} \int_0^l \left[\frac{1}{r-h} + g_1(r,h) + g_2(r,h) \right] b_1(s)ds = -p \left[S_f \frac{\sigma_\theta^h}{\sigma_u} + 1 \right]; R_i \le r \le R_i + l, \theta = 0^o \qquad (4.36)$$

where, S_f is the strength factor defined by the ratio of the ultimate strength σ_u of the base material B to the applied internal pressure p. Equation (4.36) is the singular integral equation for two diametrically-opposed edge cracks in a homogenized cylinder. The stress intensity factors determined by using this equation represent the approximate values of stress intensity factors for the thick-walled cylinder with FGM coating of the same geometry.

4.2.2.1 Normalization and solution of the integral equation

The close form solution of the singular integral equation given by Eq. (4.36) is not possible. Therefore, a numerical method is adopted for its solution. In order to obtain the numerical solution of Eq. (4.36), it is first necessary to normalize the equation over the interval [-1, +1]. This is performed by following substitutions,

$$r = R_i + t \qquad h = R_i + s \qquad (4.37a)$$

$$H = \frac{2t}{l} - 1 \qquad (4.37b)$$

$$T = \frac{2s}{l} - 1 \qquad (4.37c)$$

$$W = \frac{2R_o}{l} \tag{4.37d}$$

Substitution of Eq. (4.37) into Eq. (4.36) yields

$$\frac{2\mu_0}{\pi(\kappa_0+1)} \int_{-1}^{1} \left[\frac{B(T)}{H-T} dT + G_1(H,T)B(T)dT + G_2(H,T)B(T)dT \right]$$

$$= -p\left[S_f \frac{\sigma_\theta^h(H)}{\sigma_u} + 1 \right] ; -1 \le H \le 1 \tag{4.38}$$

where

$$B(T) = b_1\left(\frac{l}{2}T \right) \tag{4.39a}$$

$$G_1(H,T) = g_1\left(\frac{l}{2}H, \frac{l}{2}T \right) \tag{4.39b}$$

$$. \; G_2(H,T) = g_2\left(\frac{l}{2}H, \frac{l}{2}T \right) \tag{4.39c}$$

The density function $B(T)$ can be expressed as the product of a fundamental function $w(T)$ which characterizes the bounded-singular behavior of $B(T)$ and a bounded continuous function $\varphi(T)$ in the closed interval $-1 \le T \le +1$. Thus we can formulate as [55]

$$B(T) = w(T)\varphi(T) \tag{4.40}$$

In the present case, the fundamental function is given by

$$w(T) = \sqrt{\frac{1+T}{1-T}} \tag{4.41}$$

Using the Gauss-Jacobi integral formula corresponding to the weight function in Eq. (4.41) in the manner developed by Erdogan *et al*. [55], Eq. (4.38) is converted to a system of linear algebraic equations to determine the unknowns $\varphi(T_j)$ as follows

$$\frac{2\mu_0}{(\kappa_0+1)} \left[\sum_{j=1}^{N} \varphi(T_j)(1+T_j)\left\{ \frac{1}{H_i-T_j} + G_1(H_i,T_j) + G_2(H_i,T_j) \right\} \right]$$

$$= -\frac{2N+1}{2} p\left[S_f \frac{\sigma_\theta^h(H_i)}{\sigma_u} + 1 \right] \tag{4.42}$$

Here, the collocation and integration points are given by

$$H_i = \cos\left(\frac{2i\pi}{2N+1} \right), \; i = 1,2,3,......,N \tag{4.43a}$$

29

$$T_j = \cos\left(\frac{2j-1}{2N+1}\pi\right), \quad j = 1,2,3,......,N \tag{4.43b}$$

The solution of Eq. (4.42) gives the discrete values of where $\varphi(T_j)$ behind the crack tip. However, the determination of stress intensity factor requires the value of $\varphi(T_j)$ at the crack tip which is determined using the values of $\varphi(T_j)$ behind the crack tip in Krenk's interpolation formula [56] given by

$$\varphi(+1) = \frac{2}{2N+1}\sum_{j=1}^{N}\frac{\sin\left(\frac{2j-1}{2N+1}N\pi\right)}{\tan\left(\frac{2j-1}{2N+1}\frac{\pi}{2}\right)}\varphi(T_j) \tag{4.44}$$

Now the stress intensity factor [54]

$$K_I = \sqrt{\pi l}\,\frac{2\mu_0}{(\kappa_0+1)}\sqrt{2}\varphi(+1) \tag{4.45}$$

4.2.3 Approach of evaluating apparent fracture toughness

In this article, an approach is introduced to evaluate AFT using the formulations of SIFs discussed in the articles 4.2.1and 4.2.2. Equations (4.42) to (4.45) determine the SIF due to combined effect of the eigenstrain and applied internal pressure. Therefore, the critical value of SIF at the crack tip determined from Eqs (4.42) to (4.45) must be equal to the intrinsic fracture toughness, determined form the Eq (3.4) of the point of crack tip position. It is noted that the right hand side of Eq. (4.42) is the function of eigenstrains and applied internal pressure. The eigenstrain, on the otherhand, is a function of material distribution in the cylinder. Therefore, for a prescribed material distribution and crack length, this equation can be solved in terms of unknown internal pressure p in the form of

$$K_I = k_e + k_p p \tag{4.46}$$

Where k_e is the SIF associated with the eigenstrain and k_p is the factor associated with the coefficient of p in Eq. (4.42). Then, Eqs. (3.4) and (4.46) are equated to determine the critical value of internal pressure P_C corresponding to given crack length. Note that the right hand side of Eq. (3.4) is known as the material distribution is already prescribed from which E can be determined by using the mixture rule formula given by Nan *et al*. [51]. The critical value of internal pressure p_C is then used in Eq. (3.3) to determine the AFT of the point of the crack tip position. Eqs. (4.42) to (4.45) are repeatedly solved by

varying the crack length and the AFT is determined at the position of crack tip following the above procedure.

4.3 Direct Problem

In direct problems, the fracture characteristics of cylinders with an FGM coating are analyzed for assumed functions of the material distribution. To calculate the stress intensity factors, first, the effective properties of the FGM coated cylinder are determined for an assumed material distribution in the cylinder by using the mixture rule given by Eqs. (3.5a) to (3.5e). Then we can calculate the equivalent eigenstrain by using Eq. (4.18) and the resultant stress σ_θ^h from Eq. (4.19b). From Eqs. (4.42) to (4.45), we can then determine the stress intensity factor for the FGM coated cylinder. To calculate apparent fracture toughness for a given material distribution, first, we calculate the critical pressure p_C from the condition,

$$K_I = K_C \qquad (4.47)$$

where the SIF, K_I, is determined by using Eqs. (4.42) to (4.45) and the intrinsic fracture toughness K_C is found from Eq. (3.4).

Then the apparent fracture toughness can be calculated from Eq. (3.3). The geometric factor F is taken from Fig. 3.2 or Table 3.1.

4.4 Inverse Problem

The inverse problem of evaluating material distributions intending to realize prescribed apparent fracture toughness in the cylinder with FGM coating is solved by using the formulations developed for the approximation method of finding stress intensity factors. Suppose that a profile of apparent fracture toughness K_{IC}^a is prescribed over a region of radial length L measured from the inner surface of the cylinder. The FGM coating portion of the cylinder is divided into n number of layers of infinitesimal thickness. Note that the infinitesimal thickness of the layers can be given by $\Delta l = (R_{CT} - R_i)/n$. Now assume two diametrically opposed radial edge cracks of equal length emanating from the inner surface of the cylinder. The crack length l_i is varied by taking the crack length as $l_i = \Delta l/2 + (i-1)\,\Delta l$ until l_i approaches $L\%$ of the cylinder wall thickness. The volume fraction of material A varies only in FGM coating portion. Considering the volume

fractions V_A^i ($i=1,2,.....,n$) of the constituent A in each FGM coating layer of the infinitesimal thickness as design variables and V_A^i ($i= n+1$) $=0.0$, the optimum material distribution i.e. the optimum values of V_A^i ($i=1,2,.....,n$) can be evaluated by solving the optimization problem set up as

Minimize: $F_{obj}\,(V_A^1, V_A^2, ..., V_A^n) = \sum_{i=1}^{N}\left(K_I^i - K_C^i\right)^2$

Subject to: $0 \le V_A^i \le 1;$ $i =1,2,\dots, n$ (4.48)

where $N= \dfrac{L}{\Delta l}$ and K_I^i is the stress intensity factor at the tip of crack of length l_i and K_c^i is

the intrinsic fracture toughness of the ith layer of the cylinder. In determining K_I^i by using Eqs.(4.42) to (4.45), P is replaced by P_C obtained from Eq. (3.3). The intrinsic fracture toughness K_C^i is determined from Eq. (3.4).

The optimization problem in Eq. (4.48) is solved by using a numerical optimization program ADS [57] in which the Broydon-Fletcher-Goldfarb-Shanno (BFGS) variable metric method is used for the unconstrained minimization sub-problem, and the one-dimensional search is used for minimizing the unconstrained function by first finding bounds and then using polynomial interpolation. The minimum value of the objective function $F_{obj}\,(V_A^1, V_A^2, ..., V_A^n)$ obtained by the ADS program is compared with a small positive quantity ε_k to satisfy the condition

$F_{obj}\,(V_A^1, V_A^2, ..., V_A^n) \le \varepsilon_k$ (4.49)

and the corresponding set of the design variables $V_A^i (i = 1,2, ... n)$ is taken as the solution of the optimization problem.

The solution of the optimization problem gives the values of material distribution at discrete points i ($i=1, 2, ..., n$).Then the continuous profile of the material distribution is obtained by spline interpolation. In order to solve the optimization problem in Eq. (4.48), it is necessary to determine the material properties of the cylinder. These properties are determined by using the mixture rule given by Eq. (3.5) according to which the shear modulus of elasticity μ and the bulk modulus γ are first determined from Eqs. (3.5a), (3.5b), and (3.5d).

Then the Young's modulus E is calculated by using Eq. (3.5e), and the Poisson's ratio is determined from,

32

$$\nu = \frac{E}{2\mu} - 1 \tag{4.50}$$

The coefficient of thermal expansion α is determined by using the relation given in Eq. (3.5c).

CHAPTER 5
NUMERICAL RESULTS AND DISCUSSIONS

It is mentioned earlier that for any specific requirement, thick-walled cylinder with entire wall thickness made of FGM (referred as FGM cylinder from this point forward) is not necessary, only a thin FGM coating can serve the purpose adequately. So, to obtain the results for cylinder with FGM coating, simulation codes developed in earlier studies [45] are modified. The previous codes were developed for cylinder with gradation of material throughout the entire wall. In this study, those codes are modified for the cylinder with FGM coating at the inner surface. The modified codes can deal any arbitrary material distributions in FGM coating portion including the cylinder with gradation of material throughout the entire wall thickness. These can also consider the FGM coating of any thickness. The modified codes are thus more general than the earlier codes. The codes are still applicable for both single and double radial edge cracks. The effect of various parameters like cylinder wall thickness, strength factor, number of cracks, coating thickness etc can be evaluated by using the code for direct problem. In the code for inverse problem any arbitrary apparent fracture toughness over any thickness of cylinder can be prescribed. And it gives the corresponding material distribution for FGM coating of any thickness. Another code is developed to evaluate the stress intensity factor as a function of difference between sintering temperature and application temperature.

The flow diagrams for determination of SIF by using direct method for an FGM cylinder and a cylinder with FGM coating are presented in Figs. 5.1 and 5.2, respectively. On the other hand, Figs. 5.3 and 5.4 respectively, show the flow diagrams for inverse problem of material distribution to realize prescribe apparent fracture toughness for an FGM and a cylinder with FGM coating. FGM cylinder means that the entire wall of the cylinder is made of FGM. The modifications of the original codes (Figs.5.1 and 5.3) required for the cylinder with FGM coating are shown by the shaded blocks in Figs. 5.2 and 5.4.

In the present study, some numerical results are obtained for a cylinder with TiC/Al$_2$O$_3$ FGM coating at the inner surface. The material A and B correspond to TiC and Al$_2$O$_3$ respectively, whose mechanical and thermal properties are shown in Table 5.1[58-63]. It is worthwhile to mention that although the method developed can be applied to any

materials, TiC and Al_2O_3 have been chosen here merely as an example. In case of solving direct problems the difference between sintering and room temperature, ΔT is taken as 1000° C and FGM coating thickness (CT) is taken as 20% of the whole cylinder thickness..The code of the main program to evaluate SIF and AFT by applying direct method is provided in Appendix I.

5.1 Verification of the Method

The approximation method of calculating stress intensity factors for two diametrically-opposed edge cracks at the inner surface of cylinder with FGM coating is first verified by applying the method for a homogeneous cylinder. By setting $V_A = 0$ or uniform distribution of V_A throughout the wall thickness of the cylinder, one obtains a homogeneous cylinder. The normalized stress intensity factors F_I $(=K_I(1-R_i^2/R_o^2)/2p\sqrt{\pi l})$ are calculated for such a homogeneous cylinder for $R_o/R_i = 2.5$ and compared with those available in literatures as shown in Fig. 5.5. The black line represents the results obtained by the present method while the red line represents the results obtained by Wu and Janne [48]. It is observed that the results obtained by the present method agree well with those obtained by Wu and Janne [48] for the entire range of normalized crack length $l/(R_o-R_i)$.

5.2 Stress Intensity Factors for Prescribed Material Distributions

In this study, the stress intensity factors are calculated for two diametrically-opposed edge cracks in a cylinder with FGM coating for four different prescribed material distributions as shown by the curves in Fig.5.6. The volume fraction of material A varies only in FGM coating portion. Although any material distribution can be considered, these four distributions are considered here merely as examples. For these prescribed material distributions and $R_o/R_i= 2.5$, strength factor $S_f=1.0$, normalized stress intensity factor F_I versus normalized crack length $l/(R_o-R_i)$ is plotted in Fig.5.7. For all these cases of material distributions, the SIF is less at inner region of the cylinder, and then it increases over rest of the wall thickness. The lowest value of SIF is obtained for the uniform material distribution. However, the uniform distribution is not recommended as it has a sharp interface that causes the problem of delamination. Further, among rest of the three distributions, the stress intensity factor for parabolic upward distribution is the minimum for the lower range of crack length. This is due to the fact that this material

distribution has the higher gradient near surface of the cylinder which produces more incompatibility in the eigenstrain giving higher magnitude of compressive eigenstress. This compressive eigenstress attributes to the reduction in the stress intensity factor. Thus, it can be said that the FGM coating having the higher gradient would have the lower stress intensity factor.

The effect of thickness of the cylinder is shown in Fig. 5.8. Here, the stress intensity factors are plotted for different values of R_o/R_i for linear material distribution in Fig. 5.6 and 20% FGM coating thickness. It is observed that for higher thickness of the cylinder, the stress intensity factor is less, thus has more toughness against crack propagation.

The effects of strength factor S_f on the stress intensity factor are also examined and shown in Fig. 5.9. The results corresponds to the linear material distribution in Fig. 5.6 and R_o/R_i= 2.5 and CT=20%. The stress intensity factor decreases as the strength factor increases. This is because the higher value of strength factor represents the lower value of applied load p .

A comparison between the stress intensity factors for a single radial edge crack and two diametrically opposed edge cracks is depicted in Fig.5.10. The stress intensity factors for a single radial edge crack can be calculated by setting G_2 (H_i,T_j)= 0 in Eq. (4.42). The results are obtained for S_f=1.0, R_o /R_i = 2.5 and CT=20%. Note that the stress intensity factor is higher in the case of two diametrically-opposed cracks for any of the material distributions especially over the outer region of the cylinder. The comparison of stress intensity factors for a single and two diametrically-opposed edge cracks in cylinder with FGM coating of linear material distribution are shown in Fig.5.11. The stress intensity factors calculated for R_o/R_i= 2.5 and S_f=1.0 for single and double edge cracks are the same over the inner region of the cylinder wall. It shows that the stress intensity factors of the cylinder with two diametrically-opposed edge cracks are much higher than those with a single radial edge crack over the outer region of the cylinder. So, the cylinder with two diametrically-opposed edge cracks is more critical than that with a single radial edge crack.

The effect of ΔT that represents the difference between sintering and application temperatures of the cylinder with 20% FGM coating on the stress intensity factor can also be examined by the present method. If the FGM coated cylinder is used in an application of elevated temperature (higher than the room temperature), the value of ΔT will be smaller. Its effect is shown in Fig. 5.12 which is plotted for the linear material distribution in the coating portion of the cylinder shown in Fig 5.6. It is observed that the stress intensity factor rises as the value of ΔT decreases, i.e. at higher application temperature of the FGM coated cylinder. This conforms to the physical phenomenon that at lower value of ΔT, the eigenstrain developed in the cylinder becomes lower. A comparison between the stress intensity factors for a single radial edge crack and two diametrically opposed edge cracks as a function of ΔT is shown in Fig. 5.13. The stress intensity factor for the two diametrically opposed cracks is more critical than that for the single crack. The code of the main program to express the SIF as a function of ΔT is attached in Appendix II.

Figure 5.15 shows the effect of the FGM coating thickness on the stress intensity factor. To investigate this effect, FGM coatings of various thicknesses are considered as shown in Fig. 5.14. The coating thicknesses are expressed in terms of the percent of the cylinder wall thickness. In all cases, linear material distribution in FGM coating portion is considered. Outside the FGM coating, the cylinder wall is composed of Al_2O_3 only. For each coating thickness, the corresponding stress intensity factor is shown in Fig. 5.15. The results correspond to R_o/R_i=2.5, $\Delta T = 1000^{\circ}$C. From the graph it is noted that at the inner portion of the cylinder stress intensity factor decreases with the increase of the coating thickness up to 60% of the cylinder wall thickness. After this value of the coating thickness, the stress intensity factor starts to increase as the coating thickness further increases.

5.3 Apparent Fracture Toughness for Prescribed Material Distribution

The apparent fracture toughness for prescribed material distributions of Fig. 5.6 is also evaluated numerically. The apparent fracture toughness K_{IC}^a is normalized by the intrinsic fracture toughness K_C^B of Al_2O_3. This normalized apparent fracture toughness K_{IC}^a / K_C^B is plotted in Fig. 5.16 for R_o/R_i=2.5, $\Delta T = 1000^{\circ}$C and CT= 20%. For all the cases of

material distributions, the AFT initially increases over certain inner region of the cylinder wall. Then it decreases over the rest of the wall thickness. The incompatible eigenstrain induces an eigenstress, which is a self-equilibrated internal stress. The compressive eigenstress reduces the crack driving force that eventually increases the apparent fracture toughness. On the other hand, the tensile eigenstress has the reverse effects on the apparent fracture toughness. The composition profiles shown in Fig. 5.6 induce compressive eigenstress over certain portion of the wall thickness at the inner side of the cylinder and a balancing tensile eigenstress over the remaining portion of the wall thickness at the outer side. And that is why the apparent fracture toughness increases from the inner surface up to a certain length and then it decreases as seen from Fig. 5.12. This type of fracture characteristic is desirable as it ensures the protection of catastrophic failure. Once the crack starts to propagate under a certain pressure, it immediately stops propagating as the region ahead of the crack tip has a higher toughness. For its further propagation, the internal pressure should be increased. The maximum peak value of AFT is obtained for the uniform material distribution. However, the uniform material distribution is not recommended as it has sharp interface causes delimitation. Among other three material distributions, it is noted that parabolic upward distribution in Fig. 5.6 gives the maximum peak value of apparent fracture toughness. This is due to the fact that parabolic upward material distribution is steeper near the inner surface that induces compressive eigenstress with a higher absolute magnitude than those obtained for the other two profiles. Because, the material distributions whose steepness is less, induce eigenstress with smaller absolute magnitude. It is also noted that apparent fracture toughness for all material distributions has the value, which is significantly higher than the intrinsic fracture toughness K_C^B of the base material of Al_2O_3 over most of the cylinder wall except those at and near the outer surfaces of the cylinder.

The effect of cylinder wall thickness on the AFT is exhibited in Fig. 5.17. The results are obtained for the linear material distribution of Fig. 5.6 and $\Delta T = 1000\,^\circ C$ and CT= 20%. It is found that, for the same type of material distribution, AFT improves with the increase of wall thickness.

Figure 5.18 shows AFT as a function of application temperature. The parameter ΔT refers to the difference between the sintering and the application temperature. Thus, a

lower value of ΔT indicates the higher application temperature. It is evident from Fig. 5.18 that the cylinder has better fracture resistance at low application temperature. It is also noted that the AFT is worse than the intrinsic fracture toughness of the base material Al_2O_3 if the value of parameter ΔT falls below 400°C.

To investigate the effect of the FGM coating thickness on the AFT, FGM coatings of various thicknesses are considered as shown in Fig. 5.19. The coating thickness (CT) is expressed in terms of the percent of the cylinder wall thickness. In all the cases, the volume fraction of TiC varies linearly from 1.0 to 0 over the coating. For each CT, the corresponding AFT is shown in Fig. 5.20. For any CT, the AFT rises to a peak value with radial distance over the inner region of the cylinder wall. Then it starts decreasing over rest of the region of the wall. The position of the peak value of the AFT shifts toward the outer surface as the CT increases. Further the peak value of AFT increases with the increase of CT until the CT is 60% of the cylinder wall thickness. After this value of CT, the AFT start degrading as the CT further increases.

Shown in Fig. 5.21 is the comparison of AFT for a single and two diametrically-opposed edge cracks. The results correspond to the linear material distribution of Fig. 5.6, R_o/R_i=2.5, $\Delta T = 1000°C$ and CT= 20%. For both the cases of single and double cracks, the AFT is same over the inner region of the cylinder wall. However, it only differs significantly over the outer region of the cylinder wall.

5.4 Material Distribution for Prescribed Apparent Fracture Toughness

The inverse problem of evaluating optimum material distributions is solved to realize prescribed apparent fracture toughness in the thick-walled cylinder with FGM coating, which is higher than the intrinsic toughness of the constituent materials shown in Table 5.1. Although it is possible to control the higher apparent fracture toughness of various profiles in order to meet the requirement of an application, in this study, we consider only two examples as shown by the solid portions of curves I and II in Fig. 5.22. The normalized apparent fracture toughness in example I is controlled such that it increases linearly from 2.0 to 2.85 over the normalized crack length 0.75. In example II, the normalized value of the apparent fracture toughness is 2.0, that does not vary over the same crack length. The difference between the sintering and room temperature ΔT is

taken as 1000°C. The value of ε_k is taken as 0.1 in Eq. (4.49). The code of the main program to solve the inverse problem is provided in Appendix III.

For the prescribed apparent fracture toughness of Fig. 5.22, the corresponding optimal material distribution profiles evaluated by the inverse calculations are shown in Fig. 5.23. It exhibits the volume fraction V_A of TiC versus the normalized radial distance for the parameter $R_o/R_i=1.5$. In order to know the characteristics of the cylinder after the controlled region, the apparent fracture toughness in that region is calculated for the material distribution profiles of Fig. 5.23 and shown by the dotted portions of the curves I and II in Fig. 5.22. It is noted that apparent fracture toughness in both cases reduces drastically after the controlled region.

The prescribed apparent fracture toughness shown in Fig. 5.22 is realized by designing the thick-walled cylinder with FGM coating having the material distribution profiles as shown in Fig. 5.23. Thus it can be concluded that the apparent fracture toughness of a thick-walled cylinder with FGM coating can be controlled within possible limits by choosing an optimal material distribution profile in FGM coating portion of the cylinder.

Material distribution profile corresponding to the prescribed apparent fracture shown in Fig. 5.24 is presented in Fig. 5.25 for two different types of cylinders, namely (i) a cylinder with gradation throughout the entire wall (ii) a cylinder with FGM CT of 20% of the cylinder wall at the inner surface. It establishes the fact that to achieve any desirable fracture behavior in a thick-walled cylinder, material gradation throughout the wall thickness of the cylinder is not necessary. Only a thin FGM coating can satisfy the requirements.

Figure 5.26 shows the effects of the wall thickness of the cylinder on the material distribution. The results are obtained for the example I of the prescribed apparent fracture toughness shown in Fig. 5.22 and CT=20%. It is noted that up to a certain thickness at the inner side of the cylinder the value of V_A increases as the parameter R_o/R_i decreases for the same type of prescribed apparent fracture toughness. Although there is a significant difference between the results corresponding to $R_o/R_i=1.5$ and 2.0, the difference between the results for $R_o/R_i=2.0$ and 2.5 is not significant.

Figure 5.27 shows the effects of FGM coating thickness on the material distributions. These results correspond to the prescribed fracture toughness I shown in Fig. 5.22 and R_o/R_i=2.5.

The inverse method developed in this study can also be applied to evaluate material distribution corresponding to a prescribed profile of apparent fracture toughness against a single radial edge crack by setting the function G_2 (H_i, T_j) in Eq. (4.42) to zero. For the example II of prescribed apparent fracture toughness in Fig. 5.22 against a single and two diametrically- opposed cracks, the evaluated material distributions are compared in Fig. 5.28. From the graph it is found that the material distributions differ only in the region of $(r\text{-}R_i)/(R_o\text{-}R_i)$=0.05 to 0.18.

CHAPTER 6
CONCLUSIONS AND RECOMMENDATION

6.1 Concluding Remarks

A method is developed to analyze brittle fracture characteristics of a thick-walled cylinder having an FGM coating at its inner surface. The method is valid for any arbitrary variation of material properties instead of some presumed functional forms of material properties. The effect of eigenstrain developed in the cylinder as a result of cooling from sintering temperature due to nonuniform coefficient of thermal expansion is taken into account. The procedures of evaluating material distributions for prescribed apparent fracture toughness and vice versa by using this method have been outlined. This method is equally suitable for a single edge crack. Further, it can also be applied to a homogenous cylinder with a single as well as two diametrically opposed edge cracks. To demonstrate the method, some numerical results are obtained for a thick-walled cylinder with TiC/Al_2O_3 FGM coating. From the numerical results the following salient points can be noted:

i.   The stress intensity factors of a thick-walled cylinder with an FGM coating depend on the material distribution. The SIF is less for material distribution with higher gradient.

ii. The wall thickness of the cylinder has also significant influence on the SIF and AFT.

iii. The strength factor S_f has reverse effect on the SIF, i.e. the SIF decreases as S_f increases.

iv. Like a homogeneous cylinder, two diametrically-opposed edge cracks are more critical than a single edge crack in an FGM coated cylinder.

v.   Cylinder with FGM coating has better fracture resistance at low application temperature.

vi. To achieve any desirable fracture behavior in a thick-walled cylinder, material gradation throughout the wall thickness is not necessary. Only a thin FGM coating can satisfy the requirements.

vii. The apparent fracture toughness of an FGM coated cylinder is a function of material distribution. Thus the desired apparent fracture toughness can be introduced in a cylinder with FGM coating by choosing the material distribution appropriately.

viii. The coating thickness has a significant effect on the fracture characteristics of a cylinder with FGM coating. Fracture resistance improves upto a certain amount of coating thickness. After that it starts to degrade.

6.2 Recommendations for Future Work

Some recommendations for further work are given below.

i. Investigation of the effect of unequal crack size of two diametrically opposed edge cracks can be carried out.

ii. Investigation of the effect of relative crack position of two radial edge cracks on the fracture characteristics of cylinders with FGM coating can be carried out.

iii. Investigation of the effect of multiple radial edge cracks (more than two cracks) on the fracture characteristics of cylinders with FGM coating can be carried out.

REFERENCES

[1] Yamanouchi, M., Koizumi, M., Hirai, T., and Shiota, I., *Proc. of the First Int. Sympos. on Functionally Gradient Materials,* Sendai, Japan, 1990.

[2] Holt, J.B., Koizumi, M., Hirai, T., and Munir, Z. A., *Ceramic Transactions, Functionally Gradient Materials,* The American Ceramic Society, vol. 34, pp.157-164.1993.

[3] Gdoutos, E. E., "*Fracture Mechanics: an Introduction, Solid Mechanics and its Applications*", vol. 14, Kluwer Academic Publishers, Dordrecht, The Netherlands, 1993.

[4] Mura, T., "*Micromechanics of Defects in Solids: Mechanics of Elastic and Inelastic Solids*", Kluwer Academic Publishers, Dordrecht, The Netherlands, 1987.

[5] Zhong, Z., and Yu, T., "Analytical Solution of a Cantilever Functionally Graded Beam", *Compos. Sci. Technol.,* vol.67, pp. 481-8, 2007.

[6] Zhao, F., Wang, Z., and Zhang, R., "Post-Buckling Analysis of FGM Beam Subjected to Non-Conservative Forces and In-Plane Thermal Loading", *Appl. Mech. Mat.,* vol. 152-154, 2012.

[7] Kim, K.D., Lomboy, G. R., and Han, S. C., " Geometrically Non-Linear Analysis of Functionally Graded Material (FGM) Plates and Shells Using a Four Node Quasi-Conforming Shell Element", *J. Compos. Mater,* vol. 42, pp.485-511, 2008.

[8] Afsar, A. M., Rahman, Wang, Y. Q., Shi, Y., and Song, J.I., "Finite Difference Solution of Stress and Strain in an FGM Plate", *Proc.16th Ann. Intl. Conf. Composites/Nano Engineering,* Kumming, China, 2008.

[9] Chung, Y. N., and Chang, H. X., "Mechanical Behavior of Rectangular Plates with Functionally Graded Coefficient of Thermal Expansion Subjected to Thermal Loading", *J. Therm. Stresses*, vol. 31, pp. 368-88, 2008.

[10] Mostapha, R., Reza, A., and Amirabbas, K., "Thermal Buckling of Thin Rectangular FGM Plate", *World Appl. Sci. J.,*vol. 16, pp. 52-62,2012.

[11] Chen, X. L., and Liew, K.M., "Buckling of Rectangular Functionally Graded Material Plates Subjected To Nonlinearly Distributed In-Plane Edge Loads" *Smart Mater Struct.,* vol. 2004, pp. 1430-7, 2004.

[12] Obata, Y., and Noda, N., "Steady Thermal Stresses in a Hollow Circular Cylinder and a Hollow Sphere of a Functionally Graded Material", *J. Thermal Stresses,* vol.17, pp. 471–487, 1994.

[13] Liew, K. M., Kitipornchai, S., Zhang, X. Z., and Lim, C. W., "Analysis of the Thermal Stress Behavior of Functionally Graded Hollow Circular Cylinders", *Int. J. Solids Struct.*, vol.40, pp. 2355–2380, 2003.

[14] Tutuncu, N., "Stresses in Thick-Walled FGM Cylinders with Exponentially-Varying Properties", *Engng. Struct.,* vol. 29, pp. 2032-5, 2007.

[15] Anisuzzaman, M., "Brittle *Fracture Characteristics of Thick-Walled Functionally Graded Material Cylinders*", M.Sc. Dissertation, Mech. Engng. BUET, 2003.

[16] Loghman, A., Aleayoub, S.M.A., Sadi, M. Hasani, "Time-Dependent Magnetothermoelastic Creep Modeling of FGM Spheres Using Method of Successive Elastic Solution", *Appl. Math. Model,* vol. 36, pp.836–845, 2012.

[17] Xiang, H. J., and Yang, J., "Free and Forced Vibration of a Laminated FGM Timoshenko Beam of Variable Thickness under Heat Conduction, Compos" *Part B,* vol. 39, pp. 292–303, 2008.

[18] Li, S. R., Zhang, J. H., and Zhao, Y. G., "Thermal Post-Buckling of Functionally Graded Material Timoshenko Beams," *Appl. Math. Mech.*, vol. 27, pp. 803–810, 2006.

[19] Praveen, G. N., and Reddy, J. N., "Nonlinear Transient Thermoelastic Analysis of Functionally Graded Ceramic-Metal Plates," *Int. J. Solids Struct.,* vol. 35, pp. 4457–76, 1998.

[20] Han, X., Liu, G. R., Xi Z. C., and Lam, K. Y., "Transient Waves in a Functionally Graded Cylinder", *Int. J. Solids Struct.,*vol. 38, pp. 3021–37, 2001.

[21] Han, X., Liu, G. R., and Lam, K. Y., "Transient Waves in Plates of Functionally Graded Material", *Int. J. Numer. Method Eng.,* vol. 52**,** pp**.** 851–6, 2001.

[22] Afsar, A. M. and Anisuzzaman, M., "Stress Intensity Factors of Two Diametrically Opposed Edge Cracks in a Thick-Walled Functionally Graded Material Cylinder", *Engng. Fract. Mech.*, vol. 74, pp. 1617–1636, 2007.

[23] Chen, Y. F.,and Erdogan, F., "The Interface Crack Problem for a Nonhomogenous Coatings Bonded to a Homogenous Substrate", *J. Mech. Phys. Solids*, vol. 44, pp. 771-87, 1996.

[24] Gu, P., and Asaro, R. J., "Cracks in Functionally Graded Materials", *Int. J. Solids Struct.*, vol. 34, pp. 1-17, 1997.

[25] Ozturk, M., and Erdogan, F., "Axisymmetric Crack Problem in Bonded Materials with a Graded Interfacial Region", *Int. J. Solids Struct.,* vol. 33, pp. 4101-17, 1996.

[26] Choi, H. J., "Bonded Dissimilar Strips with a Crack Perpendicular to the Functionally Graded Interface", *Int. J. Solids Struct.*, vol. 32, pp. 2853-71, 1995.

[27] Delale, F., and Erdogan, F., "The Crack Problem for a Nonhomogeneous Plane", *ASME J. Appl. Mech.*, vol. 50, pp. 609-614, 1983.

[28] Bao, G., and Wang, L., "Multiple Cracking in Functionally Graded Ceramic/Metal Coatings", *Int. J. Solids Struct.*, vol. 32, pp. 2853-2871, 1995.

[29] Hassan, H. A. Z., "Torsion of a Nonhomogenous Infinite Elastic Cylinder Slackened by a Circular CUT", *J. Engng. Math.,* vol. 30, pp. 547-55, 1996.

[30] Zou, Z. Z., Wang, X. Y., and Wang, D., "On the Modelling of Interfacial Zone Containing a Griffith Crack: Plane Problem", *Key Engng. Mater*, vol. 145, pp. 489-94, 1998.

[31] Jin, Z-H., and Noda, N., "An Internal Crack Parallel to the Boundary of a Nonhomogenous Half Plane under Thermal Loading". *Int. J. Engng. Sci.,* vol. 31, pp. 793-806, 1993.

[32] Noda, N., and Jin, Z-H,. "A Crack in Functionally Graded Materials under Thermal Shock", *Arch. Appl. Mech.*, vol. 64, pp. 99-110, 1994.

[33] Hirano, T., Wakashima, K., "Mathematical Modeling and Design", *Mater Res. Soc,* vol. 20, pp. 40-2, 1995.

[34] Makworth, A. J., and Saunders, J. H., "A Model of Structure Optimization for a Functionally Graded Material", *Matter Lett.*, vol. 22, pp. 103-7, 1995.

[35] Nadeau, J. C., and Ferrari, M., "Microstructural Optimization of a Functionally Graded Transversely Isotropic Layer", *Mech. Mater*, vol. 31, pp. 637-51, 1999.

[36] Nadeau, J. C., and Meng, X. N., "Microstructural Optimization of a Functionally Graded Layer", *Compos. B*, vol. 31, pp. 285-97, 2000.

[37] Nakamura, T., Wang, T., and Sampath, S., "Determination of Properties of Graded Materials by Inverse Analysis and Instrumented Indentation", *Acta Mater,* vol. 48, pp. 4293-306, 2000.

[38] Oatao, Y., Kawamura, R., Tanigawa, Y., and Imamura, R., "Optimization of Material Composition of Nonhomogenous Hollow Sphere for Thermal Stress Relaxation Making Use of Neural Network", *Comput. Meth. Appl. Mech. Engng*., vol. 180, pp. 185-201, 1999.

[39] Oatao, Y., Tanigawa, Y., and Nakaura, T., "Optimization of Material Composition of FGM Hollow Circular Cylinder under Thermal Loading: A Neural Network Approach", *Compos. B*, vol. 30, pp. 415-22, 1999.

[40] Oatao, Y., Kawamura, R., Tanigawa, Y., and Imamura, R., "Optimization of Material Composition of Nonhomogenous Hollow Circular Cylinder for Thermal Stress Relaxation Making Use of Neural Network", *J. Thermal Stresses*., vol. 22, pp. 1-22, 1999.

[41] Zuikar, J. R., "Functionally Graded Materials: Choice of Micromechanics Model and Limitations in Property Variation", *Compos. Engng.,* vol. 5, pp. 807-19, 1996.

[42] Afsar, A. M., and Sekine, H., "Inverse Problems of Material Distributions for Prescribed Apparent Fracture Toughness in FGM Coatings around a Circular Hole in Infinite Elastic Media", *Compos. Sci. and Tech.,* vol. 62, pp. 1063-1077, 2002.

[43] Sekine, H., and Afsar, A. M., "Composition Profile for Improving the Brittle Fracture Characteristics in Semi-Infinite Functionally Graded Materials", *JSME Int. J.*, vol. 42, pp. 592-600. 1999.

[44] Afsar, A. M., and Sekine, H., "Crack Spacing Effect on the Brittle Fracture Characteristics of Semi-Infinite Functionally Graded Materials with Periodic Edge Cracks". *Int. J. of Fracture*, vol. 102, pp.L61- L66. 2000.

[45] Afsar, A. M., and Sekine, H., "Optimum Material Distributions for Prescribed Apparent Fracture Toughness in Thick-Walled FGM Circular Pipes". *Int. J. of Press. vessels and piping*, vol. 78, pp. 471-484, 2001.

[46] Shannon, R.W.E., "Stress Intensity Factors for Thick-Walled Cylinders", *Int. J. Press. Vessels and Piping*, vol. 2, pp. 19-29. 1974.

[47] Afsar, A. M., Anisuzzaman, M., and Song, J. I., "Inverse Problem of Material Distribution for Desired Fracture Characteristics in a Thick-Walled Functionally Graded Material Cylinder with Two Diametrically-Opposed Edge Cracks", *Engng. Fract. Mech.*, vol. 76, pp. 845-55, 2009.

[48] Wu, Xue-Ren., and Janne, A., *"Weight Functions and Stress Intensity Factors Solutions"*, Pergamon Press PIC, Headington Hill, Oxford OX3OBW, England, 1991.

[49] Bowie, O. L. and Freese, C. E., "Elastic Analysis for a Radial Crack in a Circular Ring", *Engng. Fract, Mech.*, vol. 4, pp. 315-321, 1972.

[50] Nair, S. V., "Crack-Wake Debonding and Toughness in Fiber-or Whisker-Reinforced Brittle-Matrix Composites", *J. American Ceramic Society*, vol. 73, pp. 2839-2847, 1990.

[51] Nan, C.-W., Yuan, R.-Z., and Zhang, L.-M., *"The Physics of Metal/Ceramic Functionally Gradient Materials"*, *Ceramic Transaction: Functionally Gradient Materials*, vol. 34, pp. 75-82, Edited by J. B. Holt et al., American Ceramic Society, Westerville, OH, 1993.

[52] Bieniek, M., Spillers, W.R., and Freudenthal, A.M., "Nonhomogeneous Thick-Walled Cylinder Under Internal Pressure", *ARS J.*, vol.32, pp.1249-1255, 1962.

[53] Muskhelishvili, N. I., "Some *Basic Problems of the Mathematical Theory of Elasticity*" (Translated from the Russian by J.R.M.Radok), 2nd edition, Noordhoff International Publishers, The Netherlands, 1975.

[54] Hills, D. A., Kelly, P. A., Dai, D. N., and Korsunsky, A. M., "*Solution of Crack Problems: The Distributed Dislocation Technique*", Kluwer Academic Publishers, 1996.

[55] Erdogan, F., Gupta, G. D.,and Cook, T. S., "Numerical Solution of Singular Integral Equations", In: Sith GC, editor. Mechanics of fracture methods of analysis and solutions of crack problems, vol. 1, pp. 368-425, LEYDEN: Noord-hoff, 1973.

[56] Krenk, S., "On the Use of the Interpolation Polynomial for Solution of Singular Integral Equation", *Quarterly of Appl. Math.*, vol. 32, pp. 479-484, 1975.

[57] Vanderplaats, G. N., and Sugimoto, H., "*A General-Purpose Optimization Program for Engineering Design*", Computers & Structures, vol. 24, pp. 13, 1986.

[58] Ichinose, N., Komeya, K., Ognio, A., Tsuge, A., Yokomizo, Y., " *Introduction to Fine Ceramics*", *Applications in Engineering*, Edited by N. Ichinose, John wiley and Sons LTD, 1987.

[59] Lawrence, H., Vlack, V., "Physical *Ceramics for Engineers*", Addison-Wesley Publishing Company, Inc., 1964.

[60] Richarson, W. David, "*Modern Ceramic Engineering*", Properties, Processing, and use in Design, Second Edition, Marcel Dekker, Inc., 1992.

[61] McColm, I. J., "Ceramic *Science for Materials Technologists*", Leonard Hill, 1983.

[62] Wei, G. C., and Bechar, P.F, "*Journal of American Ceramic Society*", vol.67, pp.571-574, 1984.

[63] Mah, T., Mendiratta, M. G., and Lipsitt, H. A., "*American Ceramic Society Bulletin*", vol. 60, pp. 1229-1240, 1981.
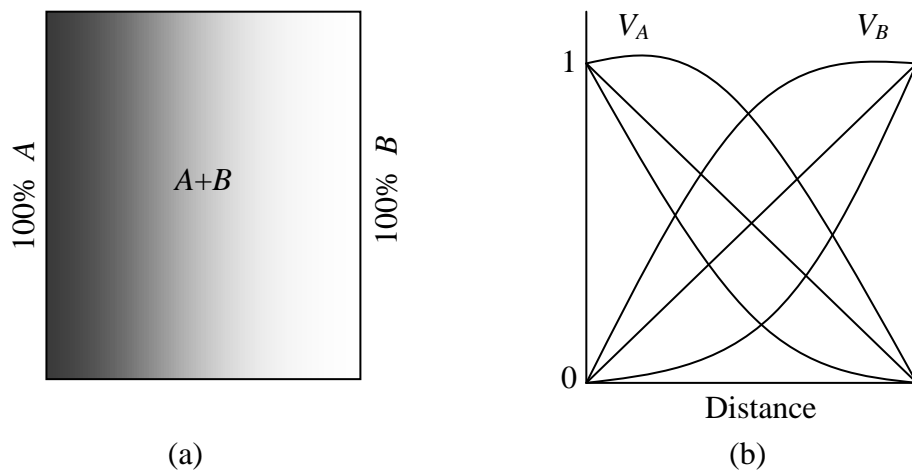
Fig.1. 1 Concept of FGM: (a) an FGM plate, (b) material distribution in the FGM plate
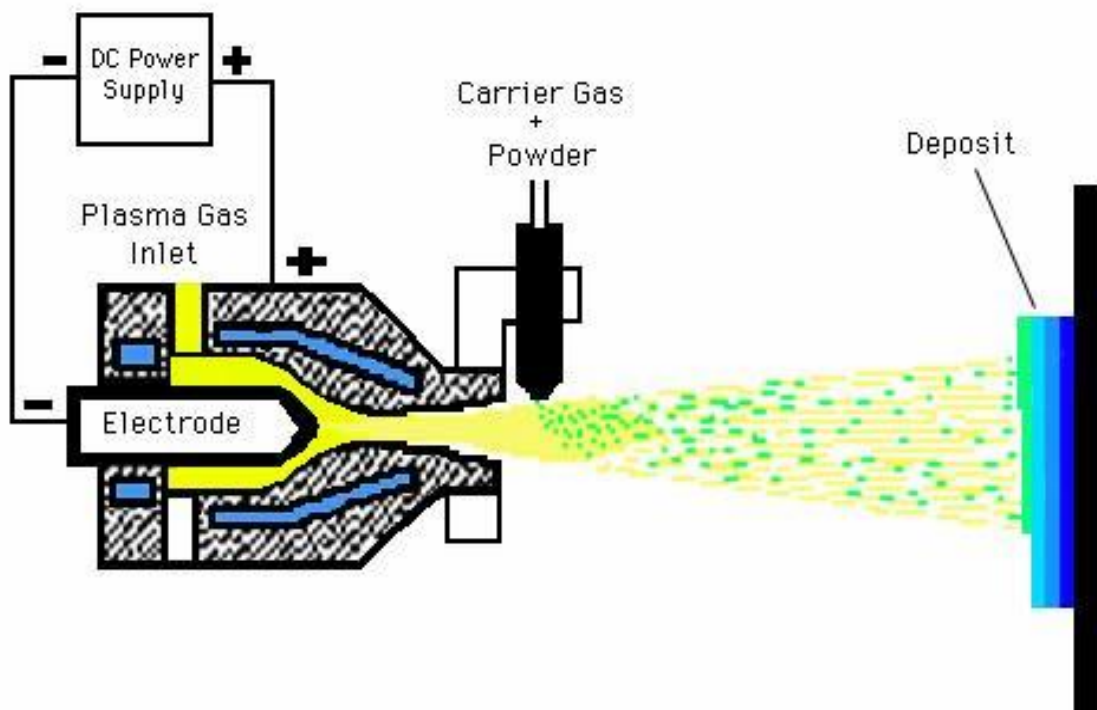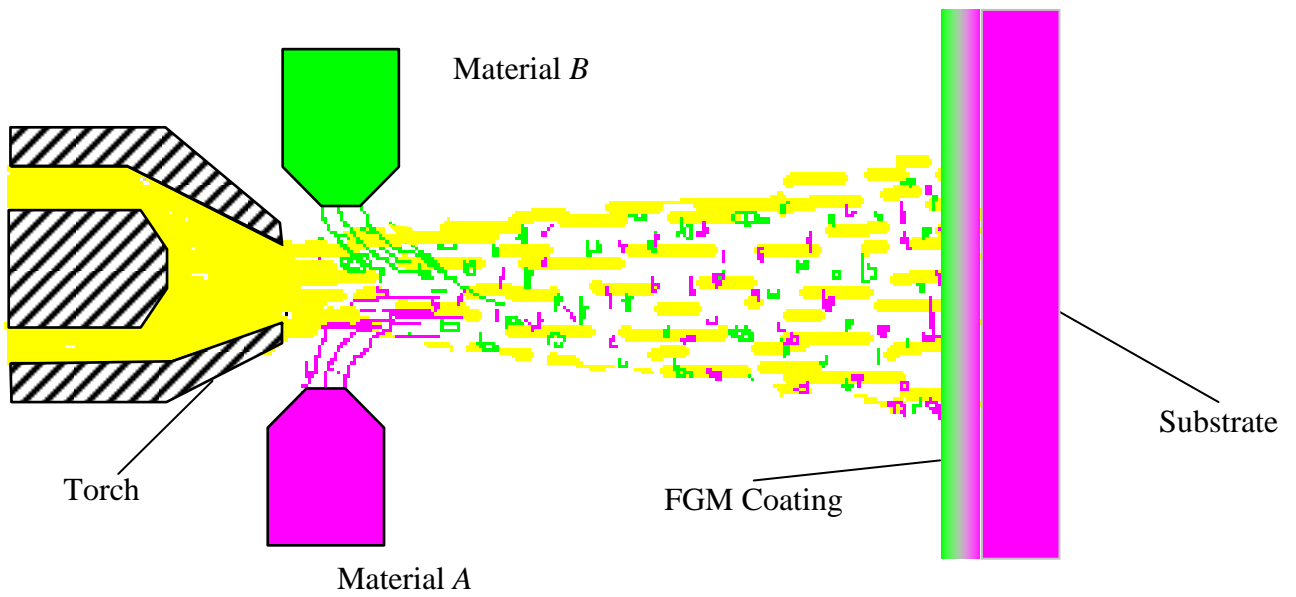

Fig.1. 2 Basic features of plasma spray method.

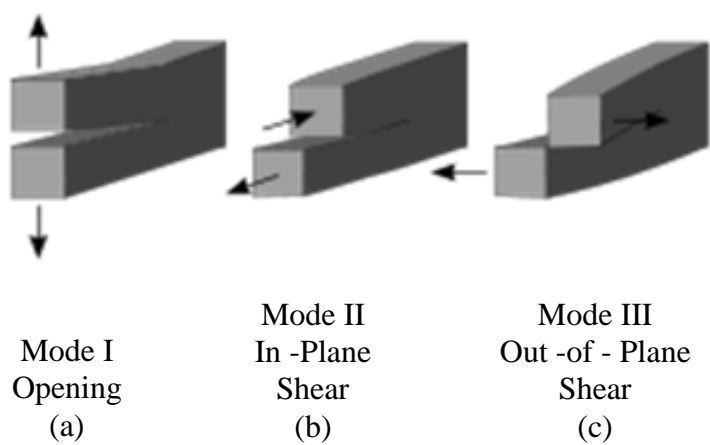**Fig.1. 3** Plasma spray method for developing FGM coating.

Mode I Opening (a)	Mode II In -Plane Shear (b)	Mode III Out -of - Plane Shear (c)

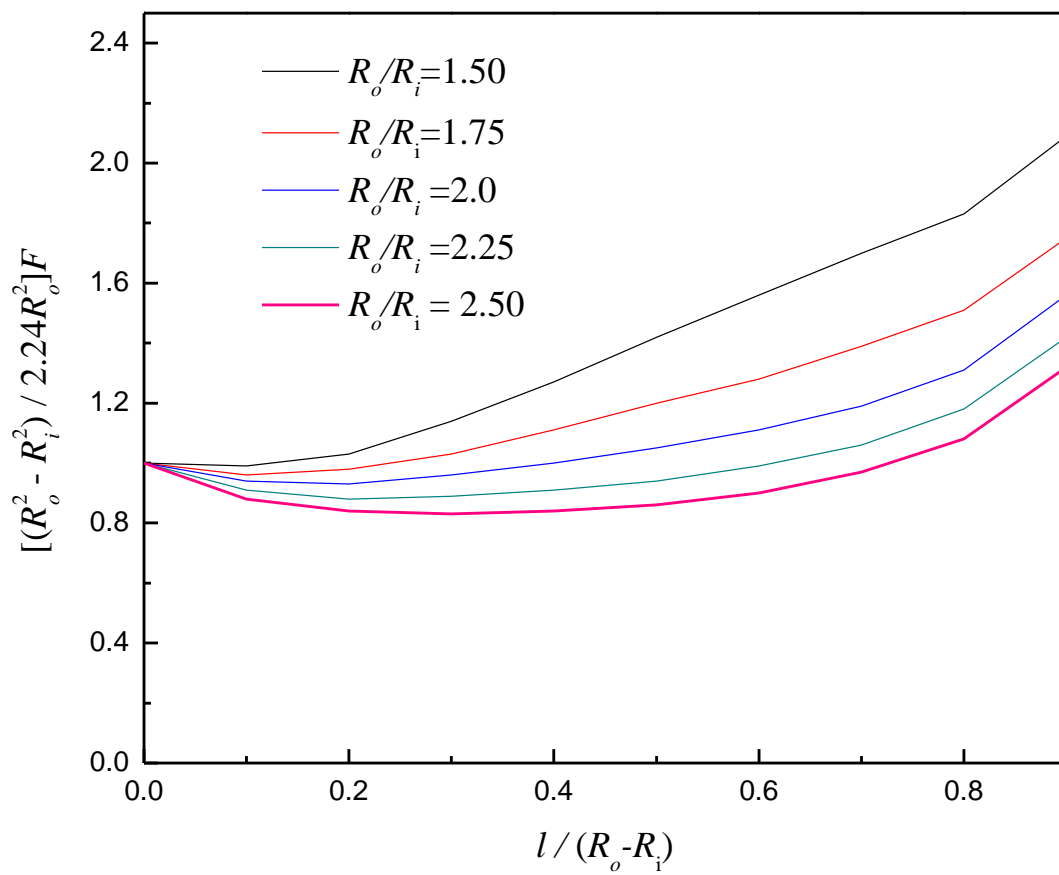**Fig. 3. 1** The three fracture modes.

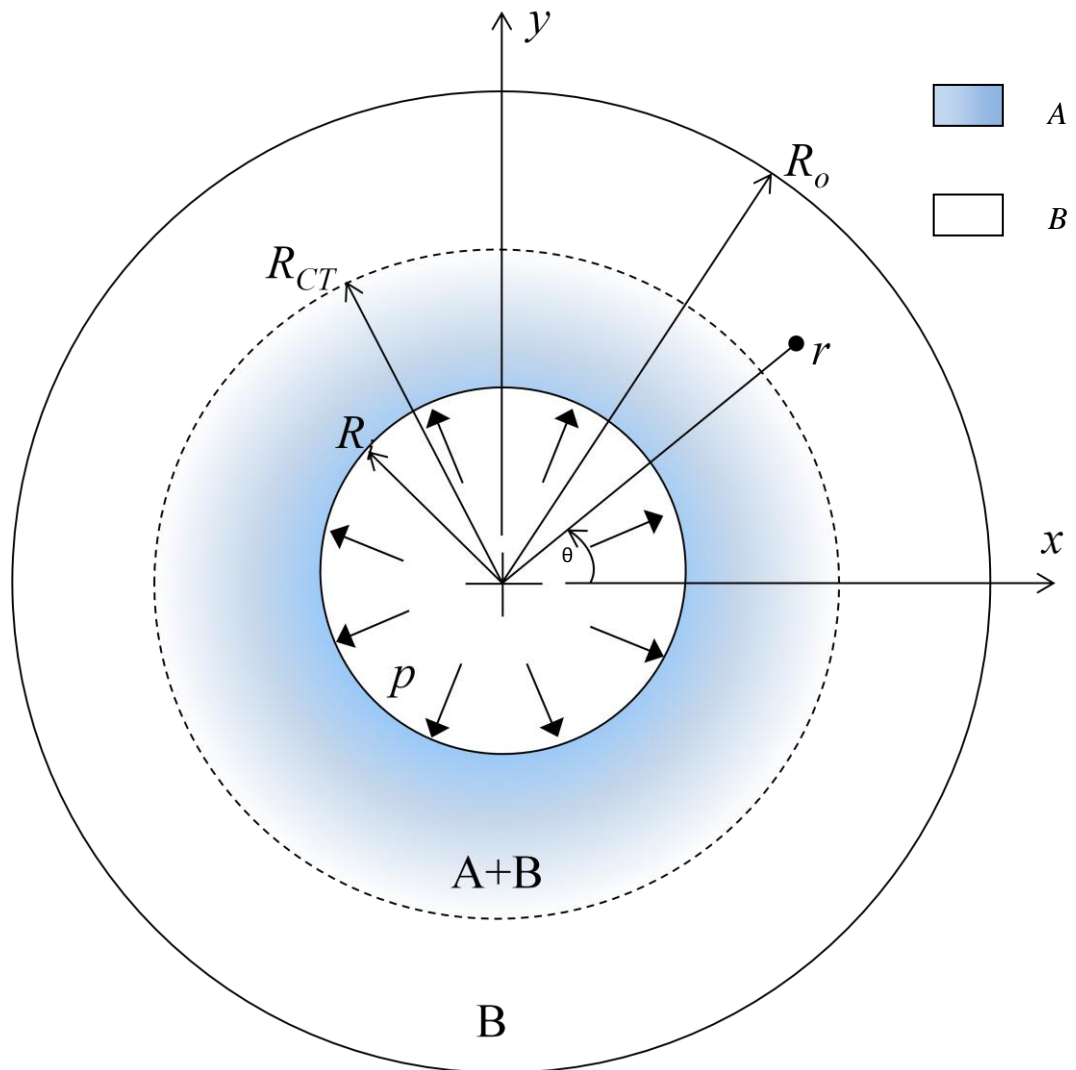**Fig. 3. 2** The normalized geometric factor.

\

Fig. 4. 1 Analytical model of a thick-walled cylinder with FGM coating.
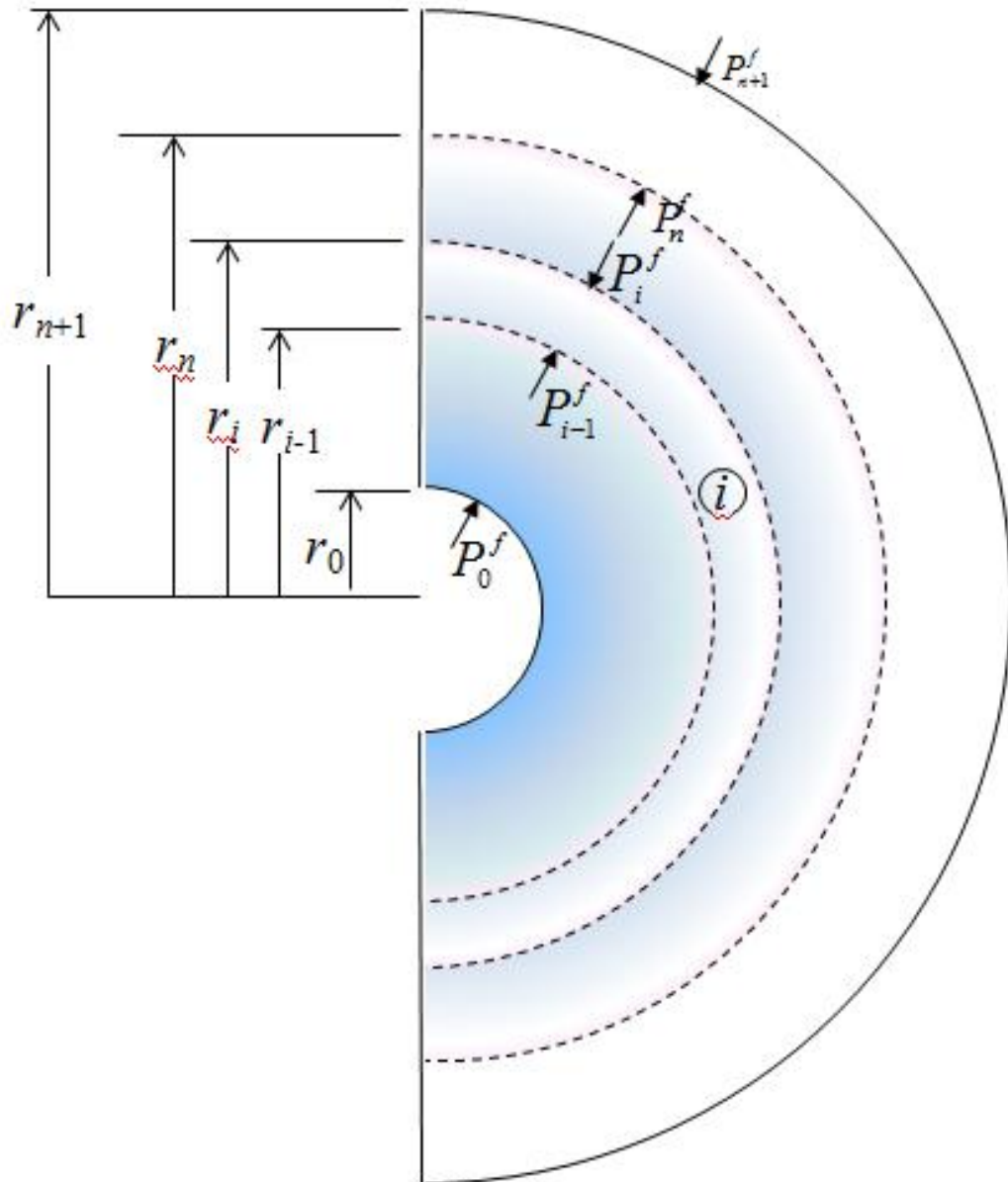
Fig. 4. 2 Model of layered cylinder with FGM coating.

Fig. 4. 3 Thick-walled homogenized cylinder with distributed incompatible and equivalent eigenstrains under a uniformly applied internal pressure.

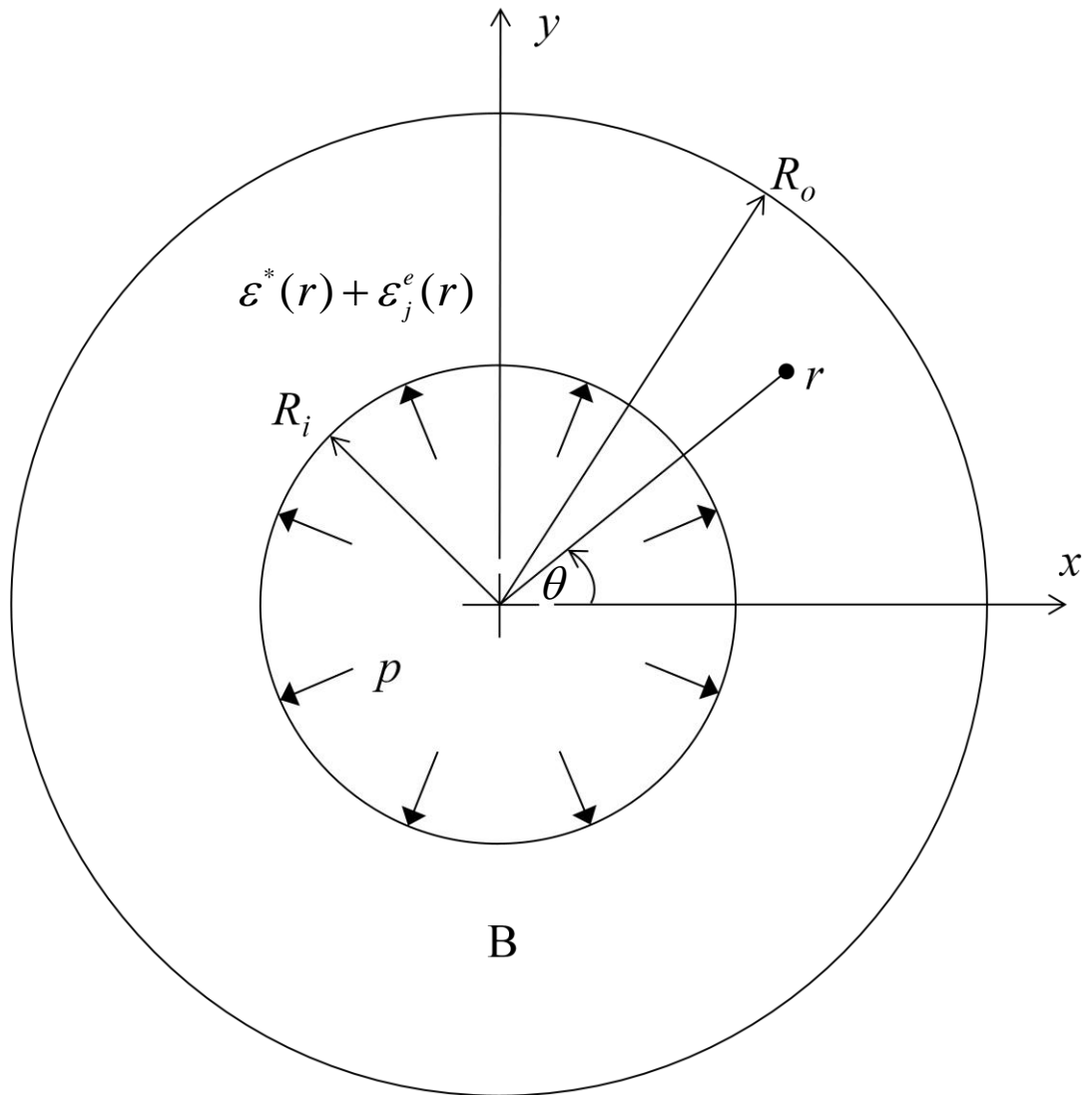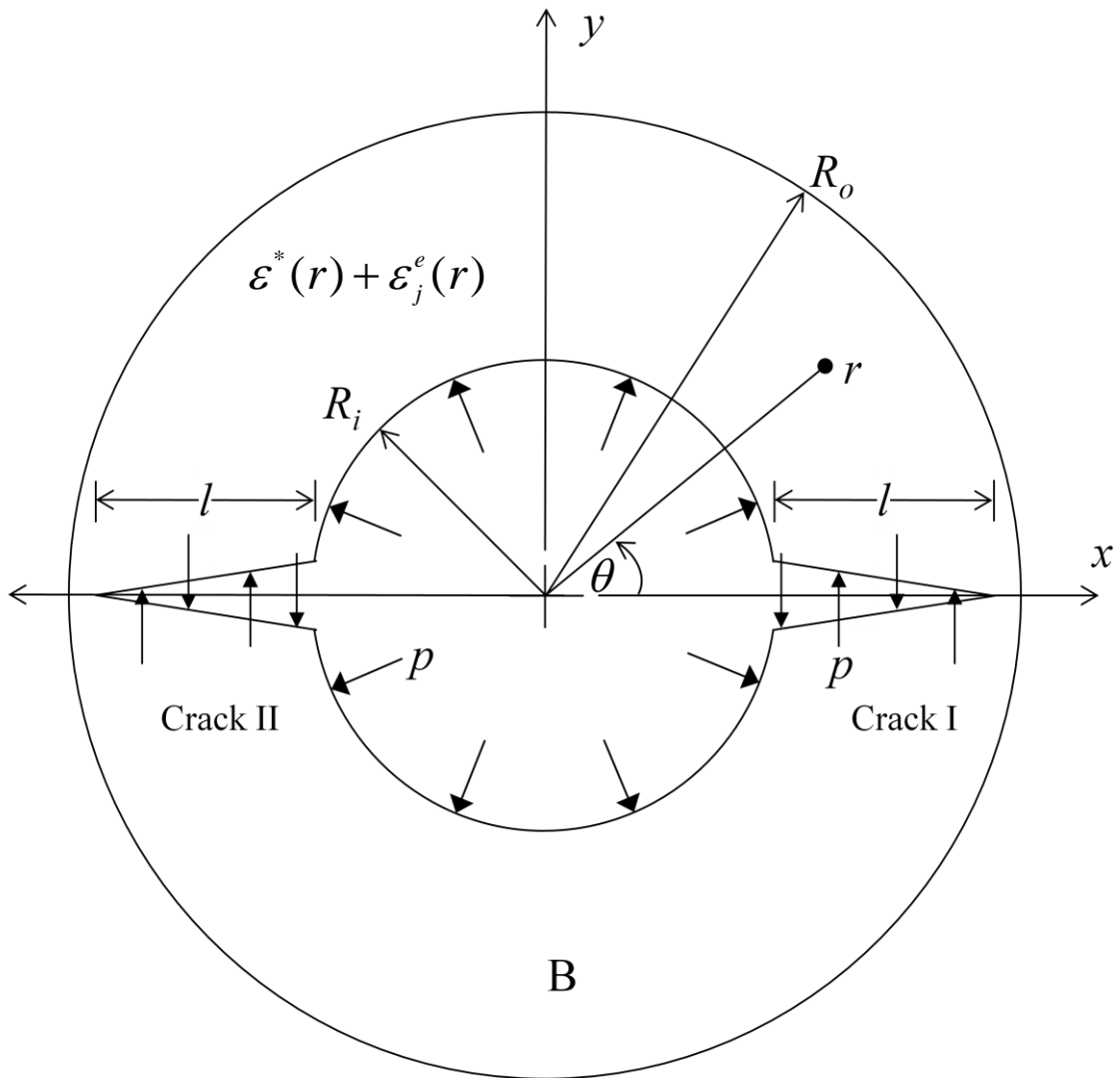**Fig. 4. 4** Two diametrically-opposed edge cracks emanating from the inner surface of a thick-walled homogenized cylinder with distributed incompatible and equivalent eigenstrains under a uniformly applied internal pressure.
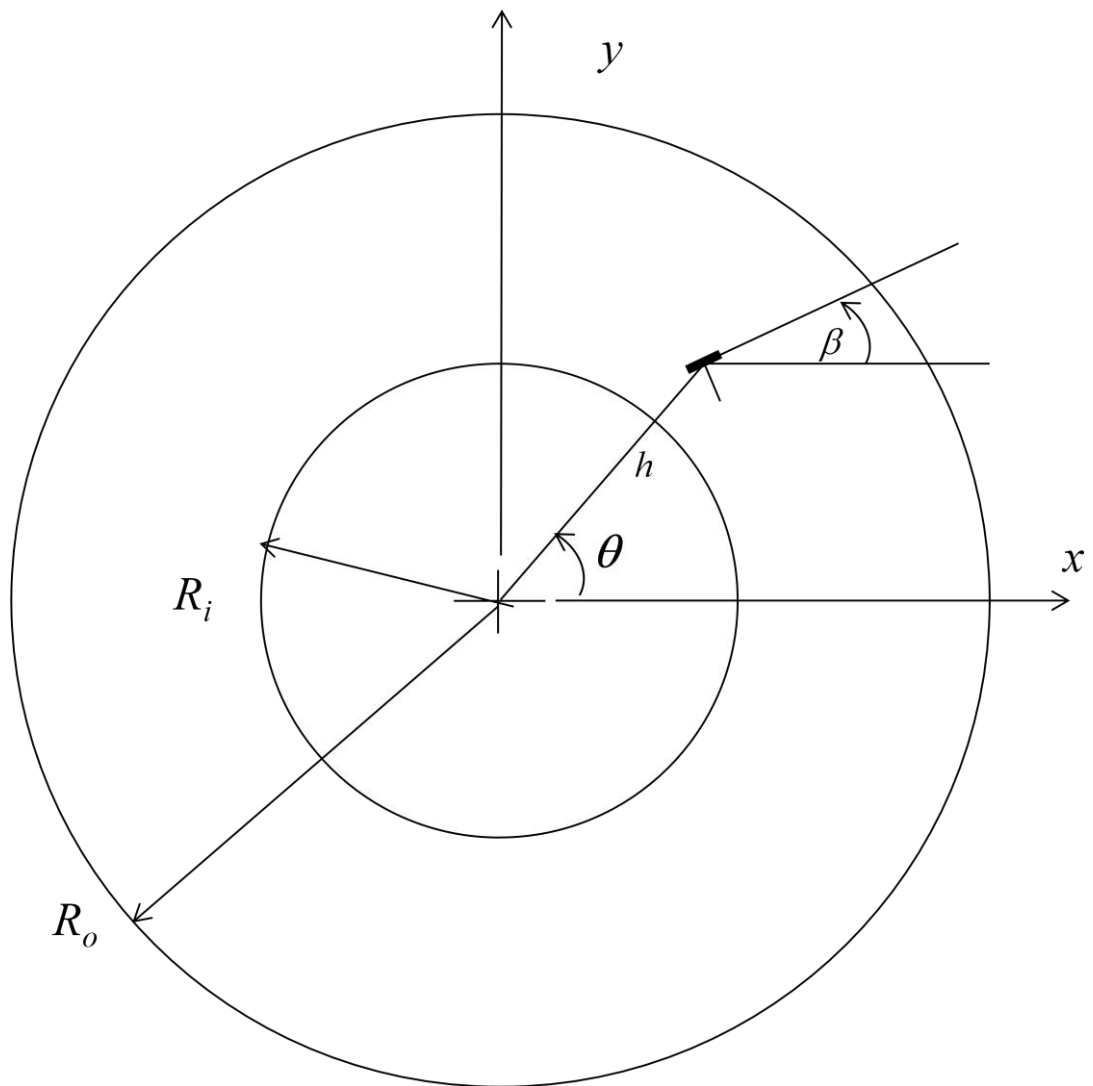
Fig. 4. 5 A discrete edge dislocation at *z=h*
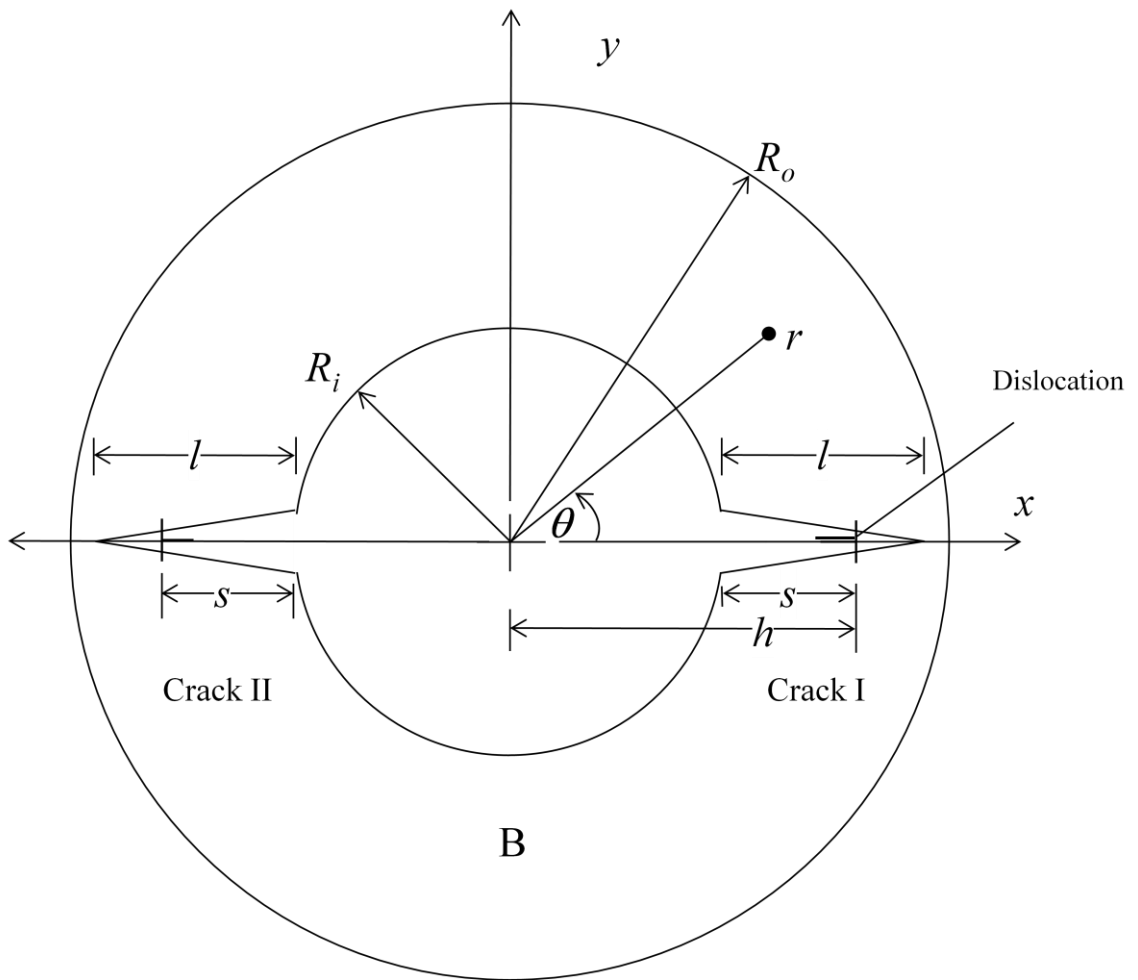
Fig. 4. 6 Two edge dislocations at $z=\pm h$ in a thick-walled homogenized cylinder

Input necessary parameters (mechanical properties, thermal properties, geometric parameters)

Prescribe material distribution in FGM cylinder

Compute effective properties of FGM at each layer by mixture rule

Determine unknown pressures P_i^f and P_i^h

Determine σ_θ^h

$K=1$

$l_k=k(\Delta l_c)$

Find $G_1(H_i,T_j)$, $G_2(H_i,T_j)$ from Eqs.(4.35)

Determine $\varphi(T_j)$ from Eq.(4.42)

$k=k+1$

Output

Determine K_I from Eq.(4.45)

$l_k \leq 0.98(R_o\text{-}R_i)$

No

Yes

Stop

Fig. 5. 1 Flow diagram for calculation of SIF by direct method for an FGM cylinder.

61

Input necessary parameters (mechanical properties, thermal properties, geometric parameters, coating thickness)

$i=1$

Prescribed material distribution, V_A^i in FGM coating only

$i=i+1$

Effective properties of FGM at each layer by mixture rule (E_i, α_i, v_i)

$V_A^i=0.0$
$i=n+1$

Material properties of base material B

Yes   No

$i \leq n$

Determine unknown pressures P_i^f and P_i^h at each layer from Eqs. (4.1) to (4.5) and (4.8) to (4.12)

Determine σ_θ^h from Eq.(4.19(b))

$k=1$

$l_k = k(\Delta l_c)$

$k=k+1$

Find $G_1(H_i,T_j)$, $G_2(H_i,T_j)$ from Eqs.(4.35)

Determine $\varphi(T_j)$ from Eq.(4.42)

Determine K_I from Eq.(4.45)

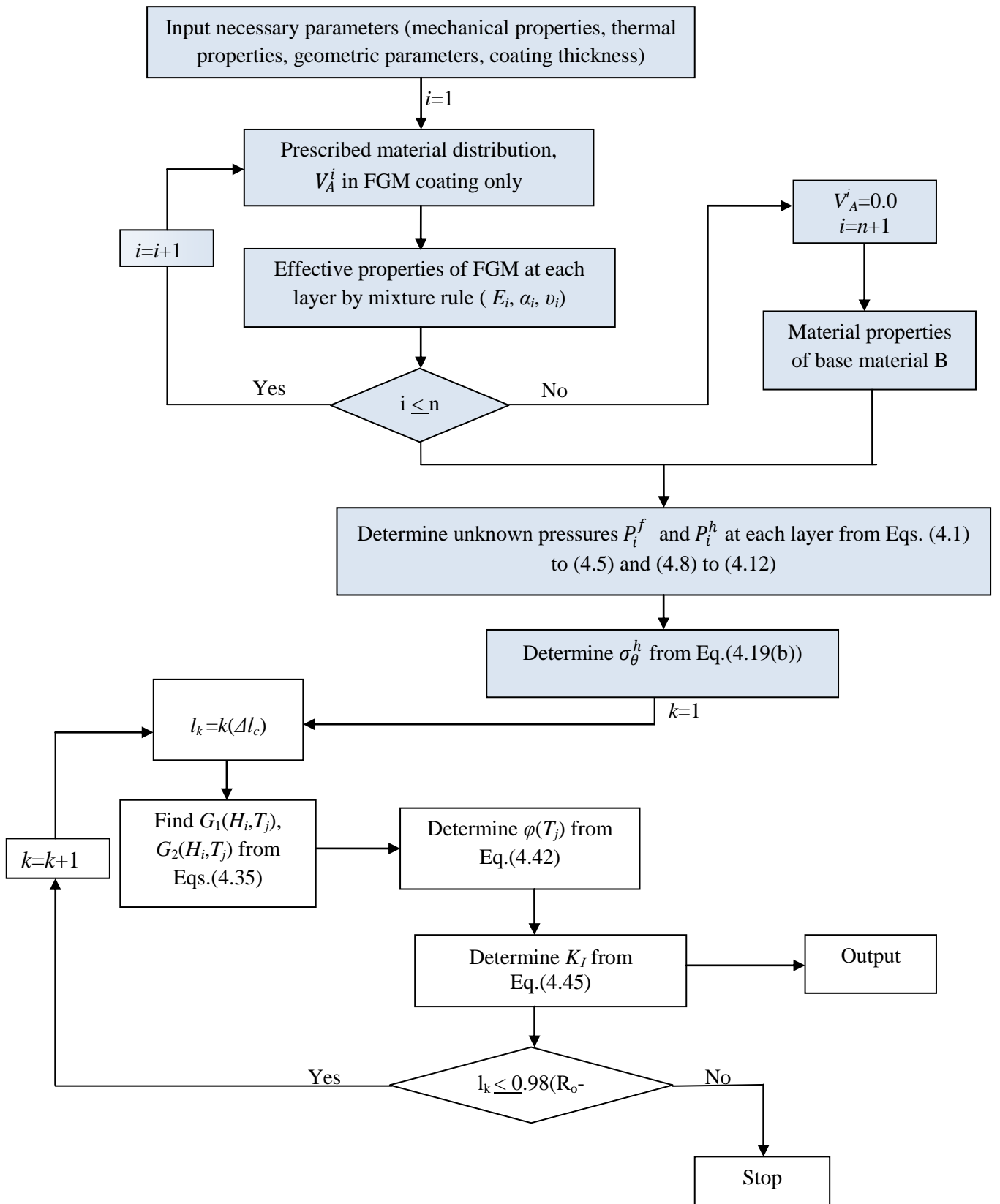Output

Yes   No

$l_k \leq 0.98(R_o-$

Stop

Fig. 5. 2 Flow diagram for determination of SIF by direct method for cylinder with FGM coating.

62

Fig. 5. 3 Flowchart for inverse problem of material distribution to realize prescribed apparent fracture toughness in an FGM cylinder.

Input all necessary parameters

Prescribe apparent fracture toughness up to $L\%$ of cylinder wall thickness.

$i=1$

Initialize V_A^i $(i=1, n)$

$i=i+1$

Yes

$i \leq n$

No

$V_A^i=0.0$, $(i=n+1)$

$l_j = j(\Delta l); j=1$

Calculate P_C from $K_{IC}^a = Fp_c\sqrt{\pi d}$ Eq.(3.3)

Calculate K_I^J using Eq.(4.42) to (4.45)

K_C^J using Eq. (3.4)

$\Delta K = K_I^J - K_C^J$

$j = j+1$
$l_j = j(\Delta l)$

Yes

$l_i < L\%$

No

Evaluate Objective Function, $F_{obj}(V_A^i) = (\Delta K)^2$

ADS

Converged to minimum?

Yes

$F_{obj}(V_A^i) \leq \epsilon_k$

Yes

Output V_A^i $(1,n)$
$V_A^i=0.0$ $(i=n+1)$

No

No

Update V_A^i
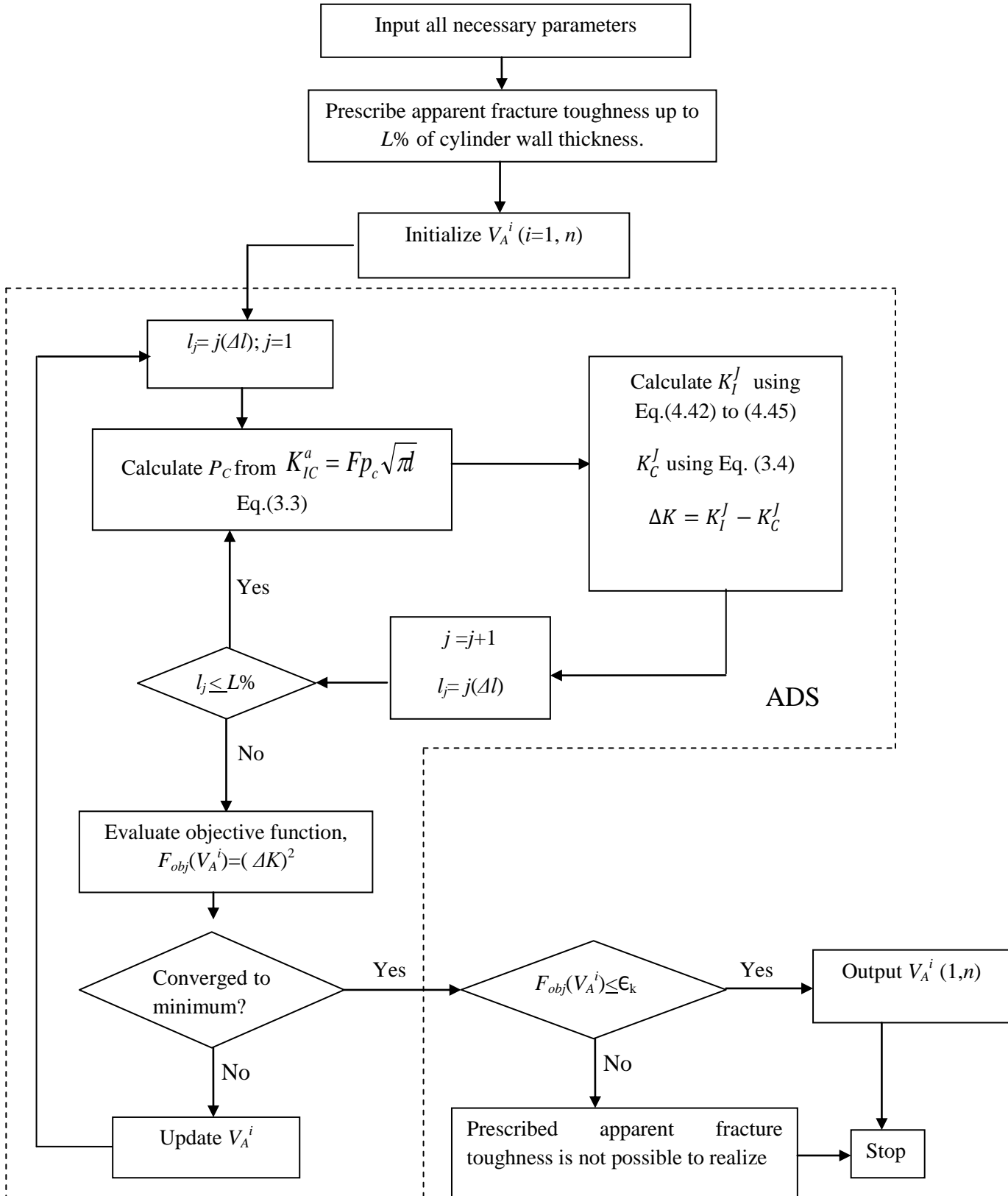
Prescribed apparent fracture toughness is not possible to realize
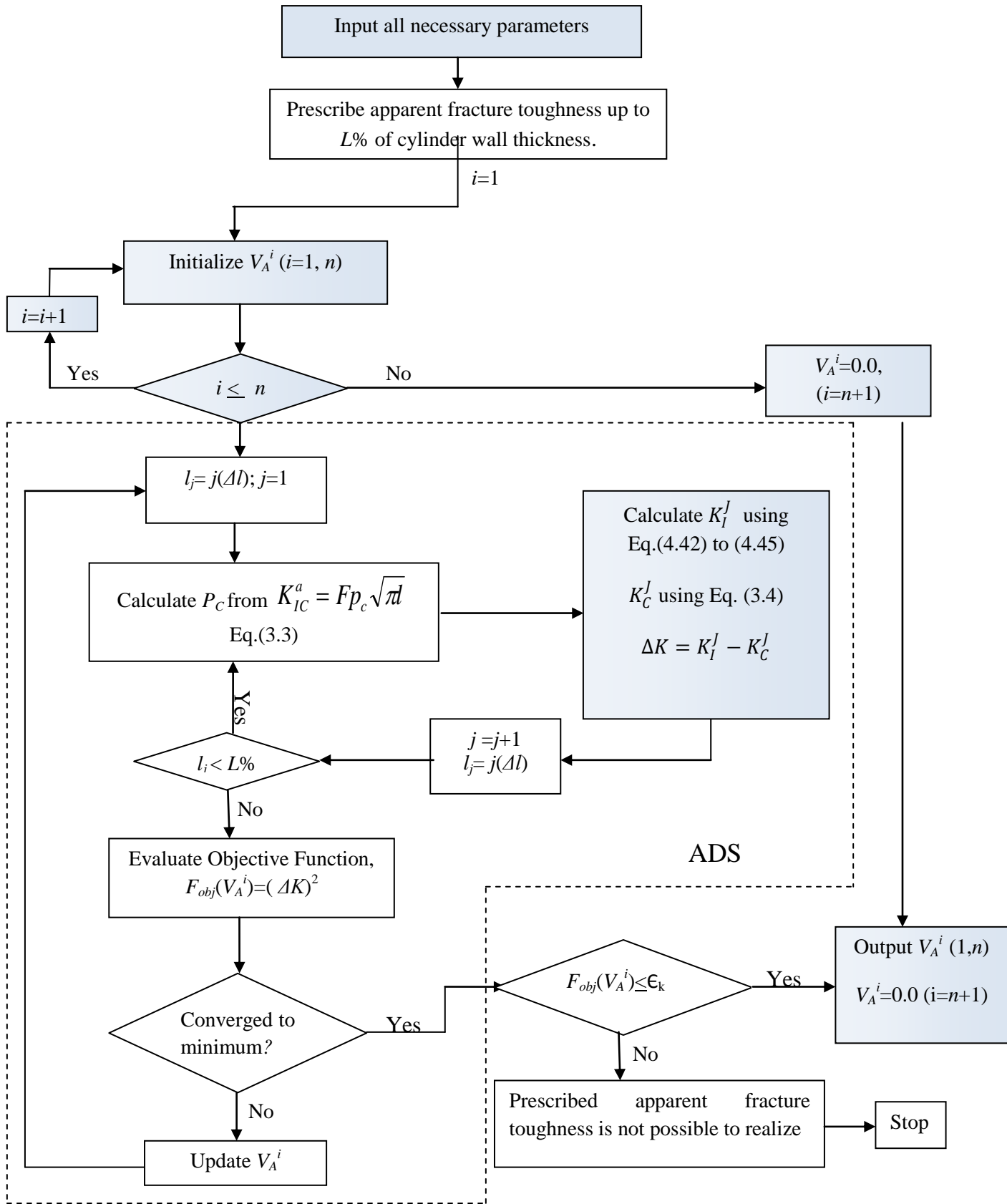
Stop

Fig. 5. 4 Flowchart for inverse problem of material distribution to realize prescribed apparent fracture toughness in a cylinder with FGM coating.
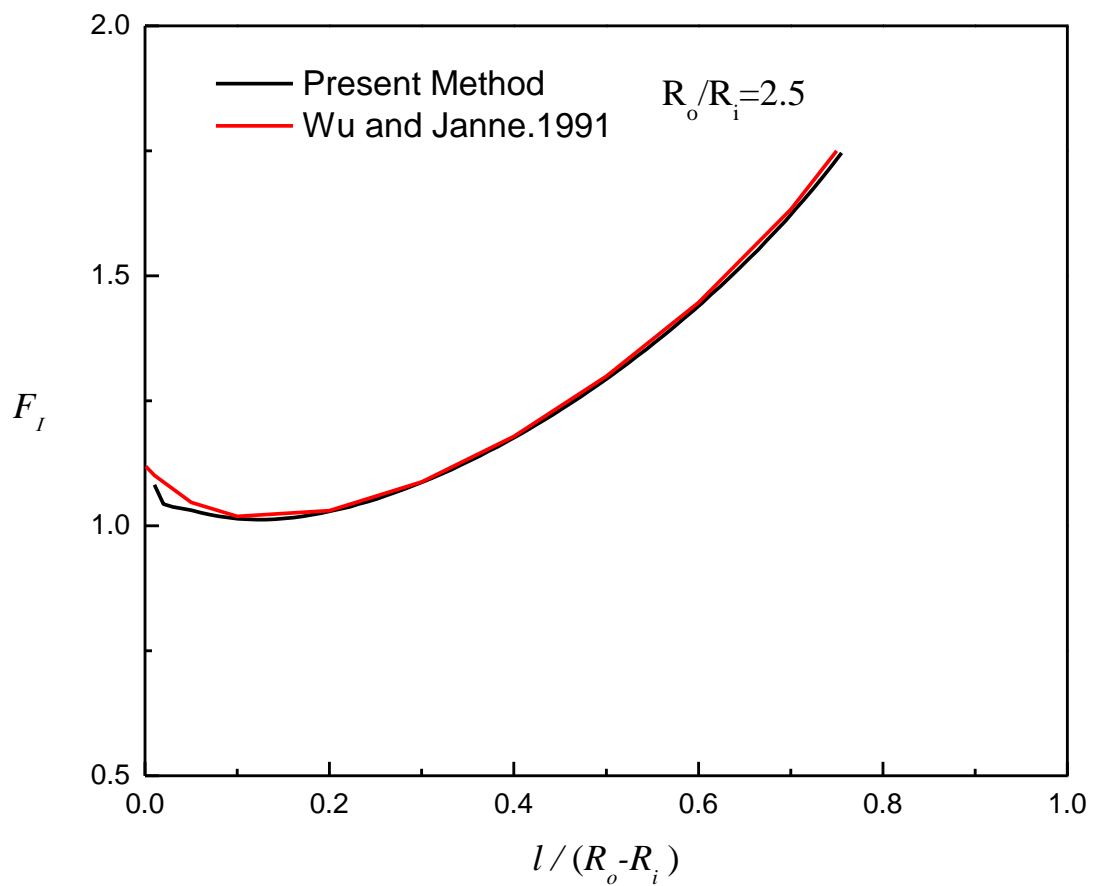
64

Fig. 5. 5 Comparison of normalized stress intensity factors for two diametrically opposed edge cracks in a homogeneous cylinder obtained by the present method and by Wu and Janne [48].
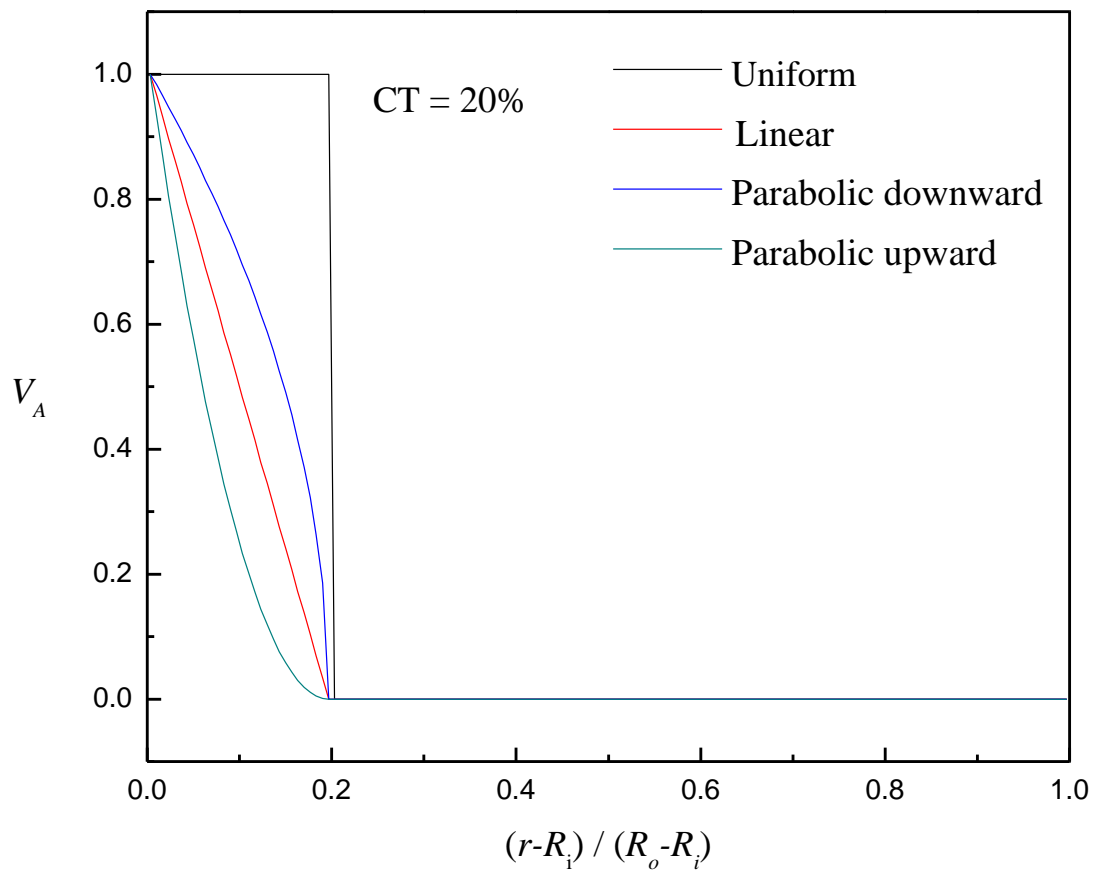
Fig. 5. 6 Prescribed material distributions of TiC in a thick-walled cylinder with TiC/Al$_2$O$_3$ FGM coating.
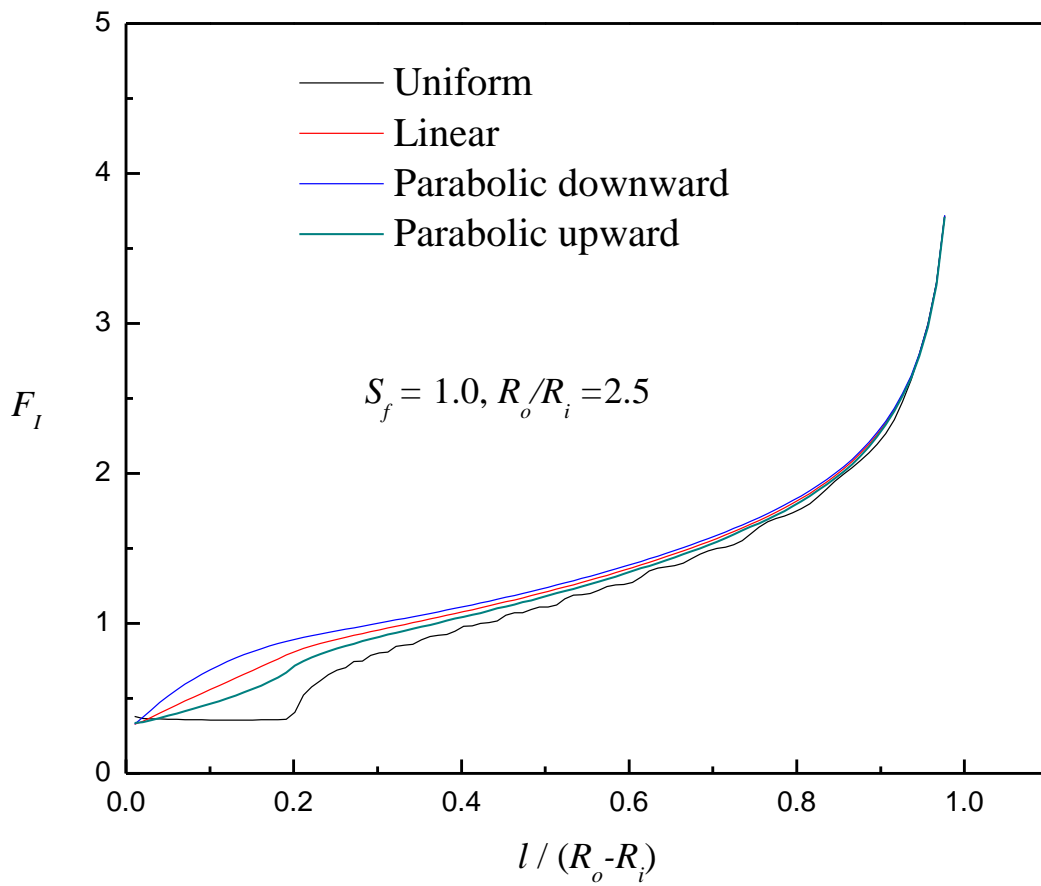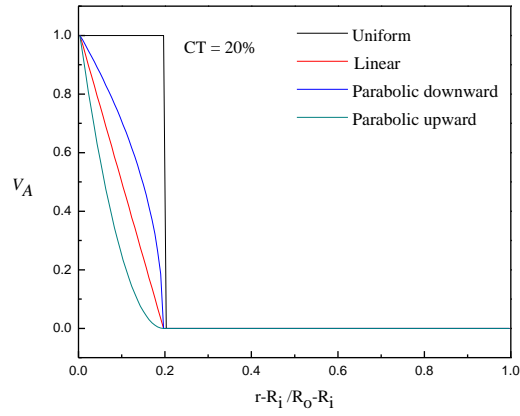
Fig. 5. 7 Effect of material distribution on normalized stress intensity factors.
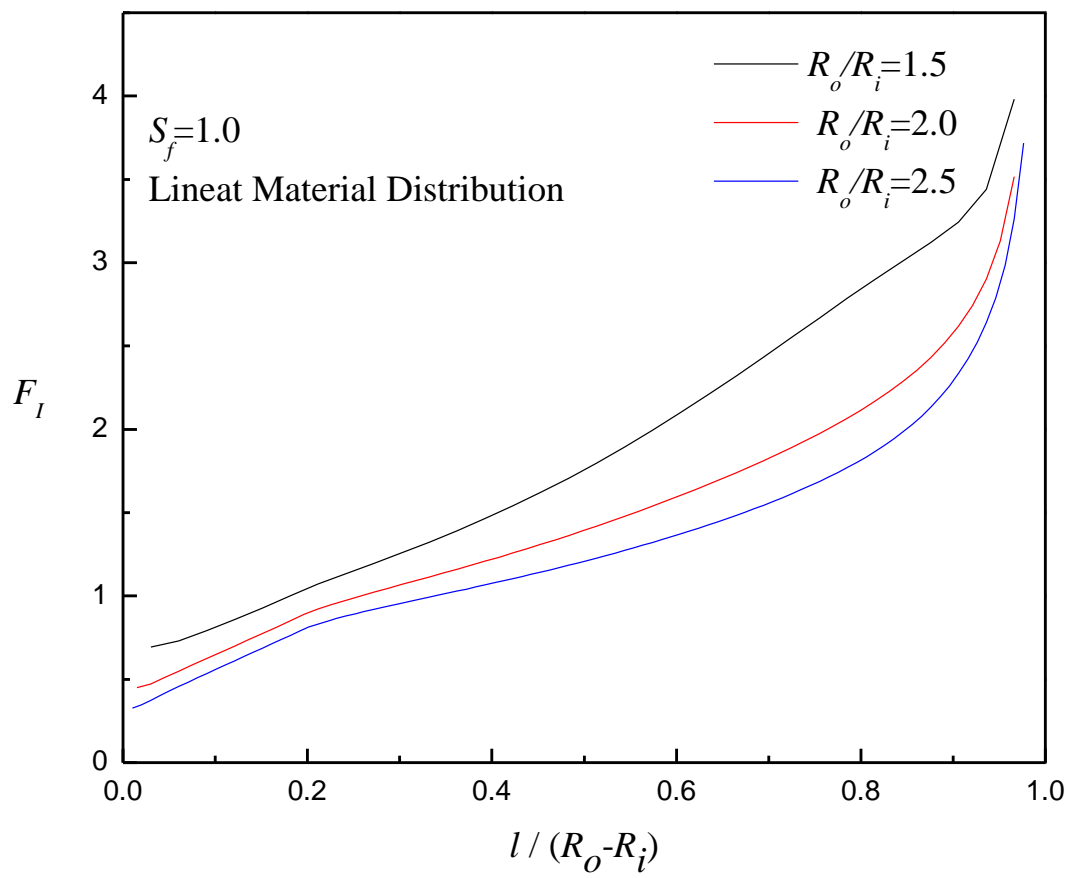
Fig. 5. 8 Normalized stress intensity factors as a function of cylinder wall thickness.
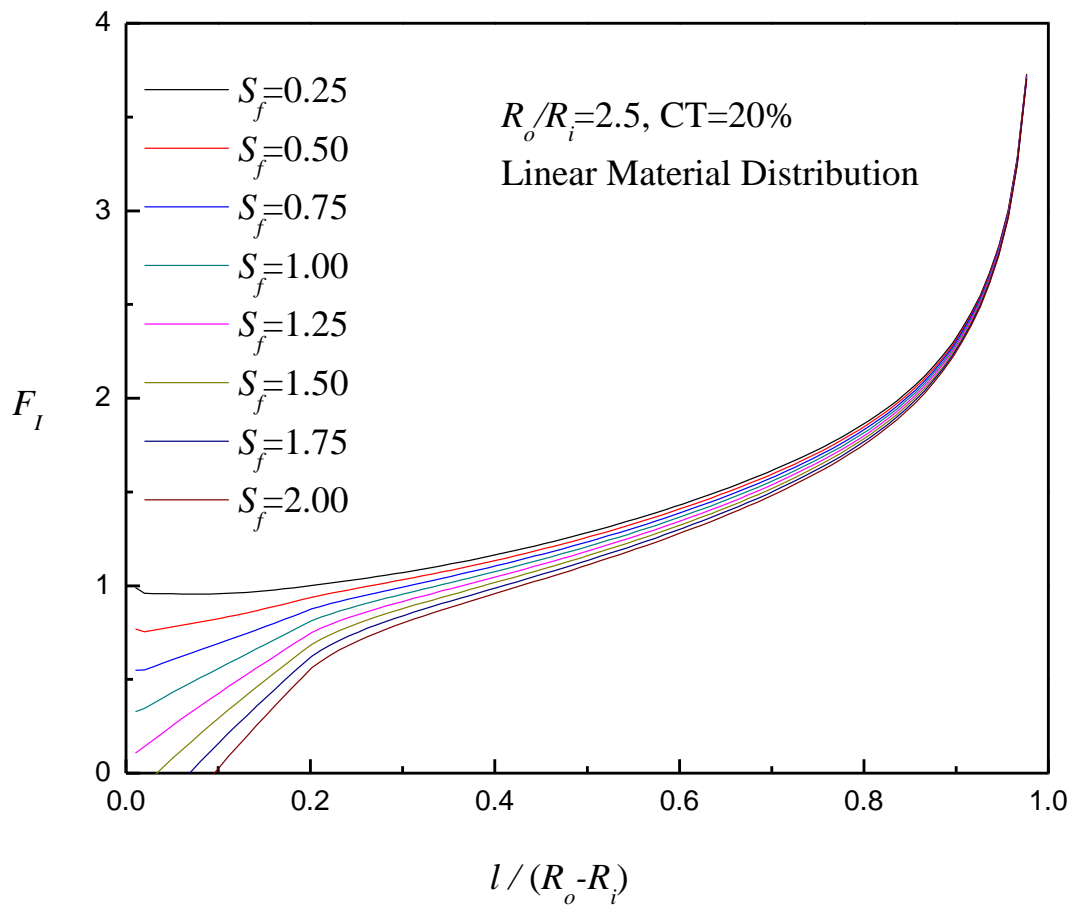
Fig. 5. 9 Normalized stress intensity factors as a function of strength factor.
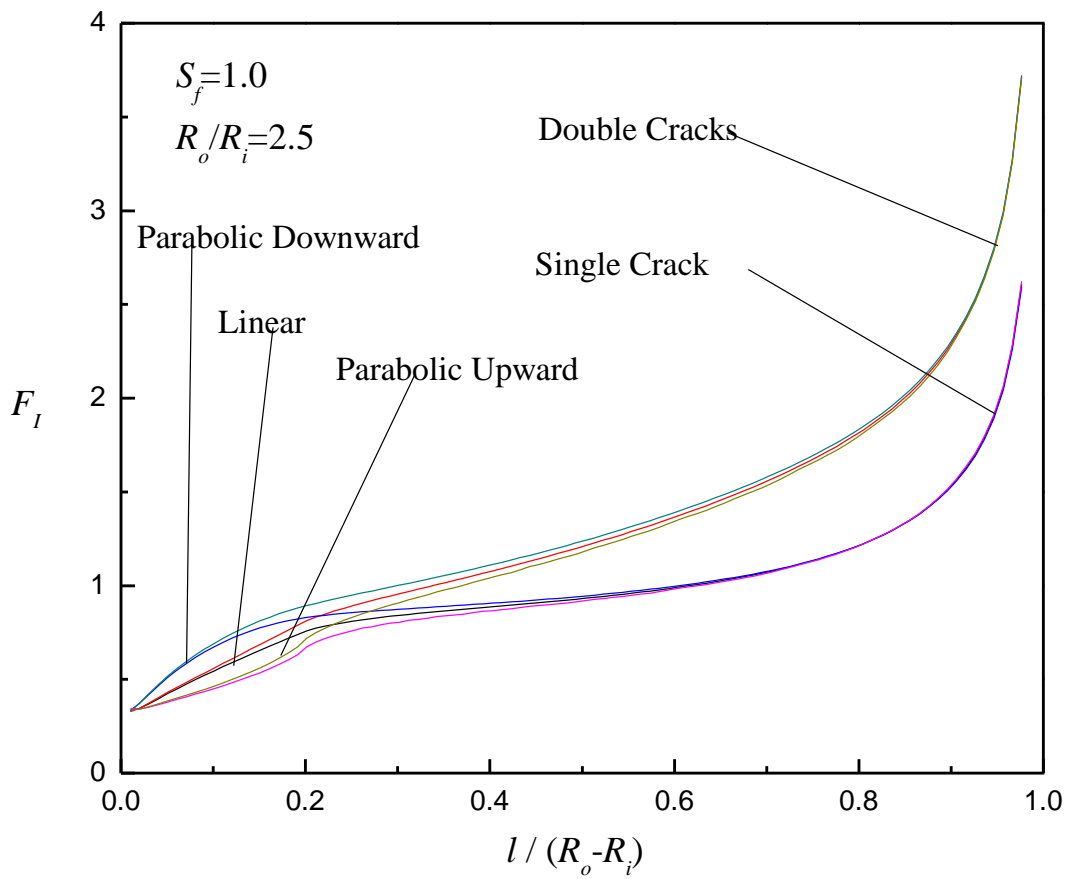
Fig. 5. 10 Comparison of normalized stress intensity factors for a single and two diametrically opposed cracks.
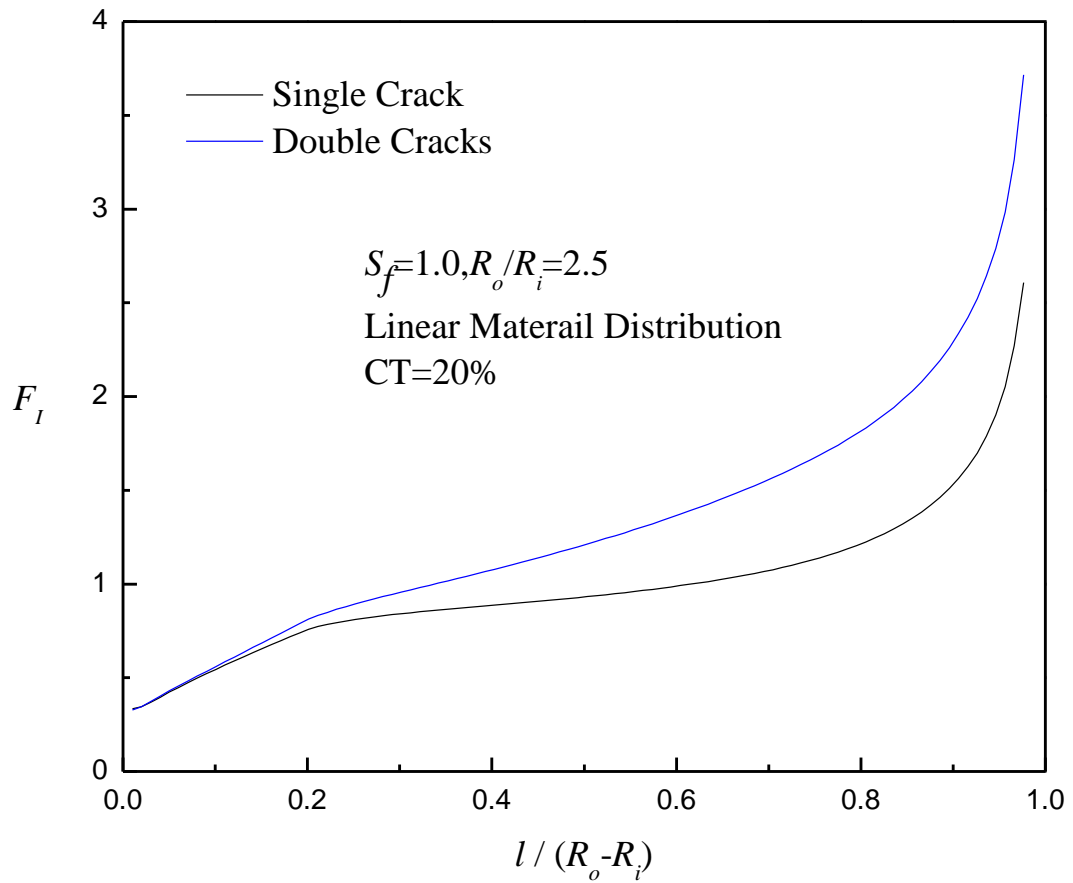
Fig. 5. 11 Comparison of normalized stress intensity factors for a single and two diametrically-opposed edge cracks.
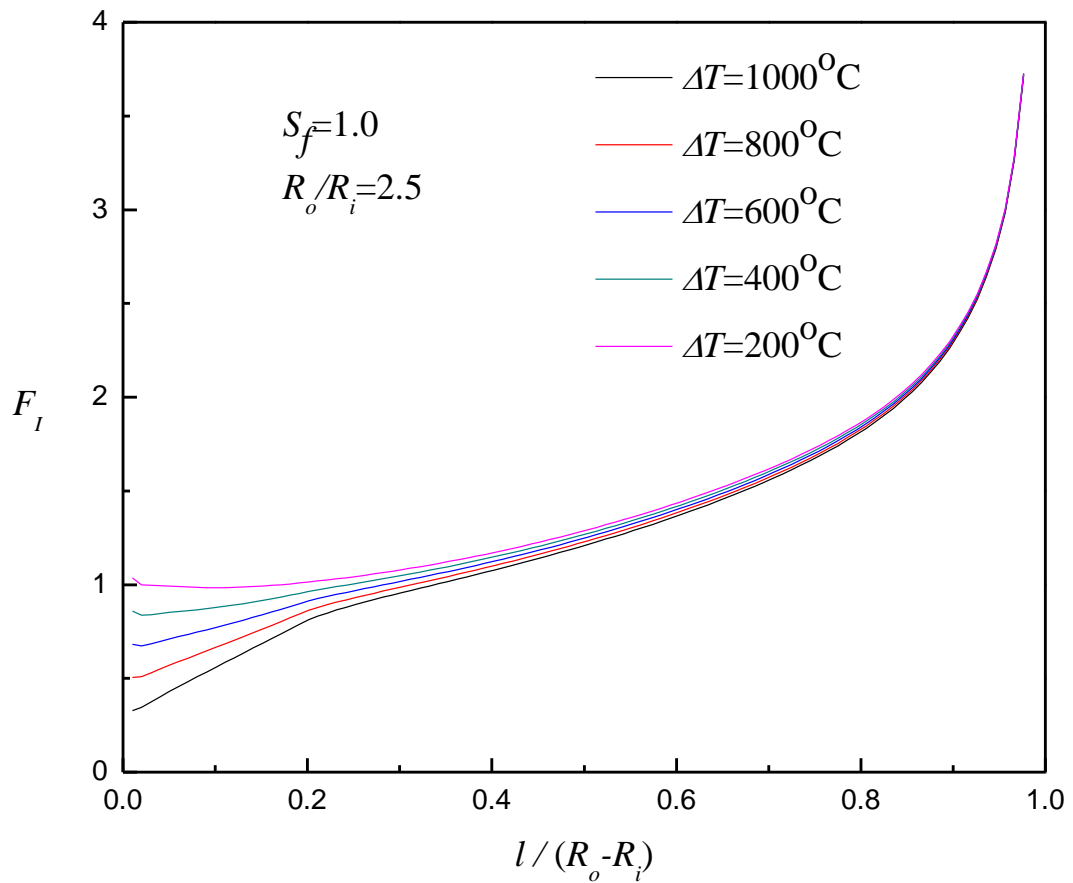
Fig. 5. 12 Normalized stress intensity factors as function of difference in sintering and application temperature.
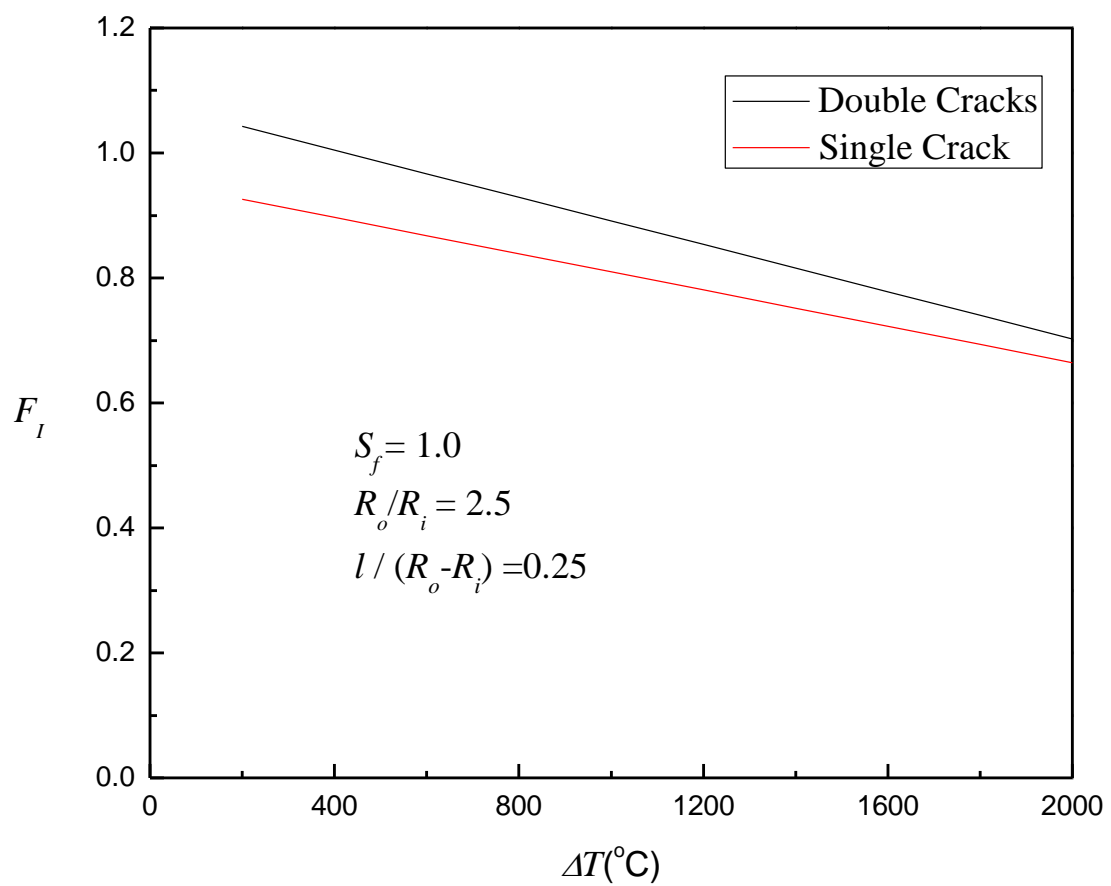
Fig. 5. 13 Comparison of normalized stress intensity factors for a single and two diametrically opposed cracks as a function of difference between sintering and application temperature.
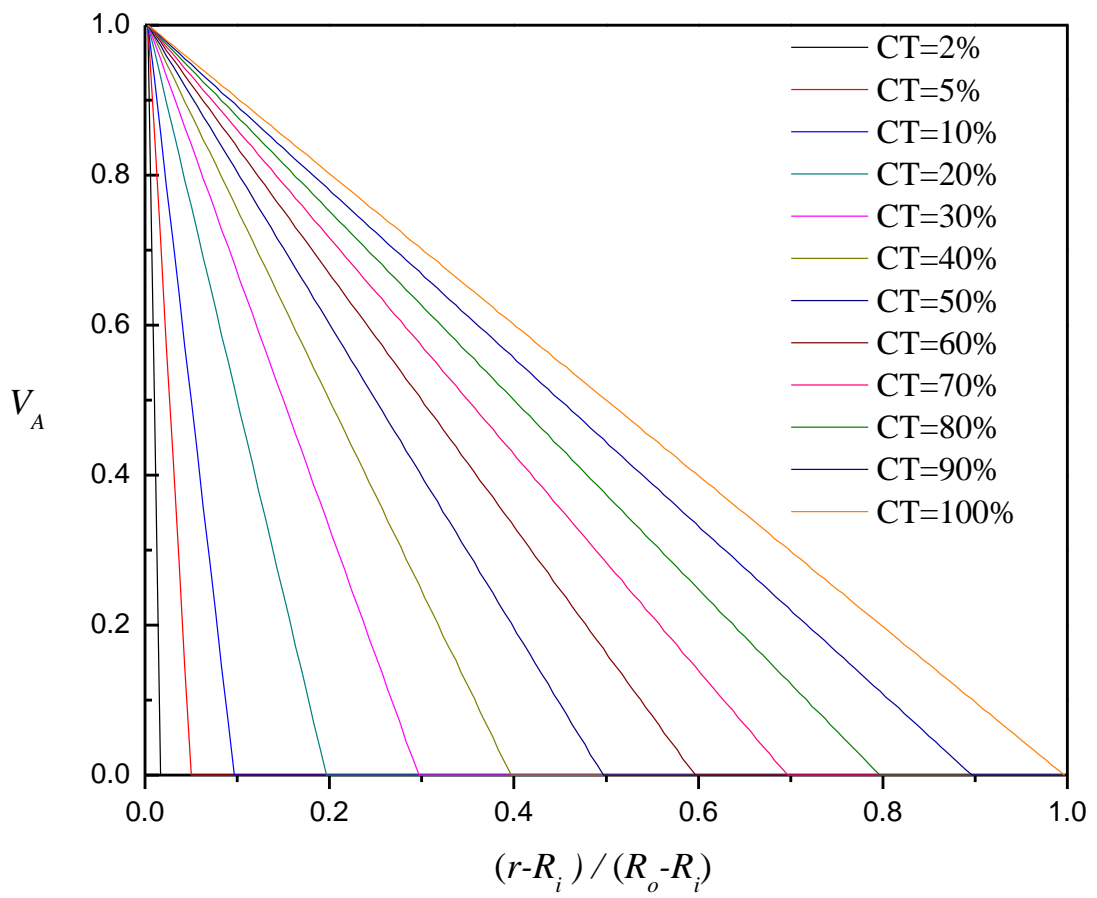
Fig. 5. 14 Coating thickness and distribution of TiC.
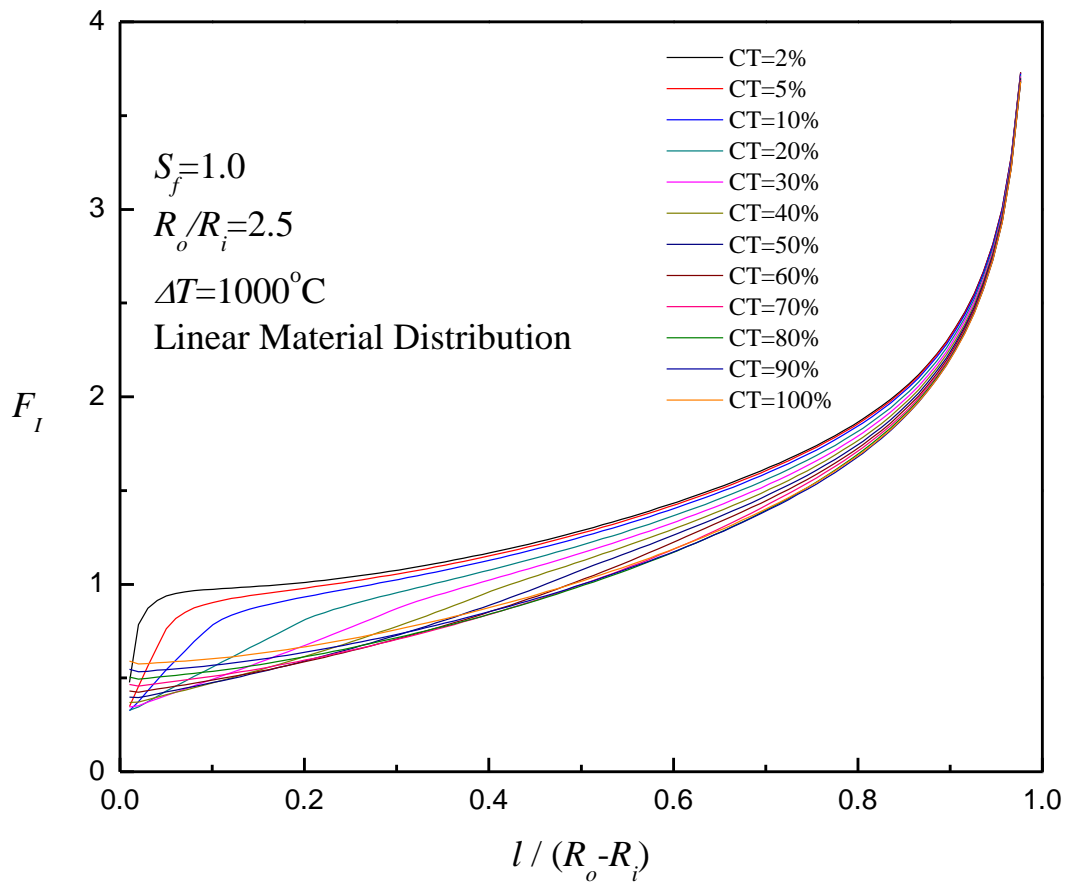
Fig. 5. 15 Effect of coating thickness on normalized stress intensity factor.
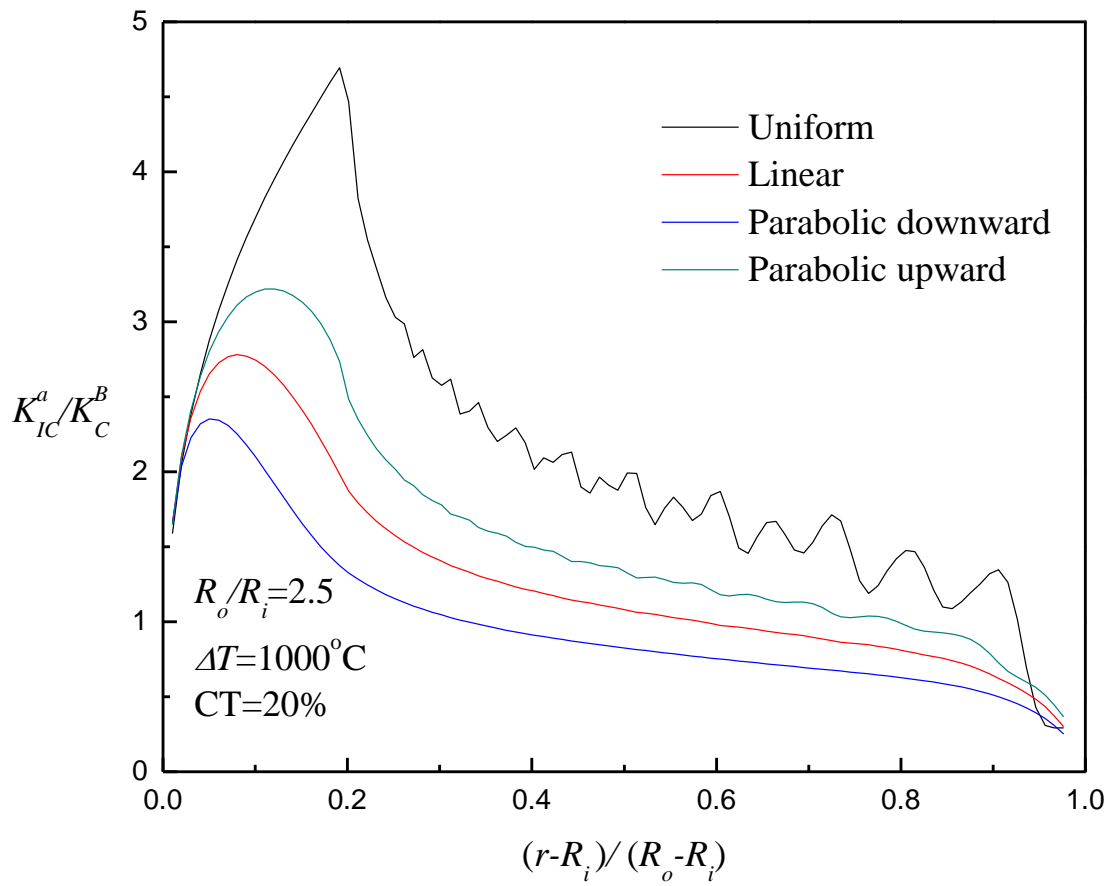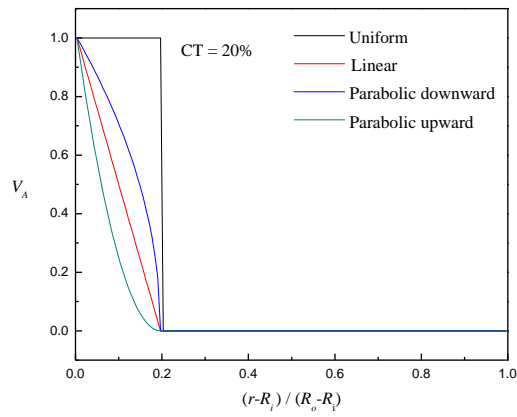
Fig. 5. 16 Effect of material distribution on apparent fracture toughness.
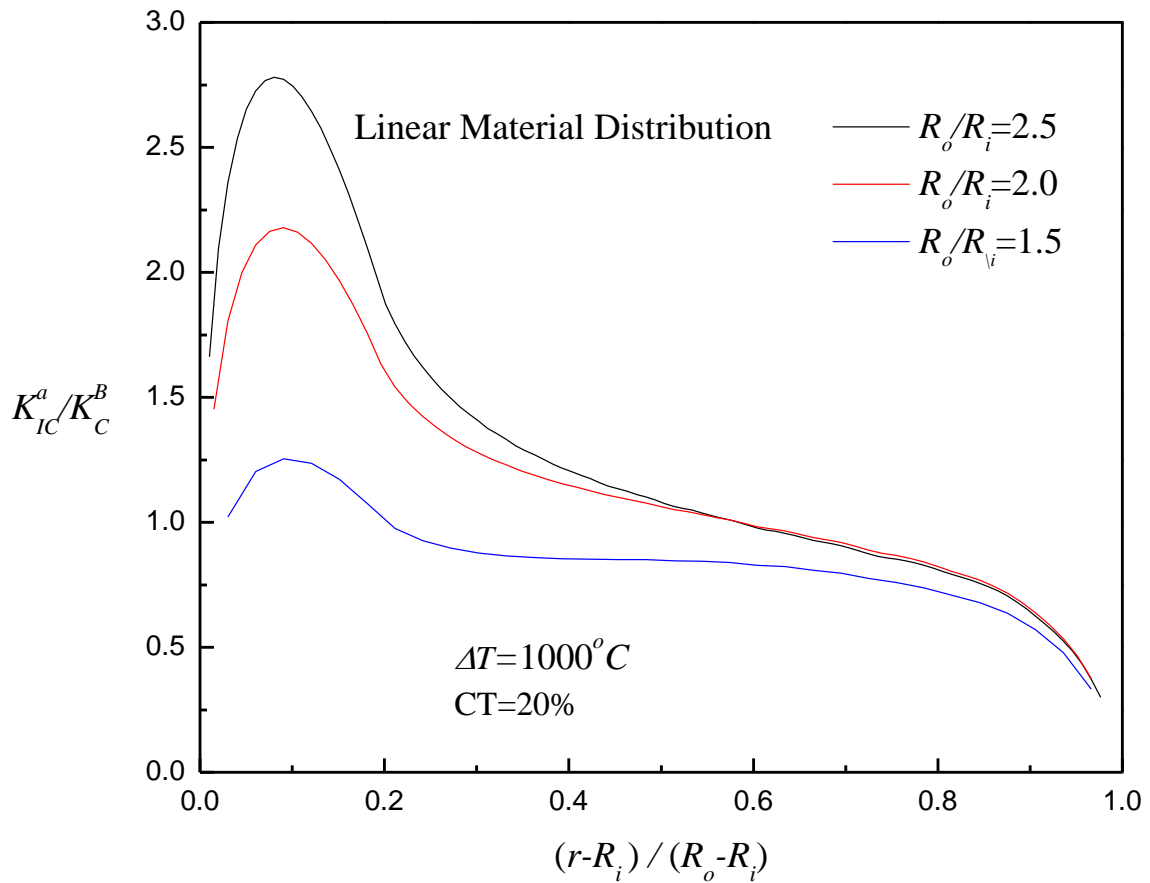
Fig. 5. 17 Effect of cylinder wall thickness on the apparent fracture toughness.
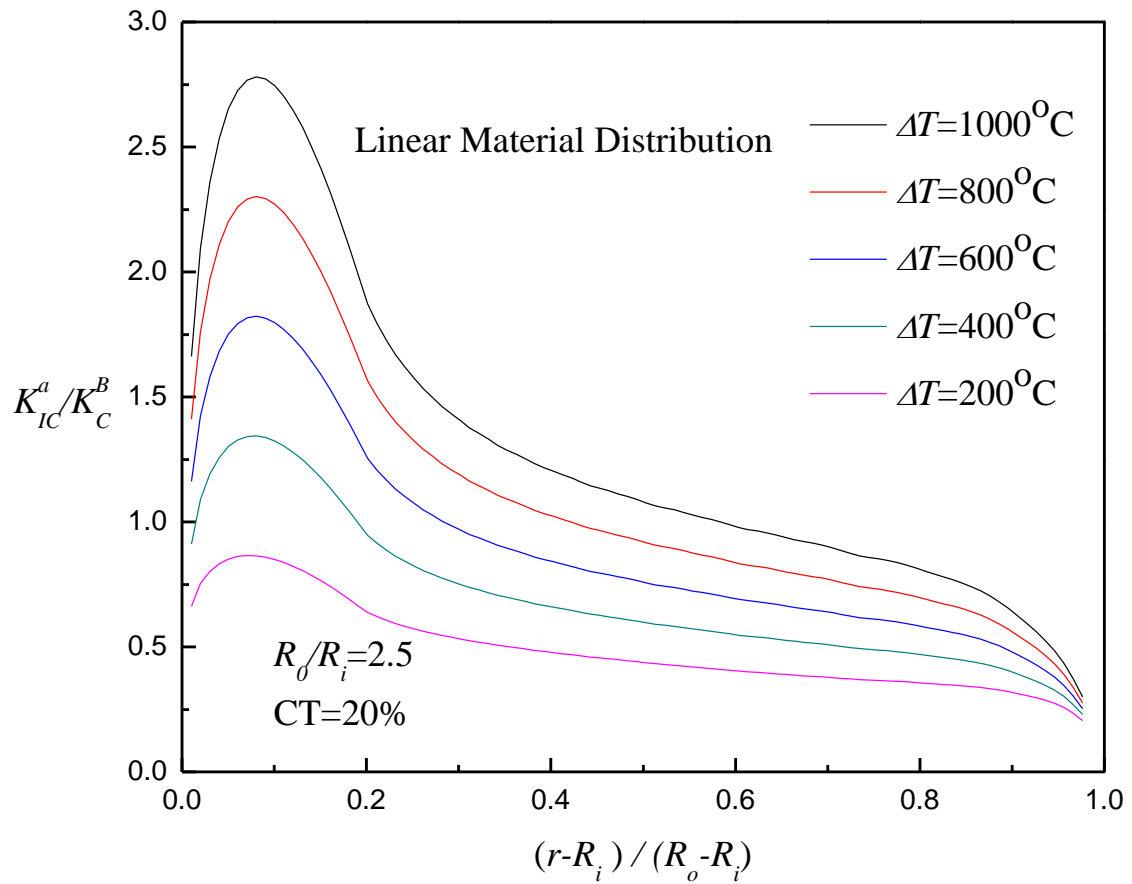
Fig. 5. 18 Effect of application temperature on the apparent fracture toughness.
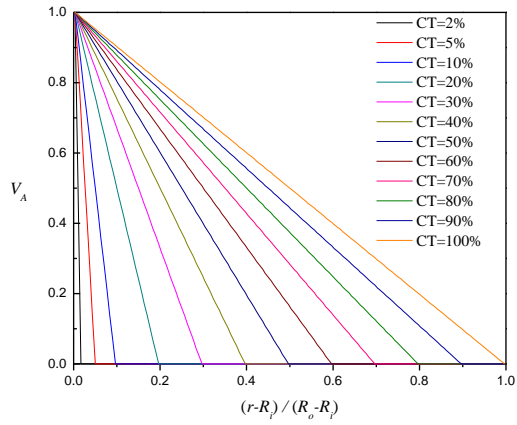
Fig. 5. 19 Coating thickness and distributioon of TiC.
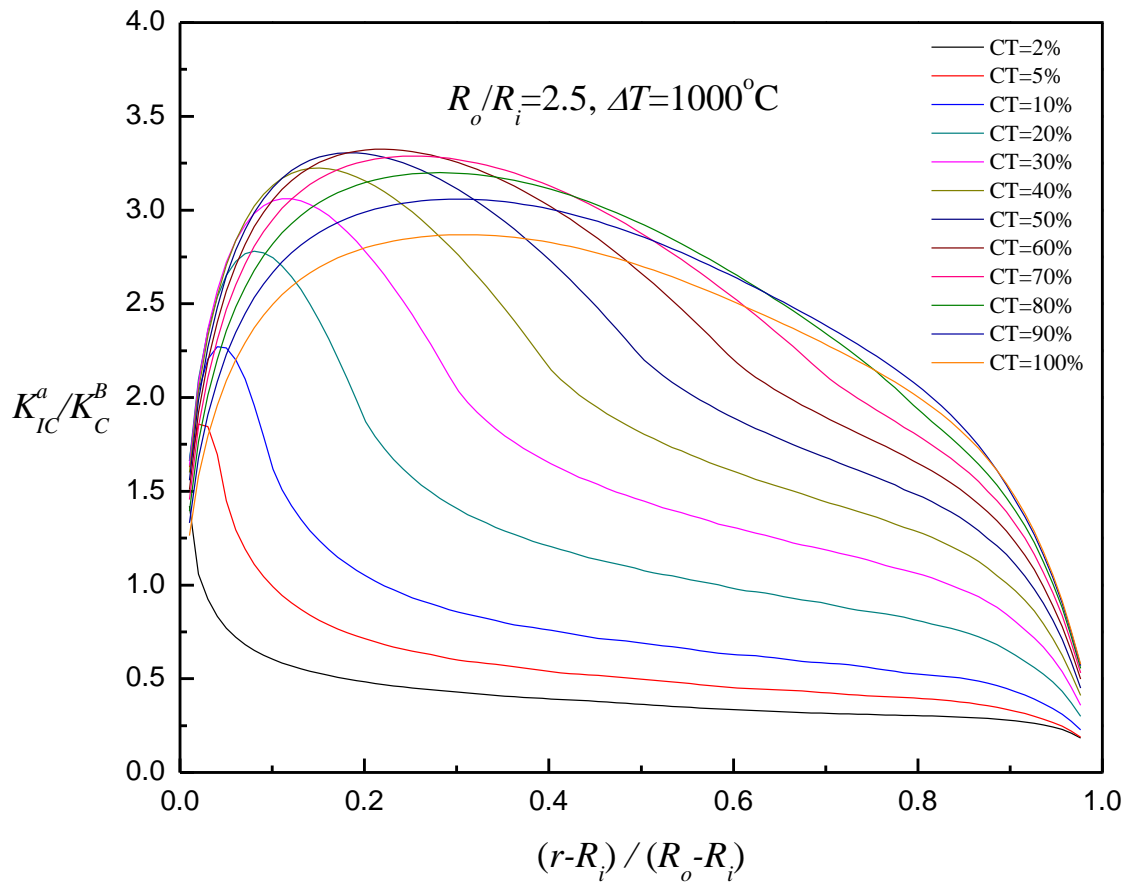
Fig. 5. 20 Effect of coating thickness on apparent fracture toughness.
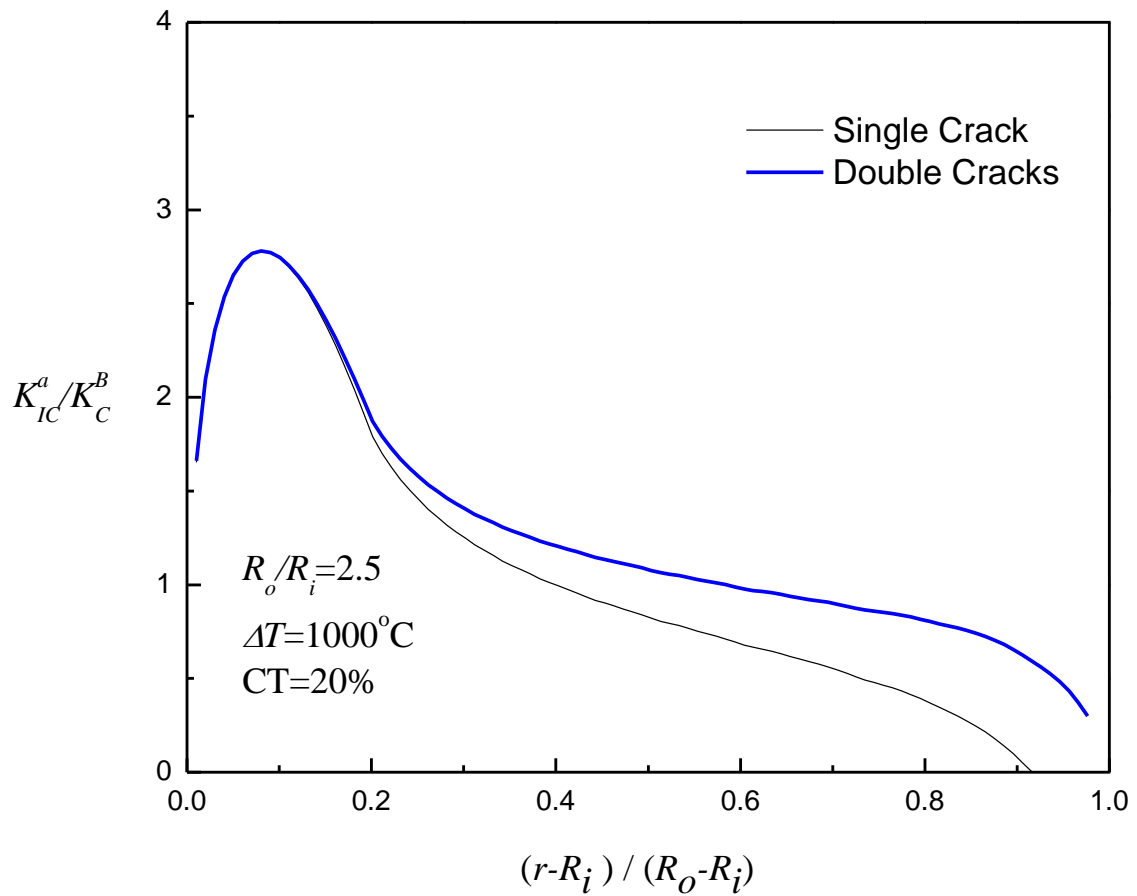
Fig. 5. 21 Effect of number of cracks on apparent fracture toughness.
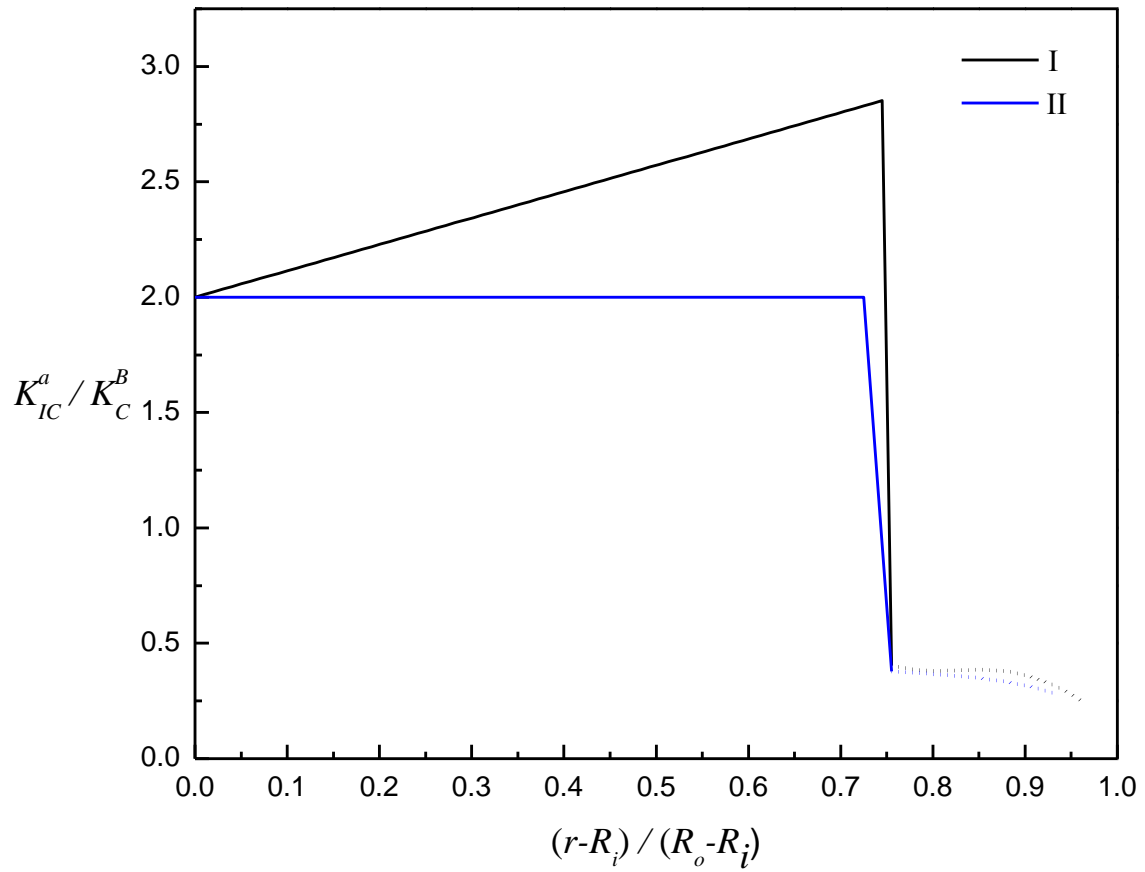
Fig. 5. 22 Prescribed apparent fracture toughness in a thick-walled cylinder with TiC/Al$_2$O$_3$ FGM coating.
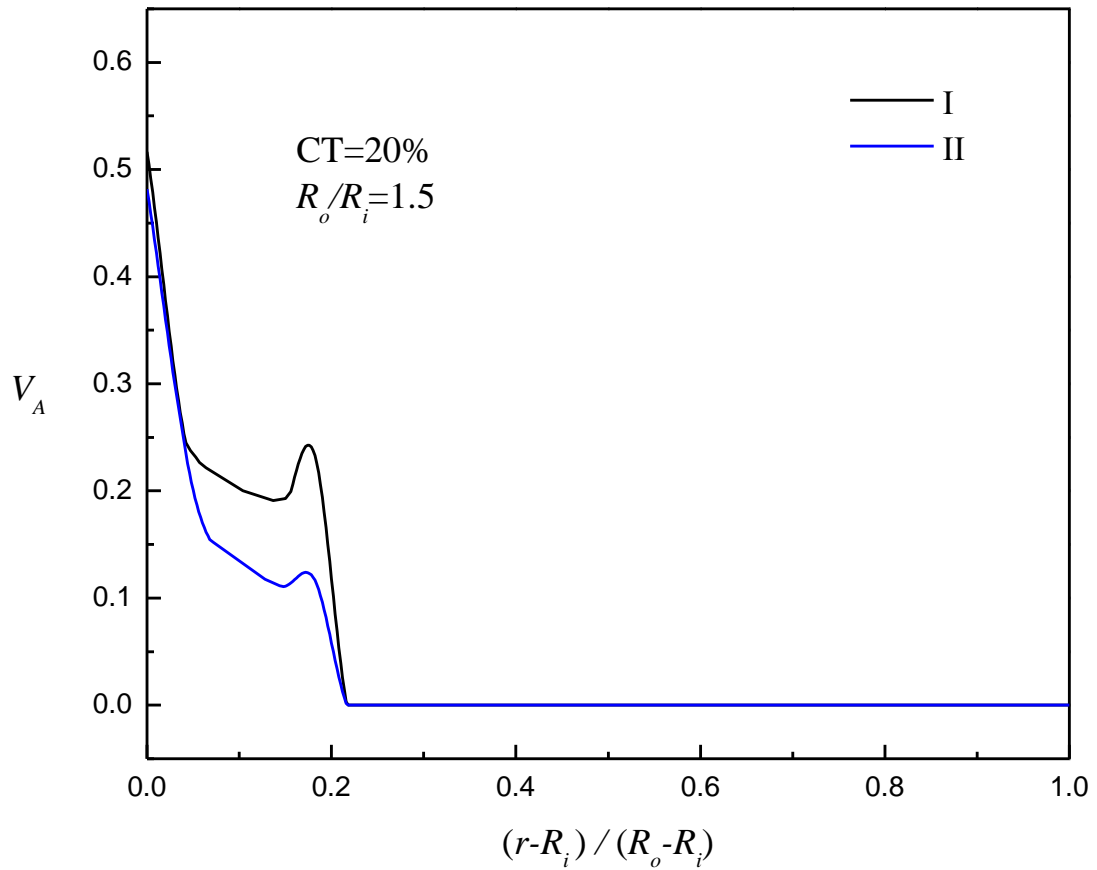
Fig. 5. 23 Material distributions of TiC in a thick-walled cylinder with 20% TiC/Al$_2$O$_3$ FGM coating at the inner surface.
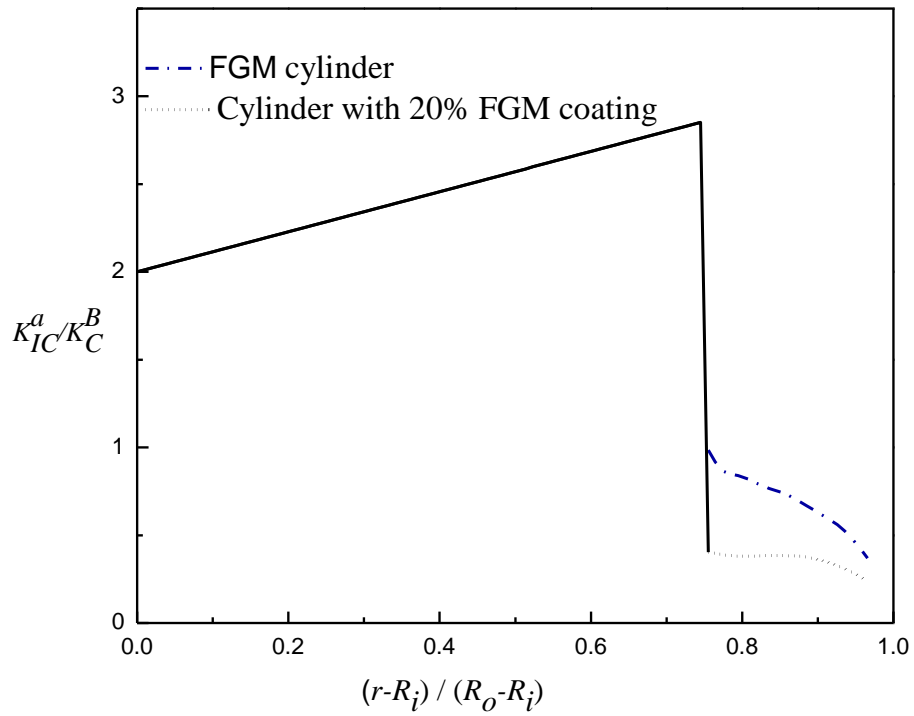
Fig. 5. 24 Prescribed apparent fracture toughness.
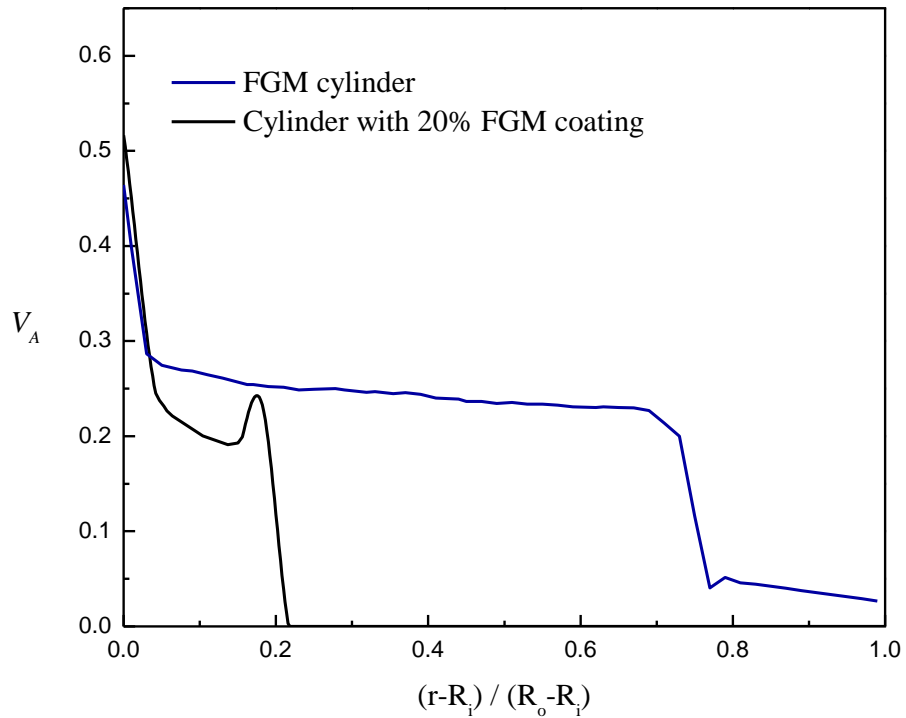
Fig. 5. 25 Comparison of material distribution for cylinder with 20% FGM coating and FGM cylinder for same prescribed apparent fracture toughness.
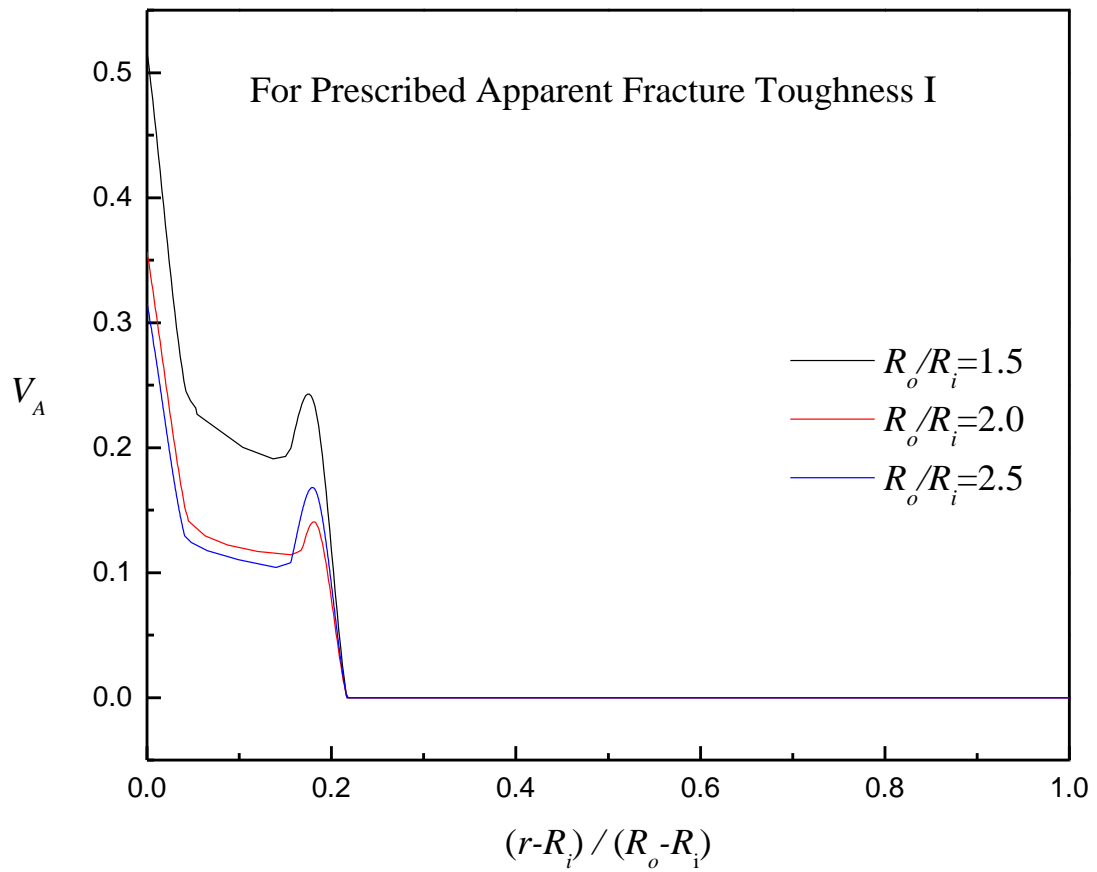
Fig. 5. 26 Effect of cylinder thickness on material distributions obtained for prescribed apparent fracture toughness of example I of Fig. 5.22.
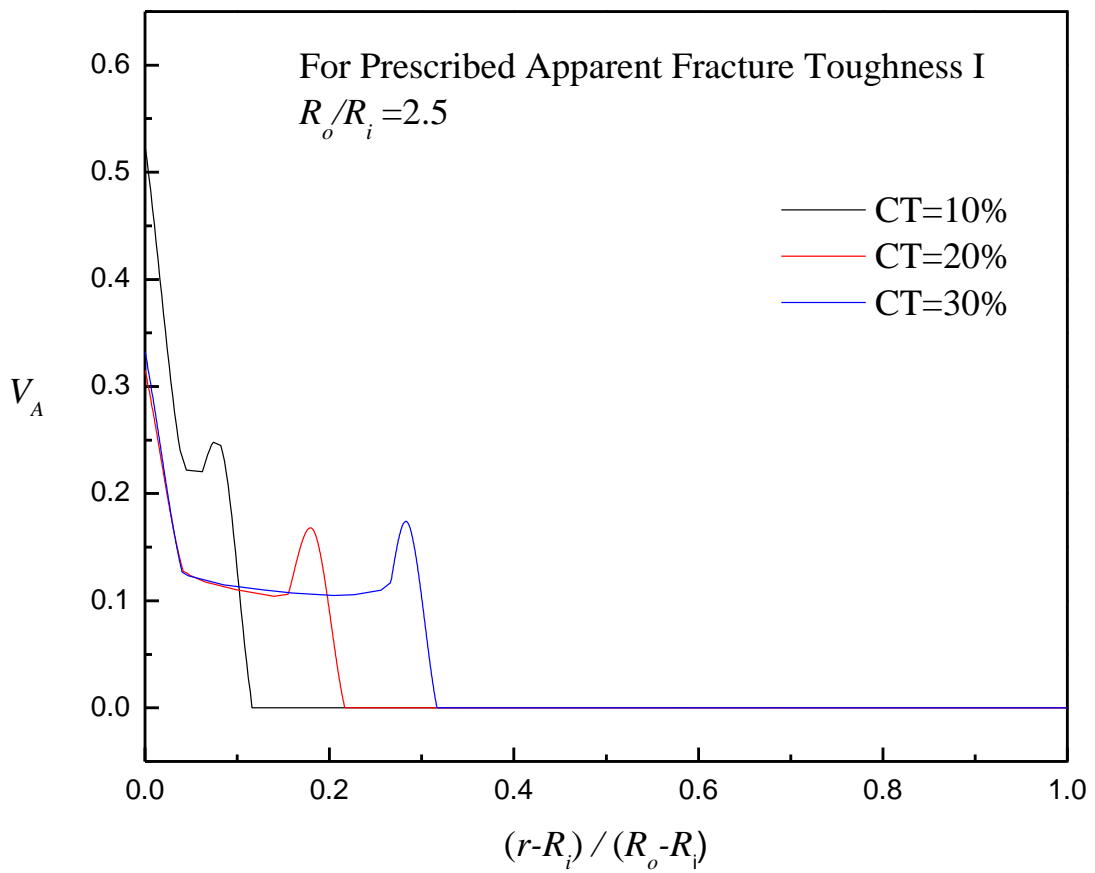
Fig. 5. 27 Comparison of material distribution for the same prescribed apparent fracture toughness I of Fig. 5.22 for different FGM coating thickness.
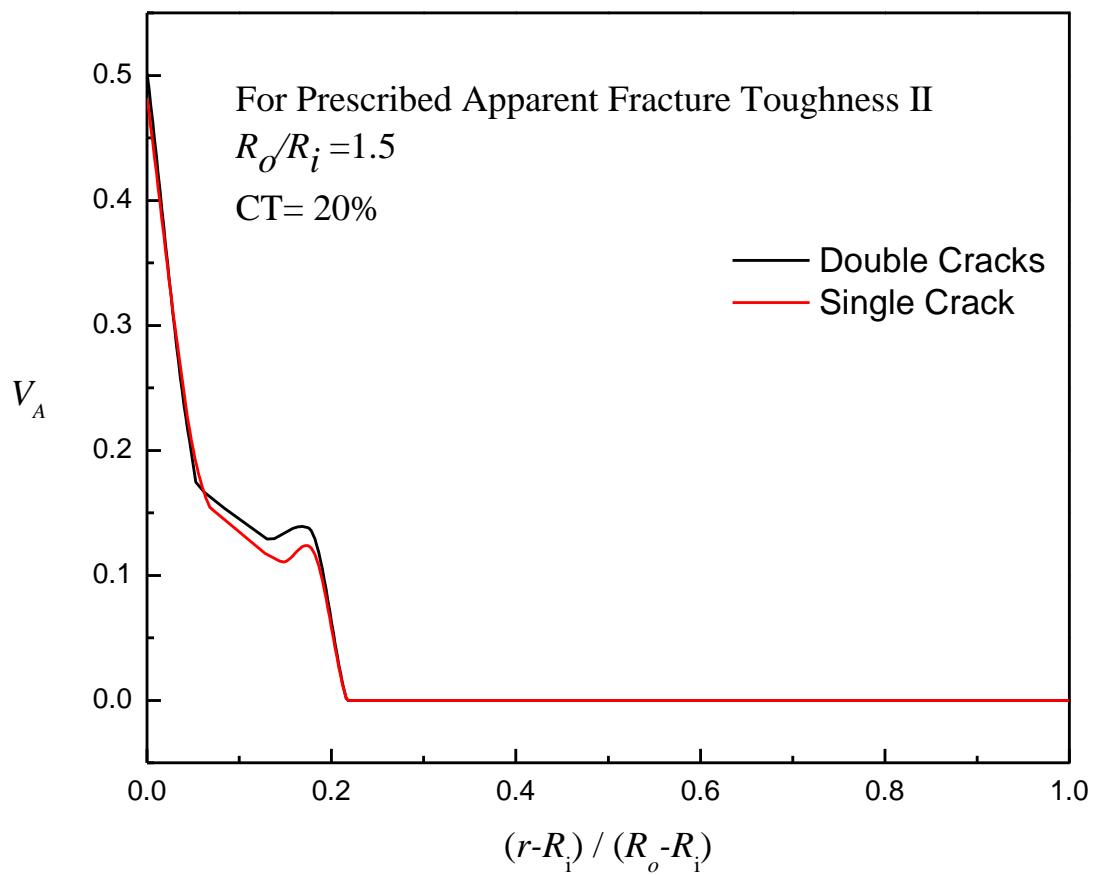
Fig. 5. 28 Comparison of material distribution for the same prescribed apparent fracture toughness II of Fig. 5.22 between a single and two diametrically-opposed edge cracks.

Table 3. 1 The normalized geometric factor $\left[(R_o^2 - R_i^2)/2.24\,R_o^2\right]F$

$l/(R_o\text{-}R_i)$	R_o/R_i					
	1.25	1.50	1.75	2.00	2.25	2.50
0.0	1.00	1.00	1.00	1.00	1.00	1.00
0.1	-	0.99	0.96	0.94	0.91	0.88
0.2	-	1.03	0.98	0.93	0.88	0.84
0.3	1.15	1.14	1.03	0.96	0.89	0.83
0.4	1.40	1.27	1.11	1.00	0.91	0.84
0.5	1.66	1.42	1.20	1.05	0.94	0.86
0.6	1.90	1.56	1.28	1.11	0.99	0.90
0.7	-	1.70	1.39	1.19	1.06	0.97
0.8	-	1.83	1.51	1.31	1.18	1.08
0.9	-	2.09	1.75	1.56	1.42	1.32

Table 4. 1 Coefficients $A_K^{'}$ and $A_K^{''}$

k	$A_k^{'}$	$A_k^{''}$
$k \geq 2$	$\dfrac{(k-1)(ib_1 - b_2)e^{i\beta} R_i^{k-2}(h\bar{h} - R_i^2)}{h^{k+1}}$ $+ \dfrac{(ib_1 + b_2)e^{-i\beta} R_i^{k-2}}{h^{k-1}}$	$(ib_1 + b_2)e^{-i\beta} \dfrac{\bar{h}^{k-1}}{R_o^k}$
$k = 1$	0	0
$k = 0$	$-\dfrac{2}{h_1^2 + h_2^2}\{(h_1 \sin\beta - h_2 \cos\beta)b_1$ $+ (h_2 \sin\beta + h_1 \cos\beta)b_2 \}$	$-\dfrac{2}{R_o^2}\{(h_1 \sin\beta - h_2 \cos\beta)b_1$ $(h_1 \cos\beta + h_2 \sin\beta)b_2 \}$
$k \leq -1$	$-(ib_1 + b_2)e^{-i\beta} \dfrac{\bar{h}^{k-1}}{R_i^k}$	$-\dfrac{(k-1)(ib_1 - b_2)e^{i\beta} R_o^{k-2}(h^2 - R_o^2)(h\bar{h} - R_o^2)}{h^{k+1}}$ $-\dfrac{(ib_1 + b_2)e^{-i\beta} R_o^{k-2}}{h^{k-1}}$

Table 4. 2 Modified coefficients $A_K^{'}$ and $A_K^{''}$

k	$A_k^{'}$	$A_k^{''}$
$k \geq 2$	$\dfrac{(k-1)R_i^{k-2}(h^2-R_i^2)}{h^{k+1}} - \dfrac{R_i^{k-2}}{h^{k-1}}$	$-\dfrac{h^{k-1}}{R_o^k}$
$k = 1$	0	0
$k = 0$	$\dfrac{2}{h}$	$\dfrac{2h}{R_o^2}$
$k \leq -1$	$\dfrac{h^{k-1}}{R_i^k}$	$-\dfrac{(k-1)R_o^{k-2}(h^2-R_o^2)}{h^{k+1}} + \dfrac{R_o^{k-2}}{h^{k-1}}$

Table 5. 1 Material properties of TiC and Al$_2$O$_3$

Material	Young's Modulus (GPa)	Shear Modulus (GPa)	Poisson's Ratio	CTE (/°C)	Ultimate Tensile Strength (GPa)	Intrinsic Apparent Fracture Toughness K_{IC} (MPa m$^{1/2}$)
TiC	462	194.12	0.19	7.4×10^{-6}	-	4.1
Al$_2$O$_3$	380	150.79	0.26	8.0×10^{-6}	0.28	3.5

APPENDIX

Appendix I

FORTRAN code to determine SIF and AFT for a cylinder with FGM coating

(Main program only)

```
c    Last change:      24 Jun 2012    2:31 am
c    This program is to directly calculate stress intensity factor and  apparent fracture
c    toughness of a thick-walled cylinder containing two diametrically opposed edge
c    cracks from a prescribed material distribution

     implicit double precision (a-h,o-z)
     parameter (ri=10.0,ro=25,ti=ri/ro,romri=ro-ri)
     parameter (delcl=0.151)
     parameter (naftad=(0.98-0.0)*romri/delcl)


c       INPUT FOR SUBROUTINE MIXTURE

     parameter (nl=150)
     dimension ye(nl),alfmix(nl),v1(nl),v2(nl),anu(nl)


c    INPUT FOR SUBROUTINE AMDIS

     parameter (nn=100,n=50)

c    INPUT FOR SUBROUTINE SIGMAP

     dimension r1(0:nl)


c    INPUT FOR SUBROUTINE SIGMAEI

     parameter (delt=1000.0)
     dimension ca2(nl-1,nl-1),b2(nl-1),p2(0:nl),xs2(nl-1),cc2(nl)

     dimension rops(nl+2),sigma2st(nl+2),sigma2sr(nl+2),sigma2sz(nl+2)


c       INPUT FOR SUBROUTINE TLEDD

     parameter (e=1.0d-16,PI=3.141592653589793d0)

c    INPUT FOR SUBROUTINE SPLINE

     parameter(nlp2=nl+2)
     dimension ryes(nl),yesp(nlp2)
```

```fortran
      open (7,file='v1.dat')
      open (8,file='v1s.dat')
      open (9,file='apft.dat')
      open (10,file='stressp.dat')
      open (11,file='stressei.dat')
      open (12,file='sifad.dat')
      open (13,FILE='SIF.dat')

      p2(0)=0.0
      p2(nl)=0.0

      d=ti
      dosl=(ro-ri)/nl+0.0001
      obti=ro/ri

      do 80 i=1,nl
      ryes(i)=i*(ro-ri)/nl+ri-(ro-ri)/nl/2.0
 80   continue


      do 16 i=1,nl

c     v1(i)=(1.0-float(i-1)/(nl-1))              !lin: linear
c     v1(i)=(1.0-float(i-1)/(nl-1))**2            !pd: parabolic downward
c     v1(i)=dsqrt(1.0d0-float(i-1)/(nl-1))         !pu: parabolic upward

c     *********** for coating *********************
      IF(i.gt.30) GOTO 37

c      IF(i.le.30) v1(i)=1.0                ! UNIFORM OVER PART OF THE
THICKNESS

      v1(i)=(1.0-float(i-1)/(30-1))               !lin  :close this statement if graded whole
thickness


c     v1(i)=(1.0-float(i-1)/(30-1))**2          !pd: parabolic downward


c     v1(i)=dsqrt(1.0d0-float(i-1)/(30-1))        !pu: parabolic upward

 37    IF(i.gt.30) v1(i)=0                ! close this statement if graded whole thickness

      v2(i)=1.0-v1(i)

      call MIXTURE(V1,V2,YE,ALFMIX,i,nl,anu)
```

```
    yesp(i+1)=ye(i)

 16   continue

    yesp(1)=ye(1)
    yesp(nlp2)=ye(nl)

    CALL SIGMAEI(ANU,RO,RI,NL,YE,ALFMIX,DELT,CA2,B2,CC2,r1)

119  format(9(f10.4),4x,f10.4)

    CALL TLEDD(NL-1,CA2,B2,XS2,NL-1,E,INDER)

    do 9 i=1,nl-1
 9   p2(i)=xs2(i)

    do 14 dx2=0.,30.0,0.2

      frac=(ro-ri)*dx2/30.0
      rop=ri+frac
      i=idint(1.0+frac/dosl)

 14    continue
131   format(f10.4,3x,f12.8)

    sp1=(ro-ri)/nl

    do 76 ji=1,nl+2

    rop=ri+sp1*(ji-1)-sp1/2.0
    if(ji.eq.1) rop=ri
    if(ji.eq.nl+2) rop=ro

    rops(ji)=rop
    i=idint(1.0+(rop-ri)/dosl)

     sigma2st(ji)=p2(i-1)*cc2(i)*cc2(i)*(1.0+r1(i)*r1(i)/(rop*rop))/
    &  (1.0-cc2(i)*cc2(i))-p2(i)*(1.0+cc2(i)*cc2(i)*r1(i)*r1(i)/
    &  (rop*rop))/(1.0-cc2(i)*cc2(i))

     sigma2sr(ji)=p2(i-1)*cc2(i)*cc2(i)*(1.0-r1(i)*r1(i)/(rop*rop))/
    &  (1.0-cc2(i)*cc2(i))-p2(i)*(1.0-cc2(i)*cc2(i)*r1(i)*r1(i)/
    &  (rop*rop))/(1.0-cc2(i)*cc2(i))

     sigma2sz(ji)=2.0*anu(i)*(cc2(i)*cc2(i)*p2(i-1)-p2(i))/(1.0-
    &  cc2(i)*cc2(i))+ye(i)*alfmix(i)*delt

 76   continue

    cl=0.0d0
```

94

```
   48  continue

c    CALCULATION OF SIF AFTER DESIGN

cCCCCCCCCCCCCCCCCCCCCCCCCCCCCCCCCCCCCCCCCCCCC

     write(12,208) obti,delt
 208  format(3x,'ro/ri=',1x,f6.3,5x,'delt='1x,f7.2/)
     write(12,206)
 206  format(5x,'Ri+cl',7x,'cl',8x,'cl/romri',5x,'sifad',10x,'sifadn')

    do 91 i=1,naftad

    cl=cl+delcl
     sf=1.0
     sigmau=.28

    call apftad(sf,sigmau,cl,p2,n,ri,dosl,cc2,r1,ro,nl,ye,anu
   & ,nn,pcrt,SIF,rops,sigma2st,nlp2,D,yesp)

    x5=cl/(ro-ri)

    ff=1.794872d0*x5**5+1.293706d0*x5**4-5.712121d0*x5**3+
   & 4.941142d0*x5**2-1.585786d0*x5+0.9988531d0      ! ro/ri=2.5

c    ff=5.0D0*x5**5-5.932401D0*x5**4+3.671329D-2*x5**3+2.77331D0*x5**2
c    & -8.599114D-1*x5+9.996224D-1                    ! ro/ri=2.0

c    ff=1.24359D+1*x5**5-2.26049D+1*x5**4+1.146795D+1*x5**3+
c    & 5.300117D-1*x5**2-2.365291D-1*x5+9.995664D-1        ! ro/ri=1.5

c    sifad=ff*pcrt*dsqrt(pi*(cl+ri))*1000.0/dsqrt(1000.0d0)
    sifad=ff*pcrt*dsqrt(pi*cl)*1000.0/dsqrt(1000.0d0)
    sifadn=sifad/3.5d0

    F1=SIF*(1-ti*ti)*sf*dsqrt(1000.0d0)/(2*sigmau*dsqrt(pi*cl)*1000)

    WRITE(13,312) x5,F1

    write(12,205) Ri+cl,cl,x5,sifad,sifadn
    print*, cl,sifadn

 91   continue
 205  format(3x,f9.6,2x,f9.6,2x,f9.6,2x,f12.8,2x,f12.8)
 312  FORMAT(5x,f9.6,7x,f12.8)

cCCCCCCCCCCCCCCCCCCCCCCCCCCCCCCCCCCCCCCCCCCCC
```

```
c    SPLINE OF VOLUME FRACTION

     write(8,209) obti,delt
209  format(3x,'ro/ri=',1x,f6.3,5x,'delt=',1x,f7.2/)
     write(8,207)
207  format(7x,'r',9x,'(r-ri)/romri',5x,'v1s')

     do 62 rv1s=ri,ro,0.01

     call spline(rv1s,v1s,ryes,v1,nl)
     write(8,111) rv1s,(rv1s-ri)/romri,v1s

62   continue

111  format(3x,f8.5,6x,f8.5,6x,f9.7)
cccccccccccccccccccccccccccccccccccccccccccccccccccccccccccccc
cccccccccccccccccccccccccccccccccccccccccccccccccccccccccccccccccc
ccccccccccccccccccccccccccccccccccc
     WRITE(7,115)
115  FORMAT(2x,'(r-ri)/(ro-ri)',6x,'v1')

     do 69 i=1,nl
     xrop=ri-romri/(2*nl)+romri/(nl)*i
     WRITE(7,116) (xrop-ri)/romri,v1(i)
  69 continue

116  FORMAT(3x,f7.3,5x,f8.3)
cccccccccccccccccccccccccccccccccccccccccccccccccccccccccccccc
cccccccccccccccccccccccccccccccccccccccccccccccccccccccccccccccc
cccccccccccccccccccccccccccccccccc

     write(7,42) nl,cl,obti
42   format(3x,'iteads=',i4,3x,'nl=',i3,3x,'cl=',f6.3,2x,
    & 'ro/ri=',1x,f6.3,/)

     write(9,43) nl,cl,obti
43   format(3x,'iteads=',i4,3x,'nl=',i3,3x,'cl=',f6.3,2x,
    & 'ro/ri=',1x,f6.3,/)

     write(7,41)
41   format(16x,'obj',12x,'r',11x,'cl/romri',8x,'v1')

     write(9,112)
112  format(7x,'cl',11x,'cl/romri',6x,'apft',11x,'apftn',
    & 11x,'inft',11x,'csif')

     do 22 i=1,nl

     xaxis=ri+i*(ro-ri)/nl-romri/2.0/nl
     write(7,40) xaxis,(xaxis-ri)/romri,v1(i)
```

```
 22   continue

 40   format(13x,f9.6,5x,f9.6,5x,f9.6,5x,f9.6)

      do 61 i=1,nlp2

      write(10,110) rops(i)
      write(11,110) rops(i),sigma2sr(i),sigma2st(i),sigma2sz(i)

 61   continue
110   format(3x,f7.4,2x,3(f12.9,2x))

 88   stop
      end
c
c
```

Appendix II

FORTRAN code for expressing SIF as a function of *ΔT* for a cylinder with FGM coating containing two diametrically opposed edge cracks.

(Main program only)

```
c    Last change:  L    27 Apr 2012   10:07 pm
c    This program is to directlyly calculate SIF as a function
c     of application temperature for a cylinder with FGM
c    coating containing two diametrically opposed edge
c     cracks from a prescribed material distribution

        implicit double precision (a-h,o-z)


      parameter (ri=10.0,ro=25,ti=ri/ro,romri=ro-ri)
c     parameter (delcl=0.151)
c     parameter (naftad=(0.98-0.0)*romri/delcl)
c     parameter (sf=1.0,sigmau=0.28)




c       INPUT FOR SUBROUTINE MIXTURE

      parameter (nl=150)
      dimension ye(nl),alfmix(nl),v1(nl),v2(nl),anu(nl)


c    INPUT FOR SUBROUTINE AMDIS

      parameter (nn=100,n=50)

c    INPUT FOR SUBROUTINE SIGMAP

      dimension r1(0:nl)


c    INPUT FOR SUBROUTINE SIGMAEI

c     parameter (delt=1000.0)
      dimension ca2(nl-1,nl-1),b2(nl-1),p2(0:nl),xs2(nl-1),cc2(nl)

      dimension rops(nl+2),sigma2st(nl+2),sigma2sr(nl+2),sigma2sz(nl+2)


c     INPUT FOR SUBROUTINE TLEDD

      parameter (e=1.0d-16,PI=3.141592653589793d0)
```

```fortran
c    INPUT FOR SUBROUTINE SPLINE

     parameter(nlp2=nl+2)
     dimension ryes(nl),yesp(nlp2)


     open (7,file='v1.dat')
     open (8,file='v1s.dat')
     open (9,file='apft.dat')
     open (10,file='stressp.dat')
     open (11,file='stressei.dat')
     open (12,file='sifad.dat')
     open (13,FILE='SIF.dat')


     p2(0)=0.0
     p2(nl)=0.0


     d=ti
     dosl=(ro-ri)/nl+0.0001
     obti=ro/ri

     do 80 i=1,nl
     ryes(i)=i*(ro-ri)/nl+ri-(ro-ri)/nl/2.0
 80  continue

     do 16 i=1,nl

c    v1(i)=1.0                              ! uniform
c    v1(i)=(1.0-float(i-1)/(nl-1))          !lin: Linear
c    v1(i)=(1.0-float(i-1)/(nl-1))**2        !pd: parabolic downward
c    v1(i)=dsqrt(1.0d0-float(i-1)/(nl-1))    !pu: parabolic upward

c    *********** for coating *******************
     IF(i.gt.30) GOTO 37

c     IF(i.le.30) v1(i)=1.0             ! uniform over part of the thickness

      v1(i)=(1.0-float(i-1)/(30-1))      !lin :close this statement if graded whole thickness

c    v1(i)=(1.0-float(i-1)/(30-1))**2          !pd: parabolic downward

c     v1(i)=dsqrt(1.0d0-float(i-1)/(30-1))        !pu: parabolic upward

 37    IF(i.gt.30) v1(i)=0              ! close this statement if graded whole thickness
      v2(i)=1.0-v1(i)

      call MIXTURE(V1,V2,YE,ALFMIX,i,nl,anu)
```

99

```fortran
      yesp(i+1)=ye(i)
16    continue

      yesp(1)=ye(1)
      yesp(nlp2)=ye(nl)

      WRITE(13,309)
309   FORMAT(5x,'DELT',7x,'F1')

      delt=0.d0
      do 91 p=1,5,1

      delt=delt+200


      CALL SIGMAEI(ANU,RO,RI,NL,YE,ALFMIX,DELT,CA2,B2,CC2,r1)
119   format(9(f10.4),4x,f10.4)

      CALL TLEDD(NL-1,CA2,B2,XS2,NL-1,E,INDER)

      do 9 i=1,nl-1
9     p2(i)=xs2(i)

      do 14 dx2=0.,30.0,0.2

        frac=(ro-ri)*dx2/30.0
        rop=ri+frac
        i=idint(1.0+frac/dosl)

14      continue
131     format(f10.4,3x,f12.8)

      sp1=(ro-ri)/nl

      do 76 ji=1,nl+2

      rop=ri+sp1*(ji-1)-sp1/2.0
      if(ji.eq.1) rop=ri
      if(ji.eq.nl+2) rop=ro

      rops(ji)=rop
      i=idint(1.0+(rop-ri)/dosl)

      sigma2st(ji)=p2(i-1)*cc2(i)*cc2(i)*(1.0+r1(i)*r1(i)/(rop*rop))/
     & (1.0-cc2(i)*cc2(i))-p2(i)*(1.0+cc2(i)*cc2(i)*r1(i)*r1(i)/
     & (rop*rop))/(1.0-cc2(i)*cc2(i))

      sigma2sr(ji)=p2(i-1)*cc2(i)*cc2(i)*(1.0-r1(i)*r1(i)/(rop*rop))/
     & (1.0-cc2(i)*cc2(i))-p2(i)*(1.0-cc2(i)*cc2(i)*r1(i)*r1(i)/
     & (rop*rop))/(1.0-cc2(i)*cc2(i))
```

```fortran
      sigma2sz(ji)=2.0*anu(i)*(cc2(i)*cc2(i)*p2(i-1)-p2(i))/(1.0-
     & cc2(i)*cc2(i))+ye(i)*alfmix(i)*delt


 76   continue

      cl=3.75

 48   continue

c    CALCULATION OF SIF AFTER DESIGN

cCCCCCCCCCCCCCCCCCCCCCCCCCCCCCCCCCCCCCCCCCCCC

      write(12,208) obti,delt
 208  format(3x,'ro/ri=',1x,f6.3,5x,'delt='1x,f7.2/)


      write(12,206)
 206  format(5x,'Ri+cl',7x,'cl',8x,'cl/romri',5x,'sifad',10x,'sifadn')


      sf=1.0
      sigmau=.28

      call apftad(sf,sigmau,cl,p2,n,ri,dosl,cc2,r1,ro,nl,ye,anu
     & ,nn,pcrt,SIF,rops,sigma2st,nlp2,D,yesp)

      x5=cl/(ro-ri)

      ff=1.794872d0*x5**5+1.293706d0*x5**4-5.712121d0*x5**3+
     & 4.941142d0*x5**2-1.585786d0*x5+0.9988531d0            ! ro/ri=2.5


c     ff=5.0D0*x5**5-5.932401D0*x5**4+3.671329D-2*x5**3+2.77331D0*x5**2
c     & -8.599114D-1*x5+9.996224D-1                         ! ro/ri=2.0

c     ff=1.24359D+1*x5**5-2.26049D+1*x5**4+1.146795D+1*x5**3+
c     & 5.300117D-1*x5**2-2.365291D-1*x5+9.995664D-1          ! ro/ri=1.5

c     sifad=ff*pcrt*dsqrt(pi*(cl+ri))*1000.0/dsqrt(1000.0d0)


      sifad=ff*pcrt*dsqrt(pi*cl)*1000.0/dsqrt(1000.0d0)
      sifadn=sifad/3.5d0

      write(12,205) Ri+cl,cl,x5,sifad,sifadn


      F1=SIF*(1-ti*ti)*sf*dsqrt(1000.0d0)/(2*sigmau*dsqrt(pi*cl)*1000)
```

```
      PRINT*,delt,F1

      WRITE(13,312) delt,F1

 91   continue
 205  format(3x,f9.6,2x,f9.6,2x,f9.6,2x,f12.8,2x,f12.8)
 312  FORMAT(5x,f7.2,7x,f12.8)

cCCCCCCCCCCCCCCCCCCCCCCCCCCCCCCCCCCCCCCCCCCC

c    SPLINE OF VOLUME FRACTION

      write(8,209) obti,delt
 209  format(3x,'ro/ri=',1x,f6.3,5x,'delt=',1x,f7.2/)
      write(8,207)
 207  format(7x,'r',9x,'(r-ri)/romri',5x,'v1s')

      do 62 rv1s=ri,ro,0.01

      call spline(rv1s,v1s,ryes,v1,nl)
      write(8,111) rv1s,(rv1s-ri)/romri,v1s

 62   continue

 111  format(3x,f8.5,6x,f8.5,6x,f9.7)

cccccccccccccccccccccccccccccccccccccccccccccccccccccccccccccc
cccccccccccccccccccccccccccccccccccccccccccccccccccccccccccccc
cccccccccccccccccccccccccccccccccccc
      WRITE(7,115)
 115  FORMAT(2x,'(r-ri)/(ro-ri)',6x,'v1')

      do 69 i=1,nl
      xrop=ri-romri/(2*nl)+romri/(nl)*i
      WRITE(7,116) (xrop-ri)/romri,v1(i)
   69 continue

 116  FORMAT(3x,f7.3,5x,f8.3)
cccccccccccccccccccccccccccccccccccccccccccccccccccccccccccccc
cccccccccccccccccccccccccccccccccccccccccccccccccccccccccccccc
cccccccccccccccccccccccccccccccc


c     write(7,42) nl,cl,obti
c 42  format(3x,'iteads=',i4,3x,'nl=',i3,3x,'cl=',f6.3,2x,
c     & 'ro/ri=',1x,f6.3,/)

      write(9,43) nl,cl,obti
 43   format(3x,'nl=',i4,3x,'cl=',f6.3,2x,'ro/ri=',f6.3,/)
```

```
c      write(7,117)
c 117   format(1x,'obj',2x,'r',2x,'cl/romri',3x,'v1')

       write(9,112)
 112  format(7x,'cl',11x,'cl/romri',6x,'apft',11x,'apftn',
     & 11x,'inft',11x,'csif')

c      do 22 i=1,nl

c      xaxis=ri+i*(ro-ri)/nl-romri/2.0/nl
c      write(7,118) xaxis,(xaxis-ri)/romri,v1(i)
c 22   continue

c 118   format(13x,f9.6,5x,f9.6,5x,f9.6)

c      do 24 i=1,naft
c 24     write(9,113) scl(i),x5s(i),saft(i),saftn(i),sifin(i),ssif(i)
c 113     format(f12.7,3x,f12.7,3x,f12.7,3x,f12.7,3x,f12.7,3x,f12.7)

      do 61 i=1,nlp2

      write(10,110) rops(i)
      write(11,110) rops(i),sigma2sr(i),sigma2st(i),sigma2sz(i)

 61   continue
 110  format(3x,f7.4,2x,3(f12.9,2x))

 88   stop
      end
c
c
```

Appendix III

FORTRAN code for inverse problem of material distribution to realize prescribed apparent fracture toughness.

(Main program only)

```
c    Last change:  L    24 Jun 2012    3:29 am
c    This program is to inversely calculate composition profile
c    of thick-walled cylinder with FGM coating
c    containing two radial edge cracks from a prescribed
c    apparent fracture toughness.

     implicit double precision (a-h,o-z)


     parameter (ri=10.0,ro=25.0,ti=ri/ro,romri=ro- ri,clmax=0.75*romri)
     parameter (delcl=0.151,naft=clmax/delcl)
     parameter (naftad=(0.98-0.75)*romri/delcl)
     dimension scl(naft),saft(naft),sifin(naft),objb(naft),ssif(naft)
     dimension x5s(naft),saftn(naft)


c       INPUT FOR SUBROUTINE MIXTURE

     parameter (nl=30)
     parameter (nlc=3)
     dimension ye(nl),alfmix(nl),v1(nl),v2(nl),anu(nl),v11(nlc)


c    INPUT FOR SUBROUTINE  ADS

      parameter (ndv=nlc,ncon=naft,nra=ndv+1,nrwk=30000,nriwk=1000,
     & ncola=2*ndv)

      parameter (smvfcon=0.4)

      dimension vlb(ndv+1),vub(ndv+1),g(ncon),idg(ncon),ic(ncon),
     & df(ndv+1),wk(nrwk),iwk(nriwk),a(nra,ncola)


c    INPUT FOR SUBROUTINE AMDIS

     parameter (nn=60,n=30)
     dimension ATL(nn,n),DH1(n),H(N)


c    INPUT FOR SUBROUTINE SIGMAP
```

```fortran
      parameter (pout=0.0)
      dimension p1(0:nl),ca1(nl-1,nl-1),b1(nl-1),r1(0:nl),xs1(nl-1)
     & ,cc1(nl),sigma1(n)
      dimension sigma1st(nl+2),sigma1sr(nl+2),sigma1sz(nl+2)

c     INPUT FOR SUBROUTINE SIGMAEI

      parameter (delt=1000.0)
      dimension ca2(nl-1,nl-1),b2(nl-1),p2(0:nl),xs2(nl-1),cc2(nl)
     & ,sigma2(n)
      dimension rops(nl+2),sigma2st(nl+2),sigma2sr(nl+2),sigma2sz(nl+2)

c       INPUT FOR SUBROUTINE TLEDD

      parameter (e=1.0d-16,PI=3.141592653589793d0)
      dimension B(n),XTL(n)

c     INPUT FOR SUBROUTINE SPLINE

      parameter(nlp2=nl+2)
      dimension ryes(nl),yesp(nlp2)


c     dimension for finding minimum value
      dimension objst(11),v1st(11,nl)

      open (7,file='v1.dat')
      open (8,file='v1s.dat')
      open (9,file='apft.dat')
      open (10,file='stressp.dat')
      open (11,file='stressei.dat')
      open (12,file='sifad.dat')

      p1(nl)=pout
      p2(0)=0.0
      p2(nl)=0.0

      d=ti
      dosl=(ro-ri)/nl+0.0001
      obti=ro/ri

      do 80 i=1,nl
      ryes(i)=i*(ro-ri)/nl+ri-(ro-ri)/nl/2.0
 80   continue

      igrad=0
c     initial design

      iobj=0
c      do 48 stepdv=0.0,1.0,0.1
```

```fortran
      iobj=iobj+1
      stepdv=0.8d0          !*************** initial value*********************

      do 11 i=1,nlc
      v11(I)=stepdv
 11   continue

      do 12 i=nlc+1,nl
 12   v1(I)=0.0d0
      continue

C     BOUNDS OF DESIGN VARIABLES

      do 21 i=1,nlc

        vlb(i)=0.0
        vub(i)=1.0
 21   continue

c     identify constraints as nonlinear, inequality

      do 19 i=1,naft

      idg(i)=0    ! for nonlinear inequality
c     idg(i)=2    ! for linear inequality
 19   continue

c     input

      data istrat,iopt,ioned,iprint/5,3,3,0000/

c     OPTIMIZATION BEGINS

      iteads=0
      info=0

 10   call ADS(info,istrat,iopt,ioned,iprint,igrad,ndv,ncon,v11,vlb,
     & vub,obj,g,idg,ngt,ic,df,a,nra,ncola,wk,nrwk,iwk,nriwk)

      do 36 i=1,nlc
 36   v1(I)=v11(I)
      continue


      if (info.eq.0) goto 20
      iteads=iteads+1

c     Calculate YE, ALFMIX and ANU

      do 16 i=1,nl
```

```fortran
c     v1(i)=(1.0-float(i-1)/(nl-1))

      v2(i)=1.0-v1(i)

      call MIXTURE(V1,V2,YE,ALFMIX,i,nl,anu)

      yesp(i+1)=ye(i)

c     print*,V1(i),ye(i),alfmix(i),anu(i)

 16   continue

      yesp(1)=ye(1)
      yesp(nlp2)=ye(nl)


      CALL SIGMAEI(ANU,RO,RI,NL,YE,ALFMIX,DELT,CA2,B2,CC2,r1)

c     write(7,119)((ca2(i,j),j=1,nl-1),b2(i),i=1,nl-1)
 119  format(9(f10.4),4x,f10.4)

      CALL TLEDD(NL-1,CA2,B2,XS2,NL-1,E,INDER)

      do 9 i=1,nl-1
 9    p2(i)=xs2(i)

c     do 13 i=0,nl
c 13      print*,p2(i)

      do 14 dx2=0.,30.0,0.2

        frac=(ro-ri)*dx2/30.0
        rop=ri+frac
        i=idint(1.0+frac/dosl)

        sigmao2=p2(i-1)*cc2(i)*cc2(i)*(1.0+r1(i)*r1(i)/(rop*rop))/
     &  (1.0-cc2(i)*cc2(i))-p2(i)*(1.0+cc2(i)*cc2(i)*r1(i)*r1(i)/
     &  (rop*rop))/(1.0-cc2(i)*cc2(i))

c     print*, rop, sigmao2,frac,i
c        write(7,131) rop,sigmao2

 14   continue
 131  format(f10.4,3x,f12.8)

      sp1=(ro-ri)/nl

      do 76 ji=1,nl+2
```

```fortran
      rop=ri+sp1*(ji-1)-sp1/2.0
      if(ji.eq.1) rop=ri
      if(ji.eq.nl+2) rop=ro

      rops(ji)=rop
      i=idint(1.0+(rop-ri)/dosl)

      sigma2st(ji)=p2(i-1)*cc2(i)*cc2(i)*(1.0+r1(i)*r1(i)/(rop*rop))/
     & (1.0-cc2(i)*cc2(i))-p2(i)*(1.0+cc2(i)*cc2(i)*r1(i)*r1(i)/
     & (rop*rop))/(1.0-cc2(i)*cc2(i))

      sigma2sr(ji)=p2(i-1)*cc2(i)*cc2(i)*(1.0-r1(i)*r1(i)/(rop*rop))/
     & (1.0-cc2(i)*cc2(i))-p2(i)*(1.0-cc2(i)*cc2(i)*r1(i)*r1(i)/
     & (rop*rop))/(1.0-cc2(i)*cc2(i))

      sigma2sz(ji)=2.0*anu(i)*(cc2(i)*cc2(i)*p2(i-1)-p2(i))/(1.0-
     & cc2(i)*cc2(i))+ye(i)*alfmix(i)*delt

 76   continue

      sobj=0.0d0
      cl=0.0d0


      do 23 ii=1,naft

      cl=cl+delcl
      scl(ii)=cl

      x5=cl/(ro-ri)
      x5s(ii)=x5

      ff=1.794872d0*x5**5+1.293706d0*x5**4-5.712121d0*x5**3+
     & 4.941142d0*x5**2-1.585786d0*x5+0.9988531d0        ! ro/ri=2.5

c     ff=5.0D0*x5**5-5.932401D0*x5**4+3.671329D-2*x5**3+2.77331D0*x5**2
c     & -8.599114D-1*x5+9.996224D-1                      ! ro/ri=2.0

c     ff=1.24359D+1*x5**5-2.26049D+1*x5**4+1.146795D+1*x5**3+
c     &5.300117D-1*x5**2-2.365291D-1*x5+9.995664D-1       ! ro/ri=1.5


      aft=3.0/clmax*cl+7.0   !********************* prescribed apparent fracture
     toughness ********************************

c     aft=7.0

      saft(ii)=aft
      saftn(ii)=aft/3.5
```

```fortran
      pin=aft*(1.0-ti*ti)*dsqrt(1000.0d0)/(2.24*dsqrt(pi*cl)*ff*1000.0)
c     write(8,111) scl(ii),saft(ii)
      p1(0)=pin

      call SIGMAP(ANU,RO,RI,NL,PIN,POUT,YE,CA1,B1,cc1,r1)

c     write(7,119)((ca1(i,j),j=1,nl-1),b1(i),i=1,nl-1)
c 119  format(9(f10.4),4x,f10.4)

      call   TLEDD(NL-1,CA1,B1,XS1,NL-1,E,INDER)

      do 7 i=1,nl-1
 7    p1(i)=xs1(i)

c     do 8 i=0,nl
c 8      print*, p1(i)

      do 15 dx1=0.,30.0,0.2

        frac=(ro-ri)*dx1/30.0
        rop=ri+frac
        i=idint(1.0+frac/dosl)

        sigmao1=p1(i-1)*cc1(i)*cc1(i)*(1.0+r1(i)*r1(i)/(rop*rop))/
     &  (1.0-cc1(i)*cc1(i))-p1(i)*(1.0+cc1(i)*cc1(i)*r1(i)*r1(i)/
     &  (rop*rop))/(1.0-cc1(i)*cc1(i))

c     print*, rop, sigmao1,frac,i

 15   continue

      do 78 ji=1,nl+2
      rop=ri+sp1*(ji-1)-sp1/2.0

      if(ji.eq.1)rop=ri
      if(ji.eq.nl+2)rop=ro
      rops(ji)=rop

      i=idint(1.0+(rop-ri)/dosl)

      sigma1st(ji)=p1(i-1)*cc1(i)*cc1(i)*(1.0+r1(i)*r1(i)/(rop*rop))/
     &  (1.0-cc1(i)*cc1(i))-p1(i)*(1.0+cc1(i)*cc1(i)*r1(i)*r1(i)/
     &  (rop*rop))/(1.0-cc1(i)*cc1(i))

      sigma1sr(ji)=p1(i-1)*cc1(i)*cc1(i)*(1.0-r1(i)*r1(i)/(rop*rop))/
     &  (1.0-cc1(i)*cc1(i))-p1(i)*(1.0-cc1(i)*cc1(i)*r1(i)*r1(i)/
     &  (rop*rop))/(1.0-cc1(i)*cc1(i))

      sigma1sz(ji)=2.0*anu(i)*(cc1(i)*cc1(i)*p1(i-1)-p1(i))/(1.0-
     &  cc1(i)*cc1(i))
```

```fortran
 78   continue


      w=2.0d0*ro/cl
      call AMDIS(NN,N,W,D,TI,ATL,dh1,h)

c     write(7,132) ((ATL(i,j),j=1,n),i=1,n)
c 132  format(10(f10.4))


c     B MATRIX CALCULATION

      do 17 j=n,1,-1

        frac=cl*(h(j)+1.0)/2.0
        rop=ri+frac

        i=idint(1.0+frac/dosl)

      call spline(rop,str1,rops,sigma1st,nlp2)
      sigma1(j)=str1

c       sigma1(j)=p1(i-1)*cc1(i)*cc1(i)*(1.0+r1(i)*r1(i)/(rop*rop))/
c     & (1.0-cc1(i)*cc1(i))-p1(i)*(1.0+cc1(i)*cc1(i)*r1(i)*r1(i)/
c     & (rop*rop))/(1.0-cc1(i)*cc1(i))

c       write(7,131) rop,sigma1(j)
c      print*, rop, sigma1(j),frac,i

 17   continue

      do 18 j=n,1,-1

        frac=cl*(h(j)+1.0)/2.0
        rop=ri+frac

        i=idint(1.0+frac/dosl)

      call spline(rop,str2,rops,sigma2st,nlp2)
      sigma2(j)=str2

c       sigma2(j)=p2(i-1)*cc2(i)*cc2(i)*(1.0+r1(i)*r1(i)/(rop*rop))/
c     & (1.0-cc2(i)*cc2(i))-p2(i)*(1.0+cc2(i)*cc2(i)*r1(i)*r1(i)/
c     & (rop*rop))/(1.0-cc2(i)*cc2(i))

c      print*, rop, sigma2(j),frac,i
c       write(7,131) rop,sigma2(j)

 18   continue
```

```fortran
      do 29 i=1,n
        b(i)=-(sigma1(i)+sigma2(i)+pin)*((2*n+1)/2.0d0)
c       print*, sigma1(i),sigma2(i),pin,b(i)
 29     continue

c
      call   TLEDD(N,ATL,B,XTL,NN,E,INDER)

      sum=0.0d0
      do 6 i=1,n
      an=dsin((2*i-1)*n*pi/(2*n+1))
      dn=dtan((2*i-1)*pi/((2*n+1)*2))
  6   sum=sum+an/dn*XTL(i)
      sumf=(2.0d0/(2*n+1))*sum

c  STRESS INTENSITY FACTOR

      sif=sumf*dsqrt(2.0d0*pi*cl)*1000.0d0/dsqrt(1000.0d0)
      ssif(ii)=sif
c     print*, sif,'=sif'


      call spline(cl+ri,yes,rops,yesp,nlp2)

c     ki=idint(1+cl/dosl)
c     sifi=ye(ki)*3.5/380.0

      sifi=yes*3.5/380.0
      sifin(ii)=sifi

c     print*, ye(ki),sifi,sif,cl

c     evaluate objective and constraints.

      objb(ii)=(sif-sifi)**2
      sobj=sobj+objb(ii)

 23   continue

      obj=sobj

      do 25 jj=1,naft

      g(jj)=dabs(ssif(jj)-sifin(jj))-0.7
c     print*, g(jj),obj,iteads

 25   continue

c     go continue with optimization.
```

```fortran
c     print*, obj,iteads

      go to 10

 20   continue

      objst(iobj)=obj
c     print*, objst(iobj)

      do 49 ij=1,nl
      v1st(iobj,ij)=v1(ij)
 49   continue

 48   continue

c     CALCULATION OF SIF AFTER DESIGN

cCCCCCCCCCCCCCCCCCCCCCCCCCCCCCCCCCCCCCCCCCCCCCC

      write(12,208) obti
 208  format(3x,'ro/ri=',1x,f6.3,/)
      write(12,206)
 206  format(5x,'Ri+cl',7x,'cl',8x,'cl/romri',5x,'sifad',10x,'sifadn')

      do 91 i=1,naftad

      cl=cl+delcl

      call apftad(cl,p2,n,ri,dosl,cc2,r1,ro,nl,ye,anu
     & ,nn,pcrt,rops,sigma2st,nlp2,D,yesp)

      x5=cl/(ro-ri)

      ff=1.794872d0*x5**5+1.293706d0*x5**4-5.712121d0*x5**3+
     & 4.941142d0*x5**2-1.585786d0*x5+0.9988531d0          ! ro/ri=2.5

c     ff=5.0D0*x5**5-5.932401D0*x5**4+3.671329D-2*x5**3+2.77331D0*x5**2
c     & -8.599114D-1*x5+9.996224D-1                    ! ro/ri=2.0

c     ff=1.24359D+1*x5**5-2.26049D+1*x5**4+1.146795D+1*x5**3+
c     &5.300117D-1*x5**2-2.365291D-1*x5+9.995664D-1       ! ro/ri=1.5




c     sifad=ff*pcrt*dsqrt(pi*(cl+ri))*1000.0/dsqrt(1000.0d0)
      sifad=ff*pcrt*dsqrt(pi*cl)*1000.0/dsqrt(1000.0d0)
      sifadn=sifad/3.5d0
```

```fortran
      write(12,205) Ri+cl,cl,x5,sifad,sifadn
c     print*, cl,sifad

 91   continue
 205  format(3x,f9.6,2x,f9.6,2x,f9.6,2x,f12.8,2x,f12.8)

cCCCCCCCCCCCCCCCCCCCCCCCCCCCCCCCCCCCCCCCCCC

c     SPLINE OF VOLUME FRACTION

      write(8,209) obti
 209  format(3x,'ro/ri=',1x,f6.3,/)
      write(8,207)
 207  format(7x,'r',9x,'(r-ri)/romri',5x,'v1s')

      do 62 rv1s=ri,ro,0.01

      call spline(rv1s,v1s,ryes,v1,nl)
      write(8,111) rv1s,(rv1s-ri)/romri,v1s

 62   continue

 111  format(3x,f8.5,6x,f8.5,6x,f9.7)


      goto 71

c     Find the minimum value of obj

      alarge=9.9d16
      do 50 i=1,11
      if(objst(i).le.alarge) alarge=objst(i)
      if(objst(i).le.alarge) kfv=i
      if(objst(i).gt.alarge) alarge=alarge
      if(objst(i).gt.alarge) kfv=kfv
 50   continue
      obj=alarge
      do 51 i=1,nl
      v1(i)=v1st(kfv,i)
 51   continue

c     print*, 'obj=',obj,kfv
c     print results

 71   continue

      write(7,42) iteads,nl,cl,obti
 42   format(3x,'iteads=',i4,3x,'nl=',i3,3x,'cl=',f6.3,2x,
     & 'ro/ri=',1x,f6.3,/)
```

```fortran
      write(9,43) iteads,nl,cl,obti
43    format(3x,'iteads=',i4,3x,'nl=',i3,3x,'cl=',f6.3,2x,
     & 'ro/ri=',1x,f6.3,/)

      write(7,41)
41    format(16x,'obj',12x,'r',11x,'cl/romri',8x,'v1')

      write(9,112)
112   format(7x,'cl',11x,'cl/romri',6x,'apft',11x,'apftn',
     & 11x,'inft',11x,'csif')

      do 22 i=1,nl

      xaxis=ri+i*(ro-ri)/nl-romri/2.0/nl
      write(7,40) obj,xaxis,(xaxis-ri)/romri,v1(i)
22    continue

40    format(13x,f9.6,5x,f9.6,5x,f9.6,5x,f9.6)

      do 24 i=1,naft
24      write(9,113) scl(i),x5s(i),saft(i),saftn(i),sifin(i),ssif(i)
113     format(f12.7,3x,f12.7,3x,f12.7,3x,f12.7,3x,f12.7,3x,f12.7)

      do 61 i=1,nlp2

      write(10,110) rops(i),sigma1sr(i),sigma1st(i),sigma1sz(i)
      write(11,110) rops(i),sigma2sr(i),sigma2st(i),sigma2sz(i)

61    continue
110   format(3x,f7.4,2x,3(f12.9,2x))

88    stop
      end
c
c
```